# Cerebellar output neurons impair non-motor behaviors by altering development of extracerebellar connectivity

Andrew S. Lee[1,2], Tanzil M. Arefin[3,10], Alina Gubanova[1], Daniel N. Stephen[1], Yu Liu[4,5], Zhimin Lao[1], Anjana Krishnamurthy[1,2], Natalia V. De Marco García[2,6], Detlef H. Heck[4,5], Jiangyang Zhang[3], Anjali M. Rajadhyaksha[2,7,8,11], Alexandra L. Joyner[1,2,9]*

[1]Developmental Biology Program, Sloan Kettering Institute, New York 10065, NY, USA

[2]Neuroscience Program, Weill Cornell Graduate School of Medical Sciences, New York 10021, NY, USA

[3]Bernard and Irene Schwartz Center for Biomedical Imaging, Department of Radiology, New York University Grossman School of Medicine, New York 10016, NY, USA

[4]Department of Biomedical Sciences, University of Minnesota Medical School, Duluth, MN 55812, USA

[5]Center for Cerebellar Network Structure and Function in Health and Disease, University of Minnesota, Duluth, MN 55812, USA

[6]Center for Neurogenetics, Brain and Mind Research Institute, Weill Cornell Medicine, New York 10021, NY 10021, USA

[7]Pediatric Neurology, Department of Pediatrics, Weill Cornell Medicine, New York 10021, NY, USA

[8]Weill Cornell Autism Research Program, Weill Cornell Medicine, New York 10021, NY, USA

[9]Biochemistry, Cell and Molecular Biology Program, Weill Cornell Graduate School of Medical Sciences, New York 10021, NY, USA

[10]Present Address: Center for Neurotechnology in Mental Health Research, Department of Biomedical Engineering, The Pennsylvania State University, University Park, PA 16801, USA

[11]Present address: Center for Substance Abuse Research, Lewis Katz School of Medicine, Temple University, Philadelphia, PA 19140, USA and Department of Neural Sciences, Lewis Katz School of Medicine, Temple University, Philadelphia, PA 19140, USA

*Correspondence to:

Alexandra L. Joyner

Developmental Biology Program

Sloan Kettering Institute

1275 York Avenue, Box 511

New York, NY 10065, USA

Office: 212-639-3962

Email: joynera@mskcc.org

**Abstract**

The capacity of the brain to compensate for insults during development depends on the type of cell loss, whereas the consequences of genetic mutations in the same neurons are difficult to predict. We reveal powerful compensation from outside the cerebellum when the excitatory cerebellar output neurons are ablated embryonically and demonstrate that the minimum requirement for these neurons is for motor coordination and not learning and social behaviors. In contrast, loss of the homeobox transcription factors Engrailed1/2 (EN1/2) in the cerebellar excitatory lineage leads to additional deficits in adult learning and spatial working memory, despite half of the excitatory output neurons being intact. Diffusion MRI indicates increased thalamo-cortico-striatal connectivity in *En1/2* mutants, showing that the remaining excitatory neurons lacking *En1/2* exert adverse effects on extracerebellar circuits regulating motor learning and select non-motor behaviors. Thus, an absence of cerebellar output neurons is less disruptive than having cerebellar genetic mutations.

## Introduction

The brain has a large capacity to compensate for neuronal loss due to injury when it occurs during development but not in adulthood. In contrast, germline mutations in genes that regulate neural development that result in hypoplasia can have deficits that range from minor to devastating. It is particularly important to understand the causes of behavior deficits in the context of pediatric cerebellar defects, as the degree of recovery of cerebellar function seems to be differentially influenced by the location and extent of insult or the type of genetic mutation[1,2,3,4,5]. As the cerebellum is a complex folded structure housing the majority of the neurons in the brain[6,7] and many lobules in the cerebellum share functions with another lobule that converges onto similar downstream forebrain targets[8], the cerebellum is an important structure to study developmental compensation.

The communication between the cerebellum and the rest of the brain is through the downstream cerebellar nuclei (CN) and they contribute to a wide range of motor and non-motor functions[9,10,11,12]. The CN comprise three bilaterally symmetrical nuclei and form a topographic circuit between their presynaptic Purkinje cells (PCs) based on their spatial position within lobules and along the mediolateral axis of the cerebellar cortex[13,14,15,16,17,18,19]. The circuit functions of subregions of the CN have begun to be defined in adult animals by mapping their projections and transiently inhibiting neural activity using targeted viral injections or neuronal ablation[9,10,11,12]. In addition, many studies have manipulated specific lobules in the cerebellar cortex and inferred which CN are involved in regulating motor coordination, motor learning and/or non-motor behaviors based on circuit topography. An additional consideration for ablation studies is that during development, the excitatory neurons of the CN (eCN) play a pivotal role in supporting the survival of PCs which in turn ensure the proper expansion of other cell types in the cerebellar cortex through secretion of Sonic hedgehog[18,20,21]. Thus, growth of each lobule is dependent on

the eCN targets of their PCs, and removing a subset of eCN embryonically will impact the development of both their downstream forebrain targets and presynaptic PCs and their local microcircuit. Given the crucial role eCN play in generation and circuit function of the cerebellum, it is important to develop tools to enable manipulations of the same eCN during development and in the adult to define the cerebellar-associated behaviors dependent on the neurons and uncover possible developmental compensation.

We used the medial eCN as a test case for comparing the necessity of a CN subregion during development versus in adulthood. We then determined the baseline requirement for having all eCN intact during development and compare the behavior deficits to mouse mutants lacking developmental genes in the eCN. We identified a *Cre* transgene that targets the medial eCN from embryogenesis onwards. Using this tool we demonstrate that while in adult mice medial eCN activity is required for reversal learning, the brain can compensate for embryonic loss of these neurons alleviating the behavioral deficit. Surprisingly, we find that when all eCN are killed in the embryo there is only a selective impairment in motor coordination behaviors. In contrast, genetic loss of the engrailed (EN1/2*)* developmental transcription factors in all eCN results in additional deficits in motor learning, acquisition/reversal learning, and spatial working memory, despite only half the eCN dying embryonically. Circuit mapping and diffusion MRI (dMRI) provide evidence for aberrant thalamo-cortical-striatal connectivity as a result of aberrant eCN development.

## Results

### *SepW1-Cre* targets the excitatory neurons in the medial cerebellar nucleus

We chose the medial CN as a region to compare adult inhibition and embryonic ablation of a CN subregion as it can be divided into 4-5 subregions based on transcriptomic profiling and circuit mapping[14,22]. We screened transgenic databases (Gene Expression Nervous System Atlas and

Allen Brain Atlas Transgenic Characterization) for a *Cre* driver that within the CN selectively targets the medial eCN. *SepW1*-Cre, a Selenow BAC construct[23], was found to mediate Cre recombination only in the medial eCN. Immunostaining of cerebellar sections from *SepW1-Cre* mice carrying a Cre-dependent nuclear tdTomato reporter[24] (*SepW1-Cre; Ai75D*) revealed that within the eCN 92.6% of all tdTomato+ cells are in the medial CN (**Fig. 1a-f**). Moreover, within the medial CN, 100% of tdTomato+ neurons expressed the eCN marker MEIS2+, and 8% of MEIS2+ neurons were not tdTomato+ (**Fig. 1f**). Approximately 50% of NeuN+ GCs in the internal granule cell layer (IGL) also expressed tdTomato (**Supplementary Fig. 1a,b**), as well as all TBR2+ unipolar brush cells (UBCs) (**Supplementary Fig. 1a,c** and ref[25]). Outside the cerebellum, tdTomato+ labeling was restricted to the vestibular nucleus, cerebral cortex, hippocampus, a subpopulation of hypothalamic nuclei and the nucleus of Darkschewitsch (see also Allen Brain Atlas Experiment ID: 488246361). Thus, among the CN neurons, the *SepW1-Cre* transgene selectively labels the eCN of the medial CN. Importantly, Cre is expressed in adult medial eCN, allowing targeting of subpopulations of the neurons in adult mice using viral injections (see below).

**Acute inhibition of the adult posterior medial eCN impairs reversal learning and not motor behaviors**

Leveraging *SepW1-Cre* mice, we tested the contribution of the posterior region of the medial eCN (MedP eCN) to adult cerebellar-associated motor coordination, learning and non-motor behaviors. Projections to the MedP CN[14,18,26] that are preferentially from vermis lobules 6-8 have been shown to contribute to cognitive flexibility, anxiolytic and stereotyped/repetitive behaviors[16,27,28], whereas projections to the anterior medial CN (MedA), which originate from lobules 1-5[17,18], are associated with motor functions[17,29]. We therefore tested whether acute chemogenetic inhibition of the adult MedP eCN would impair cognitive flexibility without affecting motor functions. A Cre-dependent inhibitory (hM4Di) Gi-DREADD (*AAV2-hSyn-DIO-hM4Di-mCherry*; MedP-hM4Di mice) or control vector (*AAV2-hSyn-DIO-mCherry*; Control mice) was injected bilaterally into the MedP CN of

*SepW1-Cre/+* littermates of both sexes (**Fig. 1g**). mCherry and hM4Di-mCherry expression was confirmed to be limited to the MedP (**Fig. 1i** and **Supplementary Fig. 2a,b**) and we observed the expected mCherry+ axon terminals in downstream motor and non-motor thalamic nuclei including mediodorsal (MD), centrolateral (CL), ventromedial (VM) and parafascicular (PF) thalamus (**Fig. 1h**).

The MedP eCN were acutely inhibited during a battery of motor and non-motor behaviors by injecting clozapine N-oxide (CNO, 5 mg/kg) 30 minutes before each behavioral test (**Fig. 1j**). Motor coordination and balance were tested using the footprint assay and revealed no differences in MedP-hM4Di mice compared to littermate controls injected with CNO (**Fig. 1k**). The open field assay also showed no differences in total distance travelled (**Fig. 1l** and **Supplementary Fig. 2c**) and average velocity (**Supplementary Fig. 2d**). Motor performance and learning using an accelerating rotarod test and forelimb grip strength also revealed no differences (**Fig. 1m,n** and **Supplementary Fig. 2e**). In contrast, when we tested acquisition and reversal learning as a readout of cognitive flexibility using a water Y-maze (WYM) test, we found that MedP-hM4Di mice showed normal acquisition learning for finding the submerged escape platform location, but had significantly impaired reversal learning for a new platform location compared to controls (**Fig. 1o**). As a test for spatial working memory, spontaneous alternations in a Y-maze revealed no differences between groups (**Fig. 1p**). Although the MedP-hM4Di mice showed lower total distance travelled (**Supplementary Fig. 2f**) in the Y-maze after CNO administration, the total number of entries (**Supplementary Fig. 2g**) were comparable to control mice. Altogether, these results demonstrated that acute inhibition of the MedP eCN in adult mice selectively impairs reversal learning without having a major effect on motor functions.

**Generation of mice lacking the MedP eCN by conditional knockout of *En1/2***

To examine the impact of embryonic loss of MedP eCN on reversal learning we deleted *En1/2* in the medial eCN using *SepW1*-Cre which initiates recombination at embryonic day 14.5 (E14.5;

**Supplementary Fig. 3a-d**), since deletion of *En1/2* in all eCN leads to preferential death of the MedP and posterior interposed (IntP) eCN after E14.5[18]. We confirmed that 7-week-old *SepW1-En1/2* CKO mice of both sexes (*SepW1-Cre; En1$^{flox/flox}$; En2$^{flox/flox}$*) have a loss of medial eCN by quantifying large NeuN (100-600 um$^2$) neurons as a proxy for eCN[18]. As predicted, there was a preferential loss of eCN in the posterior medial CN, with little loss in the interposed and lateral CN compared to littermate control mice (*En1$^{flox/flox}$; En2$^{flox/flox}$*)(**Fig. 2a,b**). As recently show, the loss of medial eCN (MEIS2+ cells) was observed by E17.5 and primarily in the MedP region[25]. This was confirmed in 7-week-old *SepW1-Cre; Ai75D* and *SepW1-En1/2 CKO; Ai75D* mice, with complete loss of tdTomato+ MedP eCN and approximately half of the tdTomato+ MedA eCN remaining in the mutants (**Supplementary Fig. 3e**). The CN interneurons were also lost in the MedP region as the only NeuN+ cells remaining in the region were displaced mutant UBCs (**Supplementary Fig. 3e** and ref[25]).

Given that the eCN support the survival of their presynaptic Purkinje cells (PCs), which in turn support production of GCs and interneurons[18], we confirmed that growth of the cerebellum was reduced in the vermis of 6-week-old animals with proportional scaling down of GCs and interneurons to PCs. There was a significant reduction in the vermis (20.3%) and paravermis (10.1%) sagittal area, but not the hemispheres of *SepW1-En1/2* CKOs compared to littermate controls (**Fig. 2c,d**). In addition, the areas of the molecular layer (ML) and the IGL was primarily reduced in the vermis and their proportions were conserved relative to the total cerebellar area in mutants (**Fig. 2e,f**). The density of Calbindin+ PCs, parvalbumin+ molecular layer interneurons and NeuN+ GCs were also normal throughout the cerebellum (**Fig. 2g-l**). Thus, loss of MedP eCN leads to a preferential reduction of growth in the vermis maintaining the proportions of neurons.

**Mice lacking MedP eCN have normal reversal learning as well as motor behaviors**

We next evaluated *SepW1-En1/2* CKOs and their littermate controls of both sexes in the same behavioral assays as those used in the chemogenetic manipulations of *SepW1-Cre* mice (**Fig. 1**).

Adult *SepW1-En1/2* CKOs–showed a very small increase in sway length (**Fig. 3a**) with no difference in total distance travelled compared to littermate controls (**Fig. 3b** and **Supplementary Fig. 4a,b**). Additionally no deficits were observed in motor learning and performance between the genotypes (**Fig. 3c,d** and **Supplementary Fig. 4c**). Unlike MedP-hM4Di mice (**Fig. 1o**), *SepW1-En1/2* CKOs showed both normal acquisition and reversal learning compared to littermate controls (**Fig. 3e**). There were no genotype differences in spatial working memory (**Fig. 3f**), number of entries or distance travelled in the Y-maze (**Supplementary Fig. 4d,e**). Motor coordination was also normal in early postnatal pups, using a surface righting reflex assay at P7 (**Fig. 3g**) and negative geotaxis assay at P7 and P11 (**Fig. 3h**). Together, these results demonstrate that embryonic loss of the MedP eCN does not have a major impact on motor and non-motor functions.

**Generation of mice in which all embryonic eCN are ablated using Diphtheria toxin**

One plausible explanation for the absence of a reversal learning deficit in mice with embryonic loss of the medial eCN compared to adult inhibition of the same neurons could be the sufficiency of the remaining interposed and lateral CN in the *SepW1-En1/2* CKOs. We therefore used an intersectional pharmacognetic approach to selectively kill all embryonic eCN soon after they are born[30] as a means to determine the baseline requirement for eCN in a range of adult and neonatal behaviors. Mice were engineered to express Diphtheria toxin subunit A (DTA) in the developing eCN by combining an allele that expresses DTA only in cells that express both Cre and tTA (*Igs7*$^{DRAGON\text{-}DTA/+}$; *Atoh1-tTA/+*; *En1*$^{Cre/+}$ mice) and administering doxycycline from E13.5 onwards (*eCN-DTA* mice) (**Fig. 4a**). Since the intersection of Cre and tTA expression is in immature eCN and granule cell precursors (GCPs), by administering doxycycline after E13.5 cell killing is limited to the eCN[18]. Immunostaining of sagittal sections at E17.5 revealed that 97.6% of the MEIS2+ eCN were missing in *eCN-DTA* mice compared to littermate controls (*Igs7*$^{DRAGON\text{-}DTA}$ mice with *Atoh1-tTA* or *En1*$^{Cre}$ or neither transgene and fed doxycycline)(36±6.8 cells per mutant vs

1529±95.3 per control) (**Fig. 4b,c**). Quantification of NeuN+ cells in the CN of 7-week-old mice demonstrated a major loss of large CN neurons (100-600 $um^2$) in the *eCN-DTA* mice (**Fig. 4d**). RNA *in situ* hybridization analysis confirmed the loss was mainly due to glutamatergic (*Slc17a6*) eCN (**Fig. 4e**). RNAScope triple RNA hybridization analysis (n=3 per genotype) revealed that the rare *Slc17a6*-expressing cells in *eCN-DTA* mice also expressed *Slc32a1* (GABAergic) and *Slc6a5* (glycinergic) markers and were located preferentially in the MedA CN. Furthermore, similar numbers of such triple positive cells were present in controls (**Fig. 4f** and **Supplementary Fig. 5a,b**). In the medial CN both the eCN and interneurons were absent in *eCN-DTA* mice, similar to in *SepW1-En1/2* CKOs. We found that the remaining triple positive NeuN+ cells in the MedA CN were not targeted by the *Atoh1-tTA* transgene (**Supplementary Fig. 5c**), despite being targeted with *Atoh1-Cre* (**Supplementary Fig. 5d** and see refs[18,22]). Therefore, all remaining NeuN+ cells in the *eCN-DTA* mice are GABAergic (*Slc32a1+*) inhibitory CN neurons or triple glutamate-GABA-glycine+ neurons.

We next examined the size and number of neurons in the cerebellar lobules. As expected, cerebellar size and neuron numbers were reduced across the entire mediolateral axis in *eCN-DTA* mice compared to littermate controls while the proportions and densities of each cell type were maintained (**Fig. 4h-p**) As triple neurotransmitter positive eCN remain in the MedA, we examined the growth of the vermis lobules that preferentially target the MedA. The anterior vermis lobules (1-5) showed a significant reduction in area, but the magnitude was smaller than the reduction in the central vermis (lobules 6-8) (**Supplementary Fig. 6**). The posterior vermis (lobules 9 and 10) was not significantly reduced (**Supplementary Fig. 6**), consistent with the PCs projecting outside the cerebellum to the vestibular nuclei[31,32]. Thus, pharmacogenetic killing of the developing eCN in *eCN-DTA* mice leads to loss of all *Slc17a6* single neurotransmitter positive eCN and reduced cerebellar size with proportional scaling down of cell numbers throughout the cerebellum.

**Loss of all eCN impairs motor coordination, but not motor learning and non-motor behaviors.**

We repeated the same battery of behaviors in *eCN-DTA* mice of both sexes as in *SepW1-En1/2* CKOs (**Fig. 3**). *eCN-DTA* mice of both sexes had motor coordination deficits in negative geotaxis at P7 and P11 and righting reflex at P7 (**Fig. 5a,b**). Motor coordination continued to be abnormal in adult *eCN-DTA* mice as they had a significant decrease in stride and increase in sway length (**Fig. 5c**) and significantly reduced total distance travelled compared to littermate controls (**Fig. 5d** and **Supplementary Fig. 7a**), but with no difference in average velocity (**Supplementary Fig. 7b**). Interestingly, *eCN-DTA* mice showed normal motor learning (**Fig. 5e,f** and **Supplementary Fig. 7c**). *eCN-DTA* mice showed normal reversal learning, although there was a main effect of geneotype in the WYM (**Fig. 5g**) with no change in swim speed (**Supplementary Fig. 7d**). Moreover, there was no genotype difference in spatial working memory (**Fig. 5h,i**), although the total distance travelled and number of arm entries were decreased in the Y-maze (**Supplementary Fig. 7e-h**).

Since all eCN die in the embryo we tested additional cerebellar-associated non-motor behaviors[9,11,12]. In a more challenging spatial working memory test (plus-maze), *eCN-DTA* mice showed no deficits (**Fig. 5i**), although the total distance travelled and number of arm entries were decreased (**Supplementary Fig. 7g,h**). Compared to littermate controls *eCN-DTA* mice showed no difference in social preference after normalizing for hypolocomotion (three-chambered social approach assay[33,34]; **Fig. 5j** and **Supplementary Fig. 7i,j**). We also did not find a genotype difference in anxiety-like behavior (elevated plus maze) when normalizing for hypolocomotion (**Fig. 5k** and **Supplementary Fig. 7k**,**l**). Finally, we did not find a genotype difference in total time spent self-grooming (**Fig. 5l**). Altogether, the behavior analyses reveal that *eCN-DTA* mice, lacking nearly all eCN, exhibit early motor coordination deficits that persist into adulthood, but motor learning, cognitive, social, and anxiety-like behaviors are largely intact.

**Loss of *En1/2* in all eCN impairs motor coordination and learning, cognitive flexibility, and spatial working memory**

Given a previous report that adult mice lacking excitatory activity in all eCN (*Atoh1-Slc17a6* CKO)[5] have motor learning deficits that we did not observe following loss of all eCN (*eCN-DTA* mice), we were prompted to analyze in more detail the behavior of a previously generated *En1/2* conditional knockout mice (*Atoh1-En1/2* CKOs) that has motor learning deficits[18]. In *Atoh1-En1/2* CKOs all eCN and GCs lack *En1/2* and the mice have an overall ~50% loss of eCN during embryogenesis that includes a complete loss in the MedP and IntP eCN (**Supplementary Fig. 8a-e** and ref[18]). Further characterization revealed that similar to *SepW1-En1/2* CKOs (**Supplementary Fig. 3e**) there was a significant loss of local interneurons, especially in the MedP and IntP where all neurons are missing (**Supplementary Fig. 8b**).

*Atoh1-En1/2* CKO mice of both sexes had motor coordination deficits in negative geotaxis at P7 and P11 compared to littermate controls (**Fig. 6a**), but no genotype difference in righting reflex at P7 (**Fig. 6b**). Replicating our previous findings[18], adult *Atoh1-En1/2* CKOs of both sexes had motor coordination (**Fig. 6c**) and motor learning deficits (**Fig. 6e** and **Supplementary Fig. 9c)** and reduced total distance travelled (**Fig. 6d** and **Supplementary Fig. 9a**) and slower velocity (**Supplementary Fig. 9b**) compared to littermate controls. Forelimb grip strength was normal (**Fig. 6f**). Thus, *Atoh1-En1/2* CKOs have motor coordination deficits detected by P7 that persist into adulthood and adult motor learning deficits.

In terms of non-motor behaviors, *Atoh1-En1/2* CKOs showed both acquisition (day 1) and reversal learning deficits in the WYM compared to littermate controls (**Fig. 6g**), which was not due to a difference in swim speed (**Supplementary Fig. 9d**). There was no genotype difference in spatial working memory (**Fig. 6h**) despite reduced total distance travelled and arm entries (**Supplementary Fig. 9e,f**). However *Atoh1-En1/2* CKOs showed impaired spatial working memory in the plus-maze (**Fig. 6i**) with no difference in total distance travelled or arm entries (**Supplementary Fig. 9g,h**). *Atoh1-En1/2* CKOs showed no difference in social preference when

normalizing for hypolocomotion compared to littermate control mice (**Fig. 6j** and **Supplementary Fig. 9i**,**j**). Also, genotype differences were not found in anxiety-like behavior (**Fig. 6k** and **Supplementary Fig. 9k**,**l**) and self-grooming (**Fig. 6l**). Thus, *Atoh1-En1/2* CKOs have impaired adult motor learning, acquisition/reversal learning and spatial working memory, in addition to the motor coordination deficits as seen in *eCN-DTA* mice.

### ***Atoh1-En1/2* CKOs have reduced but not ectopic cerebellothalamic projections**

One possible explanation for the differing behavioral outcomes in *Atoh1-En1/2* CKOs compared to *eCN-DTA* mice is that the remaining eCN in *Atoh1-En1/2* CKOs exhibit aberrant projections to the thalamus, a primary target region involved in behaviors studied. To address this question, we mapped the projections to the thalamus of the remaining eCN in adult *Atoh1-En1/2* CKO and littermate controls. We first examined whether the remaining MedA and IntA CN make ectopic projections by injecting an *AAV2-hSyn-mCherry* virus or biotinylated dextran amine (BDA) into the MedA or IntA, respectively (n=3 per genotype; **Fig. 7a,d**). Given the reduced neuron number in the MedA and IntA CN, *Atoh1-En1/2* CKOs showed reduced mCherry+ or BDA+ axon terminals in all thalamic nuclei compared to littermate controls (**Fig. 7b,e**), but importantly no obvious ectopic projections were observed compared to littermate controls (**Fig. 7c,f**). We next performed retrograde tracing from the intralaminar thalamic nuclei (ILM), which regulate motor learning and cognitive flexibility[35,36,37,38]. ILM receive strong projections from the MedP, interposed and lateral CN, but not MedA[22], allowing us to examine whether inputs to ILM from the remaining MedA (and other nuclei) in *Atoh1-En1/2* CKOs are altered. We injected 10% Fluoro-Ruby preferentially into the centrolateral (CL) or parafascicular (PF) thalamus, two nuclei within the ILM, of adult *Atoh1-En1/2* CKOs and littermate controls (**Fig. 7g-i**). As expected, *Atoh1-En1/2* CKOs showed no Fluoro-Ruby+ cells in the region of the MedP and IntP CN. Furthermore, no significant differences in the total number of Fluoro-Ruby+ cells in the MedA, IntA, and lateral CN were detected compared to littermate controls for CL injections (**Fig. 7j**) and PF injections (**Fig. 7k**). Thus, *Atoh1-*

*En1/2* CKOs have reduced cerebellothalamic projections, but the remaining CN do not make ectopic projections.

**Diffusion MRI shows *Atoh1-En1/2* CKOs have connectivity changes outside the cerebellum that are distinct from *eCN-DTA* mice**

Since the remaining eCN circuits in *Atoh1-En1/2* CKOs appear intact, we used high resolution *ex vivo* dMRI[39,40] to examine whether there are alterations in regional volume, connectivity, and network properties outside of the cerebellum in adult *Atoh1-En1/2* CKO of both sexes as well as *eCN-DTA* mice for comparison. We first examined regional volume in 10 distinct brain regions (**Supplementary Fig. 10a**) and as expected a large reduction in the volume of the cerebellum was detected in *Atoh1-En1/2* CKO compared to littermate controls (**Fig. 8a**). No changes in regional volumes were seen except for a small but significant reduction in the midbrain (**Fig. 8b**), when normalizing for an overall smaller brain in mutants (**Supplementary Fig. 10b,c**). Network analysis using eight brain regions as nodes revealed a significant reduction in global efficiency and small-worldness in *Atoh1-En1/2* CKOs compared to controls (**Fig. 8c-e** and **Supplementary Fig. 10d-f**). Examining the number of streamlines between the thalamus and CN revealed the expected significant reduction in *Atoh1-En1/2* CKOs compared to controls (**Supplementary Fig. 10g**). We further examined the number of streamlines between the ILM and three of its primary downstream targets; the primary somatosensory cortex (SS), primary motor cortex (MO), and dorsal striatum (DS). Interestingly, we observed a significant increase in the number of streamlines in ILM-SS, ILM-MO, and ILM-DS circuits in *Atoh1-En1/2* CKOs compared to littermate controls (**Fig. 8f-h,k-m** and **Supplementary Fig. 10h-j**). Furthermore, the number of streamlines of the SS-DS and MO-DS circuits were significantly increased in *Atoh1-En1/2* CKOs compared to littermate controls (**Fig. 8i,j,n,o** and **Supplementary Fig. 10k,l**).

In *eCN-DTA* mice, in addition to the expected reduction in cerebellum volume (**Fig. 8p**), there was a small but significant increase in the cerebral cortex but no other changes in the rest

of the brain (**Fig. 8q**) when normalized to a smaller overall brain compared to littermate controls (**Supplementary Fig. 10m-o**). There was a significant decrease in global efficiency, but no changes in small-worldness in mutants (**Fig. 8r-t** and **Supplementary Fig. 10p,q**). Examining the number of streamlines between the thalamus and CN confirmed a significant reduction in *eCN-DTA* mice (**Supplementary Fig. 10r**). There were no genotype differences in the thalamo-cortico-striatal connectivity that were detected in *Atoh1-En1/2* CKOs (**Fig. 8u-y** and **Supplementary Fig. 10s-w**). Thus, unlike *eCN-DTA* mice, *Atoh1-En1/2* CKOs show extracerebellar changes involving an aberrant increase in connectivity of ILM-cortico-striatal circuits.

## Discussion

Our study applied a novel combination of cell-type-specific genetic manipulations, chemogenetics, dMRI and mouse behavior tests to uncover the requirements during development of the eCN as a whole or the MedP in regulating motor and non-motor functions. We revealed that the main requirement for the eCN if they are all removed in the embryo is for postnatal and adult motor coordination. Furthermore, leveraging an *En1/2* CKO model we demonstrate that seemingly intact eCN that lack critical developmental transcription factors can have major adverse effects on cerebellar and extracerebellar circuits regulating adult motor learning and non-motor behaviors.

We identified a genetic tool (*SepW1-Cre*) to manipulate the medial eCN from E14.5 onwards, adding to existing tools to manipulate all eCN or several subregions[38,41,42,43,44,45,46,47]. By comparing developmental loss (*SepW1-En1/2* CKOs) to adult inhibition of MedP eCN (MedP-hM4Di) we show the neurons are critical for adult reversal learning (WYM) but dispensable if they die embryonically. The MedP-hM4Di results are in line with impaired reversal learning after indirectly inhibiting[27] or directly activating[16,28] PCs that preferentially target the MedP eCN (lobule 6-8). Also, inhibition of the adult MedP eCN to ventrolateral periaqueductal gray[48] or MD[49] circuits impairs fear extinction, another form of cognitive flexibility. Interestingly, manipulation of other

regions like Crus I neurons that target the lateral CN also show reversal learning deficits[27,28]. Furthermore, inhibiting lobule 6 versus Crus I PCs differentially alters c-Fos staining of recruited forebrain regions during reversal learning[28], likely reflecting distinct downstream pathways[16,22,50]. Therefore, in *SepW1-En1/2* CKOs it is possible that the intact lateral eCN modify their activity to carry out normal reversal learning.

On the contrary, we discovered that when all eCN are ablated embryonically, adult *eCN-DTA* mice show normal reversal learning, indicating that reversal learning must be regulated by extracerebellar brain regions in these mutants. Indeed, regional specific manipulation of the intralaminar thalamus[36], dorsal striatum[51], and cerebral cortex[52] are sufficient to impair reversal learning. Therefore, one possibility is that during development the corticostriatal or thalamostriatal circuits are altered to confer reversal learning without cerebellar input. Similarly, extracerebellar circuits can modulate social preference[53], spatial working memory[54], anxiety-like[12,55], and stereotyped/repetitive[56] behaviors independent of the CN, which may explain why *eCN-DTA* mice can perform these behaviors.

As expected for a cerebellar-specific developmental perturbation, *eCN-DTA* mice show impaired neonatal and adult motor coordination[5,57,58,59,60]. However, unlike when all eCN activity is inhibited[5] motor learning is not impaired in *eCN-DTA* mice. In addition to the eCN[58], the GABAergic CN interneurons play a role in motor learning through their projections to the inferior olive[61]. Therefore, the remaining GABAergic CN interneurons in *eCN-DTA* mutants might contribute to motor learning, as well as extracerebellar circuits[62] providing compensation. Curiously, these possible sources for compensation in *eCN-DTA* mutants also are expected to apply to mice lacking neurotransmission in all adult eCN[5]. Since *Atoh1*$^{Cre}$ was used to generate *Atoh1-Slc17a6* CKO[5] mice rather than our intersectional approach that targets eCN, one possibility is that one or more of the cell types outside the cerebellum that express *Atoh1*$^{Cre}$[63] are responsible for the motor leaning deficits in adult *Atoh1-Slc17a6* CKO.

We found that although only ~50% of eCN are lost in *Atoh1-En1/2* CKOs, adult mutants exhibit impaired motor learning, acquisition/reversal learning, and spatial working memory, which is not seen in *eCN-DTA* mice. Of likely relevance, the remaining eCN in *Atoh1-En1/2* CKOs lack the EN1/2 transcription factors, key regulators of cerebellar development[18,64,65,66,67,68,69,70,71,72,73]. The behavioral deficits in *Atoh1-En1/2* CKOs compared to *eCN-DTA* mice provides direct evidence that dysfunctional eCN circuits due to genetic mutations can have worse outcomes than losing the neurons embryonically. We propose that in *Atoh1-En1/2* CKOs, the remaining eCN while targeting the correct thalamic nuclei are dysfunctional due to altered gene expression. In line with these conclusions, removal of the cerebellum or vermis neonatally in genetically dystonic rats[74,75] or *weaver* mutants[76,77] significantly rescues the adult motor coordination deficits seen in both mutants. Circuits that comprise the ILM-cortico-striatal circuitry have been implicated in motor learning[36,37,78], cognitive flexibility[37,79,80], and spatial working memory[81]. The excessive connectivity seen in *Atoh1-En1/2* CKOs using dMRI might thus be caused by the remaining *En1/2*-lacking eCN and contribute to their behavioral deficits.

In conclusion, our study highlights the importance of developing relevant models for directly comparing developmental versus adult loss of neurons and the contribution of dysfunctional neurons to understanding behavioral defects and possible compensation (**Supplementary Fig. 11**). Moreover, our findings offer the potential to be leveraged for the development of therapeutic avenues for patients with pediatric cerebellar injuries.

## Methods

**Animals**. All animal care and procedures were performed according to the Memorial Sloan Kettering Cancer Center and Weill Cornell Medicine Institutional Animal Care and Use Committee guidelines. Mice were kept in a 12-h/12-h light/dark cycle and in temperature- and humidity-controlled rooms and had *ad libitum* access to standard laboratory mouse chow and water. All transgenic mouse lines were maintained on a mixed genetic background containing 129, C57BL/6J, and Swiss Webster. For behavior analysis, males and females were analyzed separately, but as there were no sex differences all final analyses combined the two sexes. Estrous cycle was not evaluated for females. The following mouse lines were used in the study: *Atoh1-Cre* (JAX #011104)[82], *tetO-Cre* (JAX #006234)[83], *R26*$^{LSL\text{-}nls\text{-}tdTomato}$ (Ai75D, JAX #025106)[24], 129S1/SvImJ (JAX #002448), Swiss Webster mice (Taconic Biosciences catalog #SW), *En1*$^{flox}$ (JAX #007918)[71], *En2*$^{flox}$ (JAX #008872)[64], *Atoh1-tTA*[18], *En1*$^{Cre}$ (JAX #007916)[84], *lgs7*$^{TRE\text{-}lox\text{-}tdTomato\text{-}STOP\text{-}lox\text{-}DTA*G128D}$ (or *lgs7*$^{DRAGON\text{-}DTA}$, JAX #034778)[30], and *SepW1-Cre* (MMRRC #036190-UCD)[23]. Details of all mouse strains used in the study are listed in **Table 1** and primers used for genotyping are listed in **Table 2**.

Embryonic ablation of excitatory cerebellar nuclei (eCN) was achieved by crossing *Atoh1-tTA/+; En1*$^{Cre/+}$ mice with *lgs7*$^{DRAGON\text{-}DTA/DRAGON\text{-}DTA}$ mice to generate *Atoh1-tTA/+; En1*$^{Cre/+}$; *lgs7*$^{DRAGON\text{-}DTA/+}$ mice (*eCN-DTA*). Noon of the day that a vaginal plug was discovered was designated as embryonic day 0.5 (E0.5). Doxycycline hyclate (Sigma D9891) was diluted in drinking water (0.02 mg/mL) and provided at E13.5 (when neurogenesis of eCN is complete) until postnatal day 28 (P28) for behavioral studies or otherwise until the end of the experiment and replaced with fresh doxycycline every 3-4 days. To determine if the *Atoh1-tTA* transgene targets the *Slc6a5*-expressing anterior medial eCN, *Atoh1-tTA/+; tetO-Cre/+; R26*$^{LSL\text{-}nls\text{-}tdTomato/+}$ mice were generated and administered doxycycline from E13.5 onwards. *Atoh1-En1/2* CKOs and *Atoh1-En1/2* CKO; *Ai75D* mice were generated by crossing *Atoh1-Cre/+; En1*$^{flox/flox}$*; En2*$^{flox/flox}$ males with *En1*$^{flox/flox}$*; En2*$^{flox/flox}$ or *En1*$^{flox/flox}$*; En2*$^{flox/flox}$*; R26*$^{LSL\text{-}nls\text{-}tdTomato/LSL\text{-}nls\text{-}tdTomato}$ females, respectively.

Non-littermate control *Atoh1-Cre; Ai75D* mice were generated by crossing *Atoh1-Cre/+* males with *R26*$^{LSL\text{-}nls\text{-}tdTomato/LSL\text{-}nls\text{-}tdTomato}$ females. *SepW1-En1/2* CKO and *SepW1-En1/2* CKO; *Ai75D* mice were similarly generated. *SepW1-Cre; Ai75D* mice were generated by crossing *SepW1-Cre/+* or *SepW1-Cre/Cre* males with *R26*$^{LSL\text{-}nls\text{-}tdTomato/LSL\text{-}nls\text{-}tdTomato}$ females. For all experiments and analyses, investigators were blinded to the genotypes and experimental conditions.

**Behavioral assays.** All adult behavioral tests were conducted in a behavioral suite at Weill Cornell Medicine (WCM) and early postnatal behavioral tests were conducted in an animal room at Memorial Sloan Kettering Cancer Center (MSKCC). Six-week-old mice were transferred from MSKCC to WCM two weeks prior to the start of the first behavioral test. Adult mice were acclimated to the animal suite for 1 hour the day before testing. Before conducting each behavioral test, mice were brought to the behavioral suite and left undisturbed for at least 1 hour before testing. The order of each behavior test and age of animals (in brackets) for *eCN-DTA* and *Atoh1-En1/2* CKO mice (and their littermate controls) was as follows: basal locomotor activity[33] (6 weeks), three-chambered social approach[33,34] (7 weeks), elevated plus maze[33] (8 weeks), self-grooming[27] (9 weeks), accelerating rotarod[18], grip strength[18] and footprint assay[18] (11 weeks), spontaneous alternation in dry Y-maze[33,85] (12 weeks), water Y-maze[16,59,86] (13 weeks). Plus-maze[87] was tested with different groups of mice at 15 weeks (see details below). MedP-hM4Di mice (and control) and *SepW1-En1/2* CKOs (and their littermate controls) followed the same order and age of animals as *eCN-DTA* and *Atoh1-En1/2* CKOs, but were only tested for basal locomotor activity, accelerating rotarod, grip strength, footprint assay, spontaneous alternation, and water Y-maze. For *SepW1-En1/2* CKO, *Atoh1-En1/2* CKO, and *eCN-DTA* mice, negative geotaxis[88] (at P7 and P11) and surface righting reflex[88] (P7) were tested. For MedP-hM4Di and control mice, clozapine N-oxide dissolved in 0.9% saline (5 mg/kg, CNO, Enzo Life Sciences) was injected intraperitoneally 30 minutes before the start of each behavioral testing. For accelerating rotarod and water Y-maze, CNO was injected every day of behavioral testing. All behavioral experiments

were recorded with a Logitech C920 HD Pro Webcam (30 fps) and analyzed with ANY-maze (Stoelting Co) or hand scored using BORIS software[89].

*Negative geotaxis*. Mice were tested for negative geotaxis reflex at P7 and P11 as previously described[88]. Mice were placed head down on a negative incline (-35°) platform that was covered with a sterile poly-lined drape. Time until mice turned 180° in either direction was measured using a stopwatch. The test was suspended if mice did not turn within 60 seconds (s) or fell down the slope (considered failed trials). Failed trials were assigned a 60 s latency. All mice were tested three trials per test day.

*Surface righting reflex*. Mice were tested for surface righting reflex at P7 as previously described[88]. Mice were placed in the supine position on a flat surface with a sterile poly-lined drape. The time taken for each mouse to turn onto their four paws was measured. All mice were tested for three trials per test day.

*Basal locomotor activity.* Mice were placed in a polycarbonate test chamber (27.3 cm x 27.3 cm) equipped with three infrared beam arrays. Horizontal locomotor activity was monitored by computer-assisted activity monitoring software (Med Associates). For each test session, animals were placed in the chamber and recorded for 1 hour without interruption with no incandescent lighting[33]. Locomotor activity was measured as total distance traveled in centimeters.

*Three-chamber social approach.* Mice were tested with a modified version of the three-chamber social approach and social novelty assays as described previously[33,34]. All testing was conducted in the three-chamber apparatus (Ugo Basile sociability apparatus, Stoelting Co) in a room with 30 lux lighting at the center of each chamber (1~2 lux difference across chambers) and a ceiling-

mounted camera for ANY-maze tracking. Two days before testing, age- and sex-matched 129S1/SvImJ mice were habituated to the wire cup (see ref[34] for details). After 1-hour habituation to the testing room, two 129S1/SvImJ mice were placed individually under a wire cup (3.8 cm bottom diameter, rust-proof/rust-resistant, noncorrosive, steel wire pencil cups) in the left or right chamber of the apparatus. The entrance to each chamber was blocked. 129S1/SvImJ mice were observed for 10 min for behaviors that are potentially disruptive, such as bar-biting, excessive self-grooming, circling, or clinging to the side bars with all four paws. Only 129S1/SvImJ mice showing docile behavior were used as novel mice in the social approach and novelty testing.

On the day of testing, mutant or control mice were placed in the center of an empty apparatus to freely explore all three chambers for 10 min. During the 10 min habituation, empty wire cups were placed in both left and right chamber. Mice were briefly taken out of the apparatus and a novel object (orange rectangle block) and a novel mouse were placed under each wire cup. The location of the novel mouse was randomly assigned across each subject mouse. Test mice were placed back into the center chamber and allowed to freely explore for 5 min. Test mice were kept in a separate cage until all animals from its original home cage were tested. Time spent in each chamber and time spent in the contact zone (nose within a 2 cm radius around the wire cups) were calculated by automated detection.

*Elevated plus maze.* Mice were placed in the center of an elevated plus maze (L x W x H = 50 cm x 5 cm x 50 cm and 38 cm above the floor) for 10 min with 15 lux lighting in the open arms and 5 lux lighting in the closed arms[33]. A ceiling-mounted camera for ANY-maze tracking was used to measure time spent in and entries into each arm.

*Self-grooming.* Mice were placed in a clean cage for 10 min to habituate to the test arena with 25-30 lux lighting[27]. After habituation, mouse activity was recorded for 10 min. Time spent grooming was hand scored by an experimenter blind to the genotype.

*Accelerating rotarod and grip strength.* Mice were tested using an accelerating rotarod protocol as previously described[18] with 30 lux lighting. Mice were put on a rotarod (47650, Ugo Basile) rotating at 10 rpm until all mice (3~5 mice tested simultaneously) were facing forward for at least 5 s. The rod was then accelerated from 10 rpm to 40 rpm over 5 min. Mice were tested for 3 trials per day across 3 consecutive days. Animals rested for 10 min in their home cage between each trial. Latency to fall (seconds) was recorded for each animal. If a subject mouse held onto the rod and rotated 3 consecutive times, the latency at which the mouse first started to rotate with the rod was recorded as the latency to fall and the mouse was returned to their home cage. If a subject mouse repeatedly fell within 10-15 s after the start of each trial, the mouse was excluded from the final analysis. If mice did not fall throughout the entire trial, 300 s was assigned as latency to fall. The following day after the accelerating rotarod test, forelimb grip strength was measured using a horizontal grip bar (1027SM Grip Strength meter with single sensor, Columbus Instruments). Mice were allowed to hold the triangle grip bar while being gently pulled away by the base of their tail with their body parallel to the bench. The average of 5 measurements was normalized to the mouse's body weight (force/gram). Animals rested 5 min in their home cage between each measurement.

*Footprint assay.* Mice were tested using a footprint assay as previously described with 30 lux lighting[18]. After forepaws and hindpaws were painted with different nontoxic acrylic paint colors (red/blue or orange/purple, Crayola), mice were allowed to walk through a plexiglass tunnel (L x W x H = 50 cm x 10 cm x 15 cm) lined with a strip of paper. A dark box was placed at the end of the plexiglass tunnel. Each mouse was tested three times, and three gait parameters (stride, sway, and stance) were measured from each run and averaged.

*Y-maze.* Mice were tested using a Y-shaped maze with equal length arms (L x W x H = 33.0 cm x 7.6 cm x 38.1 cm) as described previously[33,85] with 20 lux lighting at the bottom of the center of the arena. Mice were placed in the center of the arena and allowed to freely explore the arena for 5 min. A ceiling-mounted camera for ANY-maze tracking was used to record the distance travelled in the maze. The sequence of arm entries and number of entries to each arm was manually scored. The percentage of spontaneous alternation was calculated as previous described[33,85].

*Water Y-maze.* Mice were tested using an adapted version of the water Y-maze test as described previously[16,59,86] with no incandescent lighting (red light for experimenter). The same Y-shape maze used in the dry Y-maze test above was filled with room temperature water colored with non-toxic white paint to be opaque. After dry Y-maze testing and ~1 week prior to testing, mice were placed at the base of one of the Y-maze arms (filled with paint but no hidden platform) and allowed to freely swim for 3 minutes. Average velocity was measured using ANY-maze tracking software. On day 1, mice were placed in the base of one arm of the Y-maze and allowed to swim for 60 s without a platform present to further habituate the mice to the arena. On the next three days (2-4), a white platform was submerged about 1 cm below the surface of the water at the end of one of the arms of the Y-maze. The location of the platform was randomly assigned to either the left or right arm relative to the starting arm (base arm). Mice were placed in the base of the Y-maze and latency to find the platform was recorded. The number of correct trials were recorded only when the first arm entered was the arm with the platform and the mouse found the platform without entering another arm. Once the mouse found the platform, the mouse was allowed to sit on it for 15 s and removed from the Y-maze and placed under a heat lamp in an empty cage. If the mouse did not find the platform within 35 s, it was placed onto the platform for 20 s. All mice were run for the same trial before repeating the process for all 15 trials. On average 10-15 mice were run during one session. This procedure was repeated with each animal for 15 trials per day for 3 consecutive days. For days 5-7, the location of the platform was switched to the opposite arm

557 from which the mouse was initially trained on days 2-4. The same procedure as days 2-4 were
558 repeated. Each day, at the end of the set of 15 trials, the mouse was toweled dry and placed
559 under a heat lamp for 5 min before returning to its home cage. The correct choices (when the first
560 arm entered was the correct arm and the mouse found the platform) and latency to find platform
561 were hand scored using a stopwatch during each trial.
562
563 *Plus-maze.* Mice were tested using a plus-shape maze with equal length arms (L x W x H = 30.48
564 x 5.08 x 15.24 cm) as described previously[87] with incandescent lighting. Mice were placed in one
565 arm of the maze designated the base of the arena and allowed to freely explore the arena for 12
566 min each day for a total of 4 days (day 1 was considered habituation to the arena). A ceiling-
567 mounted camera for ANY-maze tracking was used to record the distance travelled in the maze.
568 The sequence of arm entries and number of entries into each arm was scored using a custom
569 MATLAB script. The percentage spontaneous alternation was calculated as previous described[87]
570 and the last 3 days of the behavioral testing was averaged for final analysis. As previously
571 described, the estimated chance level performance for the plus maze test is 22.2% spontaneous
572 alternations[87]. For *Atoh1-En1/2* CKOs, mice were tested in two different locations: Weill Cornell
573 Medicine (New York, NY) and University of Tennessee Health Science Center (Memphis, TN).
574 Data from both institutions were pooled as the results were consistent. For *eCN-DTA* mice, all
575 mice were tested at Weill Cornell Medicine (New York, NY).
576
577 **Stereotaxic Injections**. Mice were anesthetized with 2.5% isoflurane and 80% $O_2$ and head-fixed
578 in a stereotaxic frame (David Kopf Instruments, Tujunga, CA) equipped with digital manipulator
579 arms (Stoelting Co, Wood Dale, IL). A nose cone was used to deliver isoflurane to maintain
580 anesthesia. Mice were given a subcutaneous injection of meloxicam (2 mg/kg) and 0.1 mL of 0.25%
581 Marcaine around the incision site. After exposing the skill, craniotomies were made with an
582 electric drill (Stoelting CO, Wood Dale, IL) with a ball bur attached. A Neuros 7000 series 1 µL

583 Hamilton syringe with a 33-gauge needle (Reno, NV) connected to a remote automated
584 microinfusion pump (KD Scientific, Holliston, MA) was used for delivery of tracers or viral
585 constructs at a rate of 100 or 50 nL/min, respectively. Details of dye, viruses, and stereotaxic
586 coordinates are provided in **Table 3**. Following infusion, the needle was left in place for 5 min and
587 then slowly manually retracted. Mice were placed on a heat pad for at least 30 min post-surgery
588 before being returned to their home cage. Mice were monitored for three days post-surgery to
589 ensure recovery. Brains were collected and imaged (see below) to confirm viral expression and
590 injection placements and no misplacements were found.
591
592 **Tissue preparation**. For all histological analyses, mice were anesthetized with isoflurane and
593 then perfused transcardially with room temperature (RT) phosphate buffered saline (PBS) with
594 heparin (0.02 mg/mL) and then ice-cold 4% paraformaldehyde (PFA, Electron Microscopy
595 Sciences, catalog no: 15714). Brains were dissected and post-fixed in 4% PFA overnight at 4°C
596 and cryopreserved in 30% sucrose in PBS for ~2 days at 4°C. Brains were embedded in Tissue-
597 Tek OCT compound (Sakura Finetek). Coronal serial cryosectioning was performed at either 40
598 um (6 series) or 100 um (3 series) and collected in 0.01M phosphate buffer (PB) with 0.02%
599 sodium azide and kept at 4°C until further processing. For long-term storage, sections were
600 transferred to 24-well plates with cryoprotectant (30% sucrose and 30% ethylene glycol in 0.1M
601 PB) and stored at -20°C. Sagittal serial cryosectioning was performed at either 14 um (10 series)
602 or 30 um (6 series) and collected on charged glass slides (Fisherbrand ColorFrost Plus) and
603 stored at -20°C until further processing. Details of reagents are listed in **Table 1**.
604 For single molecular fluorescence *in situ* hybridization, tissue was prepared as previously
605 described[90]. Mice were anesthetized with isoflurane and then perfused transcardially with RT 0.9%
606 saline with 10 units/mL heparin (Sigma Aldrich, H3393-50KU) followed by RT 4% PFA in 0.2M
607 phosphate buffer (PB). Brains were dissected and post-fixed in the same fixative overnight at RT.

608 Brains were cryopreserved by incubating in 15% sucrose in 0.2M PB overnight followed by an
609 overnight incubation in 30% sucrose in 0.2M PB. Brains were embedded in Tissue-Tek OCT
610 compound and stored at -80°C until further processing. Coronal serial cryosectioning was
611 performed at 30 um and sections were stored in cryoprotectant solution at -20°C until further
612 processing. Details of reagents are listed in **Table 1**.
613
614 **Hematoxylin and eosin (H&E) staining.** All reagents for H&E staining were obtained from
615 Richard-Allan Scientific: hematoxylin 2 solution (catalog no: 7231), eosin-Y (catalog no: 7111),
616 bluing reagent (catalog no: 7301), clarifier 2 (catalog no: 7402). Slides were first washed in PBS
617 for 5 min and incubated in hematoxylin 2 solution for 3 min. Slides were rinsed in deionized water
618 (di$H_2O$) and immersed in staining reagents for 1 min each (di$H_2O$, bluing reagent, di$H_2O$, clarifier
619 2, di$H_2O$). After dehydration and defatting (d$H_2O$-70% ethanol-95%–95%-100%-100%-xylene-
620 xylene-xylene, 1 min each) slides were mounted with a coverslip and DPX mounting medium
621 (Electron Microscopy Sciences). Details of reagents are listed in **Table 1**.
622
623 **Immunofluorescence.** For slide-mounted sections, slides were washed three times in PBS for 5
624 min. If necessary, antigen retrieval was then performed by immersing slides in sodium citrate
625 buffer (10 mM sodium citrate with 0.05% Tween-20, pH 6.0) at 95°C for 20 min followed by
626 washing with PBS. Slides were then incubated in blocking buffer (5% BSA in 0.4% Triton-X100 in
627 PBS (PBST)) for 1 hour at 4°C. Primary antibody solution in blocking buffer was then applied
628 overnight at 4°C. Primary antibody information and dilutions are listed in **Tables 1 and 4**. Slides
629 were then washed with RT 0.1% PBST three times and incubated in secondary antibody solution
630 in blocking buffer (1:500) for 1 hour at RT. Slides then were incubated in Hoechst (Invitrogen,
631 catalog no: H3569 diluted 1:1000 in PBS) for 10 min and washed with PBS three times and cover-
632 slipped with Fluoro-Gel (Electron Microscopy Sciences, catalog no: 17985-10).

633 For free-floating sections, sections were first washed three times in PBS for 10 min.
634 Sections then were incubated in blocking buffer (10% normal donkey serum in 0.5% PBST,
635 Sigma-Aldrich, catalog no: D9663-10ML) for 1 hour at RT before incubating in primary antibody
636 solution (2% normal donkey serum in 0.4% PBST) for 24-48 hours at 4°C. Slides were washed in
637 PBS three times and incubated in secondary antibody solution (1:500 in 2% normal donkey serum
638 in 0.4% PBST) for 2 hours at RT. Slides then were incubated in Hoechst (1:1000 in PBS) for 10
639 min and washed with PBS three times. Sections were mounted on glass slides and after sections
640 had fully dried, cover-slipped with Fluoro-Gel (Electron Microscopy Sciences).
641
642 **Immunohistochemistry.** All steps were performed at RT, unless specified. Cryosectioned tissue
643 mounted on slides were washed three times in PBS for 5 min (hereafter PBS washes). Antigen
644 retrieval was achieved by immersing sections in sodium citrate buffer at 95°C for 40 min and
645 washing in PBS. Slides were then treated with 50% methanol (in deionized $H_2O$) with 0.03%
646 $H_2O_2$ for 1 hour and washed with PBS. Primary antibody solution in blocking buffer (5% BSA in
647 0.4% PBST) was applied overnight at 4°C. After washing in PBS, a biotinylated secondary
648 antibody in blocking buffer (1:500) was applied for 1 hour, followed by PBS washes. Vectastain
649 Elite ABC HRP solution (Vector Labs, Burlingame, CA, USA; PK-6100) in blocking buffer (1:500
650 for A and B) was applied for 1 hour, followed by PBS washes. Sections were washed in 0.175 M
651 sodium acetate (in dd$H_2O$) and incubated in either standard DAB (0.02% 3,3'-Diaminobenzidine
652 tetrahydrochloride (Sigma-Aldrich, D5905), 2.5% $H_2O_2$ in 0.175 M sodium acetate) or Nickel-
653 enhanced DAB (Ni-DAB) solution (addition of 2.5% $NiSO_4$ in standard DAB solution) for 20 min.
654 DAB or Ni-DAB reaction was stopped by washing sections in 0.175 sodium acetated followed by
655 PBS washes. Sections were mounted on glass slides and dried overnight. After dehydration and
656 defatting (d$H_2O$-70% ethanol-95%–95%-100%-100%-xylene-xylene-xylene, 1 min each) slides
657 were mounted with a coverslip using DPX mounting medium (Electron Microscopy Sciences).
658

**Single molecule fluorescence *in situ* hybridization.** Tissue was treated according to the RNAscope Multiplex Fluorescent Assay v2 manufacturer's instructions and reagents from Advanced Cell Diagnostics (Hayward, CA). Details of reagents are listed in **Table 1**. Sections were rinsed twice (5 min each) in RNAase and DNAase free PBS before mounting onto Superfrost Plus coated slides (VWR, catalog no: 48311-703) in RNase- and DNase-free PBS. Slides were dried overnight and heated for 1 hour at 60°C. Slides were pretreated with target retrieval buffer for 10 min at 95-100°C, then treated with Protease III for 30 min at 40°C, followed by a probe incubation for two hours at 40°C. The probes used were: Mm-*Slc32a1*-C1, Mm-*Slc17a6*-C2 and Mm-*Slc6a5*-C3. After probe incubation, slides underwent three amplification steps, followed by developing horseradish peroxidase signal fluorescence with TSA-based fluorophores. Hoechst 33258 was used as a counterstain and slides were dried for 15 min before cover-slipping with Fluoro-Gel.

**Double labeling by RNA *in situ* hybridization and protein immunofluorescence.** Sagittal sections (14 um) were first processed for *in situ* hybridization of *Slc6a5* as described previously[91]. Briefly, probes were *in vitro* transcribed from PCR-amplified templates prepared from cDNA synthesized from an adult cerebellum lysate. The forward (5'-GTATCCCACGAGATGGATTGTT-3') and reverse (5'- CCATACAGAACACCCTCACTCA-3') primers used for PCR amplification were based on the Allen Brain Atlas. Primers were flanked in the 5' with SP6 (antisense) and 3' with T7 (sense) promoters. After visualizing the probe, slides were incubated in 4% PFA overnight at 4°C. Following PBS washes, slides were incubated in sodium citrate buffer (10 mM sodium citrate with 0.05% Tween-20, pH 6.0) at 95°C for 40 min. Slides were placed in blocking buffer for one hour and then incubated in primary antibody solution (anti-RFP at 1:500 in blocking buffer) overnight at 4°C. Slides were washed with 0.1% PBST three times and incubated in secondary antibody solution in blocking buffer (1:500) for 1 hour at RT. Slides were then incubated in Hoechst

(1:1000 in PBS, Invitrogen, catalog no: H3569) for 10 min and washed with PBS three times and cover-slipped with Fluoromount-G (ThermoFisher Scientific, catalog no: 00-4958-02).

**Microscopy, image processing, and analyses.** All images were acquired with a DM6000 Leica fluorescent microscope (Leica Camera, Wetzlar, Germany) or NanoZoomer Digital Pathology (Hamamatsu Photonics, Shizuoka, Japan). Images were processed or analyzed using Fiji[92] or Photoshop (Adobe Inc., San Jose, CA, USA). Cell counts for littermate controls, *SepW1-En1/2* CKO, *Atoh1-En1/2* CKO; *Ai75D*, *Atoh1-Cre; Ai75D*, and *eCN-DTA* mice were manually obtained using the Cell Counter plugin for Fiji or semi-automated using a custom script using the Analyze Particle plugin for Fiji as previously described[18].

The CN subregions were delineated for quantifying the recombination efficiency in *SepW1-Cre; Ai75D* mice using MEIS2 staining and the mouse brain atlas[93]. 10-14 brain slices that were 40-um apart were analyzed. The percentage of tdTomato+ cells across the CN were calculated for each animal (total n=4 mice) and averaged. The same slides were used to calculate the percentage of tdTomato+ cells in the medial CN that were co-labeled for MEIS2 (total n=4 mice) and averaged.

**Brain sample preparation for *ex vivo* dMRI.** Mice were transcardially perfused with RT PBS containing heparin and then 4°C 4% PFA. Brains were kept inside the skull, but skin, eyeballs and muscle surrounding was removed and then kept overnight in 4% PFA at 4°C. Samples were then stored in PBS with 0.02% sodium azide until imaging. One week before imaging, samples were equilibrated with Gadodiamide (0.2 mM) in PBS at 4°C and scanned by an experimenter blind to the sex and genotype.

**High resolution *ex vivo* dMRI.** Imaging of the brains was conducted as previously described[39,40]. High resolution *ex vivo* dMRI datasets were acquired on a horizontal 7T MR scanner (Bruker

Biospin, Billerica, MA, USA) using a 72-mm conventional circularly polarized birdcage radiofrequency resonator (Bruker Biospin, Ettlingen, Germany) for homogeneous transmission in conjunction with a four-channel receive-only phased array CryoProbe (CRP, Bruker Biospin, Ettlingen, Germany) and a modified 3D diffusion-weighted gradient-and-spin-echo (DW-GRASE) sequence[94] (TE/TR: 35 ms/ 400 ms, b-value: 5000 s/mm$^2$, no. of diffusion directions: 60, resolution: 0.1 mm$^3$ isotropic, acquisition time: 10.6h).

**dMRI data processing.** dMRI rawdata was processed using a pipeline demonstrated in our earlier studies[39,40]. In brief, the following steps were followed for each subject: 1) removal of signals from non-brain tissue in the dMRI datasets using AMIRA (ThermoFisher Scientific, https://www.thermofisher.com), 2) Correction for specimen displacements using rigid alignment implemented in DTIStudio[95], 3) calculation of diffusion tensor, fractional anisotropy, and fiber orientation and distribution maps Using MRtrix[96] (https://www.mrtrix.org/), 4) regional volumetric analysis, and 5) streamline tractography between the selected pairs of brain regions or nodes.

**Volumetric analysis.** For regional brain volumetric analysis, each subject was mapped to a high-resolution mouse brain atlas[39]. Whole brain volume or 10 regional volumes (cortex – CTX, olfactory area – OLF, hippocampus – HPF, amygdala – AMY, striatum – STR, pallidum – PAL, thalamus – TH, hypothalamus – HY, midbrain – MB, and cerebellum – CB) were calculated.

**Streamline tractography and structural connectome generation.** Structural connectivity between nodes and the structural connectome were constructed as previously reported[39,40,97]. In short, eight nodes (anterior cingulate cortex – ACA, motor cortex – MO, somatosensory cortex – SS, HPF, STR, AMY, TH, and HY) were included to construct the node-to-node SC maps using streamline tractography as implemented in MRtrix by seeding (n = 50,000) within the seed region

with minimum streamline length of 3 mm, FOD cut-off 0.05, step size 0.025, and angle 45˚. Excluding the intra-regional connectivity, in total 28 connections per subject were generated, which were subsequently used to construct the subject-specific structural connectome[40].

**Global network analysis.** Brain global network properties, global efficiency (Geff) and small-worldness (SW), were evaluated as previously described[97] using principles of graph theory[98] via GRETNA software[99]. Geff represents the efficiency of distant information transfer in a network and was defined as the inverse of the average characteristic path length between all nodes in the network. Brain network with short average path length between nodes and high degree of interconnectedness in local networks is considered to have SW properties. SW was computed by normalizing the network with respect to 1000 simulated random networks with equal distribution of edge weight and node strength as reported previously[100].

**Statistics.** No statistical methods were used to predetermine sample sizes, but our sample sizes are similar to those reported previously[18,33,59]. At least three different litters were used for all experiments (cell counting and behavior). No litter-related effects were seen in behavioral studies. Experimenters were blind to mouse genotypes during behavior analysis and quantifications. All data were subject to the Shapiro-Wilk test and Q-Q plots were generated to evaluate normality. If one or more dependent variable(s) failed the normality test, a non-parametric test was used. For behavioral experiments, outliers were defined if at least one dependent variable was more than mean+2×SD or less than mean-2×SD. Some additional criteria for outliers are indicated for each behavioral test (see above). A given outlier was not consistent across experiments. All statistical analyses were carried out with GraphPad Prism 8 software. Comparisons between two groups were analyzed using parametric test (unpaired *t*-test) or non-parametric test (Mann-Whitney test). The Holm-Šídák method was used for multiple unpaired t-test comparisons. Wilcoxon signed-rank test (null hypothesis = 50%) was used to test normal social preference in the three-

762 chambered social approach test. Ordinary two-way ANOVA was used to compare means across
763 two or more dependent variables. Repeated measures two-way ANOVA with Šídák's multiple
764 comparisons test were used for basal locomotion, accelerating rotarod, and water Y-maze. A
765 three-way ANOVA was used to examine the effects of sex and genotype on behavior, but as there
766 were no sex differences (data not shown), final analyses included both males and females. Data
767 are presented as mean ± SEM or mean ± SD as indicated in each figure legend. Mean differences
768 were considered significant if $P < 0.05$.
769

770 **Acknowledgements**

771 We thank all members of the Joyner, Rajadhyaksha, Heck, and Zhang laboratories over the past
772 five years for insightful discussions and technical support. We thank Alexander Walsh, Narmin
773 Mekawy, Diego Scala Chavez, and Dr. Arlene Martinez-Rivera for their excellent support from the
774 Rajadhyaksha lab. We thank Drs. Kristen Pleil (Weill Cornell Medicine), Peter Tsai (UT
775 Southwestern), and Jacqueline Crawley (UC Davis) for their advice and input on data
776 interpretation and technical support for DREADDs and behavioral testing. We thank Dr. Choong
777 Heon Lee for his help with diffusion MRI scanning and post-processing. This work was supported
778 by grants from the NIH to Alexandra L. Joyner (R37MH085726 and R01NS092096), Andrew S.
779 Lee (NICHD T32HD060600), Anjali M. Rajadhyaksha (R01MH118934, R01MH125006,
780 R01DA029122, R01DA050454), Natalia V. De Marco Garcia (2R01MH110553, 1R01MH125006,
781 1R01NS116137), Detlef H. Heck (R01MH112143), and Jiangyang Zhang (R01NS102904).
782 Alexandra L. Joyner is also supported by an NCI Cancer Center Support Grant (CCSG, P30
783 CA08748) and the Cycle for Survival. Andrew S. Lee was supported by a Weill Cornell Medicine
784 Clinical & Translational Science Center Predoctoral Training Award (TL1TR002386) from the
785 National Center for Advancing Translational Sciences. Alina Gubanova was supported by a
786 Fordham College at Lincoln Center Dean's Undergraduate Research and Creative Practice Grant.

Anjana Krishnamurthy was supported by a Dorris J. Hutchison Predoctoral Fellowship. Anjali M Rajadhyaksha was supported by the Weill Cornell Autism Research Program.

**Contributions**

A.S.L., A.M.R., T.M.A., D.H.H., J.Z., A.L.J. formulated experiments and analysis. A.S.L., A.G., D.N.S., Y.L., Z.L., A.K. performed experiments and anlaysis. T.M.A. and J.Z. carried out the mouse diffusion MRI experiments and anlaysis. N.V.D.M.G. provided the *SepW1-Cre* mice. A.S.L., T.M.A., A.M.R., and A.L.J. prepared the manuscript.

**Competing interests**

All authors declare to have no actual or potential conflict of interest including any financial, personal, or other relationships with other people or organizations within three years of beginning the submitted work that could inappropriately influence, or be perceived to influence, their work.

**Data availability**

Any additional information and requests for reagents and resources should be directed to and will be satisfied by the lead contact ALJ.

**Code Availability**

All data reported in this study and the analysis codes used are available upon request.

807 **References**

808 1. Albazron FM*, et al.* Pediatric postoperative cerebellar cognitive affective syndrome follows
809 outflow pathway lesions. *Neurology* **93**, e1561-e1571 (2019).
810 2. Korah MP*, et al.* Incidence, risks, and sequelae of posterior fossa syndrome in pediatric
811 medulloblastoma. *Int J Radiat Oncol Biol Phys* **77**, 106-112 (2010).
812 3. Robertson PL*, et al.* Incidence and severity of postoperative cerebellar mutism syndrome
813 in children with medulloblastoma: a prospective study by the Children's Oncology Group.
814 *J Neurosurg* **105**, 444-451 (2006).
815 4. Stoodley CJ, Limperopoulos C. Structure-function relationships in the developing
816 cerebellum: Evidence from early-life cerebellar injury and neurodevelopmental disorders.
817 *Semin Fetal Neonatal Med* **21**, 356-364 (2016).
818 5. van der Heijden ME*, et al.* Glutamatergic cerebellar neurons differentially contribute to the
819 acquisition of motor and social behaviors. *Nat Commun* **14**, 2771 (2023).
820 6. Herculano-Houzel S. Coordinated scaling of cortical and cerebellar numbers of neurons.
821 *Front Neuroanat* **4**, 12 (2010).
822 7. Herculano-Houzel S, Mota B, Lent R. Cellular scaling rules for rodent brains. *Proc Natl*
823 *Acad Sci U S A* **103**, 12138-12143 (2006).
824 8. Prati JMP-S, A.; Gianlorenco, A. C. L. The cerebellum and its connections to other brain
825 structures involved in motor and non-motor functions: a comprehensive review. *Behav*
826 *Brain Res*, (2024).
827 9. Kebschull JM*, et al.* Cerebellum Lecture: the Cerebellar Nuclei-Core of the Cerebellum.
828 *Cerebellum*, (2023).
829 10. Novello M, Bosman LWJ, De Zeeuw CI. A Systematic Review of Direct Outputs from the
830 Cerebellum to the Brainstem and Diencephalon in Mammals. *Cerebellum* **23**, 210-239
831 (2024).

11. Rudolph S*, et al.* Cognitive-Affective Functions of the Cerebellum. *J Neurosci* **43**, 7554-7564 (2023).

12. Zhang XY*, et al.* A role for the cerebellum in motor-triggered alleviation of anxiety. *Neuron*, (2024).

13. Darmohray DM, Jacobs JR, Marques HG, Carey MR. Spatial and Temporal Locomotor Learning in Mouse Cerebellum. *Neuron* **102**, 217-231 e214 (2019).

14. Fujita H, Kodama T, du Lac S. Modular output circuits of the fastigial nucleus for diverse motor and nonmotor functions of the cerebellar vermis. *Elife* **9**, (2020).

15. Judd EN, Lewis SM, Person AL. Diverse inhibitory projections from the cerebellar interposed nucleus. *Elife* **10**, (2021).

16. Kelly E*, et al.* Regulation of autism-relevant behaviors by cerebellar-prefrontal cortical circuits. *Nat Neurosci* **23**, 1102-1110 (2020).

17. Liu XX*, et al.* BOD1 regulates the cerebellar IV/V lobe-fastigial nucleus circuit associated with motor coordination. *Signal Transduct Target Ther* **7**, 170 (2022).

18. Willett RT*, et al.* Cerebellar nuclei excitatory neurons regulate developmental scaling of presynaptic Purkinje cell number and organ growth. *Elife* **8**, (2019).

19. Sugihara I, Fujita H, Na J, Quy PN, Li BY, Ikeda D. Projection of reconstructed single Purkinje cell axons in relation to the cortical and nuclear aldolase C compartments of the rat cerebellum. *J Comp Neurol* **512**, 282-304 (2009).

20. Corrales JD, Blaess S, Mahoney EM, Joyner AL. The level of sonic hedgehog signaling regulates the complexity of cerebellar foliation. *Development* **133**, 1811-1821 (2006).

21. Fleming JT*, et al.* The Purkinje neuron acts as a central regulator of spatially and functionally distinct cerebellar precursors. *Dev Cell* **27**, 278-292 (2013).

22. Kebschull JM*, et al.* Cerebellar nuclei evolved by repeatedly duplicating a conserved cell-type set. *Science* **370**, (2020).

857 23. Gerfen CR, Paletzki R, Heintz N. GENSAT BAC cre-recombinase driver lines to study the
858 functional organization of cerebral cortical and basal ganglia circuits. *Neuron* **80**, 1368-
859 1383 (2013).
860 24. Daigle TL*, et al.* A Suite of Transgenic Driver and Reporter Mouse Lines with Enhanced
861 Brain-Cell-Type Targeting and Functionality. *Cell* **174**, 465-480 e422 (2018).
862 25. Krishnamurthy A*, et al.* Engrailed transcription factors direct excitatory cerebellar neuron
863 diversity and survival. *bioRxiv*, (2023).
864 26. Gruver KMJ, J. W.; Fields, E.; Song, S.; Sjöström, P. J.; Watt, A. J. Structured connectivity
865 in the output of the cerebellar cortex. *bioRxiv*, (2023).
866 27. Badura A*, et al.* Normal cognitive and social development require posterior cerebellar
867 activity. *Elife* **7**, (2018).
868 28. Verpeut JL*, et al.* Cerebellar contributions to a brainwide network for flexible behavior in
869 mice. *Commun Biol* **6**, 605 (2023).
870 29. Wang X, Yu SY, Ren Z, De Zeeuw CI, Gao Z. A FN-MdV pathway and its role in cerebellar
871 multimodular control of sensorimotor behavior. *Nat Commun* **11**, 6050 (2020).
872 30. Ahmadzadeh E*, et al.* A collection of genetic mouse lines and related tools for inducible
873 and reversible intersectional mis-expression. *Development* **147**, (2020).
874 31. Leto K*, et al.* Consensus Paper: Cerebellar Development. *Cerebellum* **15**, 789-828 (2016).
875 32. Dietrichs E. Cerebellar cortical and nuclear afferents from the feline locus coeruleus
876 complex. *Neuroscience* **27**, 77-91 (1988).
877 33. Kabir ZD*, et al.* Rescue of impaired sociability and anxiety-like behavior in adult cacna1c-
878 deficient mice by pharmacologically targeting eIF2alpha. *Mol Psychiatry* **22**, 1096-1109
879 (2017).
880 34. Yang M, Silverman JL, Crawley JN. Automated three-chambered social approach task for
881 mice. *Curr Protoc Neurosci* **Chapter 8**, Unit 8 26 (2011).

882 35. Brown HD, Baker PM, Ragozzino ME. The parafascicular thalamic nucleus concomitantly
883 influences behavioral flexibility and dorsomedial striatal acetylcholine output in rats. *J*
884 *Neurosci* **30**, 14390-14398 (2010).
885 36. Kato S*, et al.* Action Selection and Flexible Switching Controlled by the Intralaminar
886 Thalamic Neurons. *Cell Rep* **22**, 2370-2382 (2018).
887 37. Melief EJ*, et al.* Loss of glutamate signaling from the thalamus to dorsal striatum impairs
888 motor function and slows the execution of learned behaviors. *NPJ Parkinsons Dis* **4**, 23
889 (2018).
890 38. Xiao L, Bornmann C, Hatstatt-Burkle L, Scheiffele P. Regulation of striatal cells and goal-
891 directed behavior by cerebellar outputs. *Nat Commun* **9**, 3133 (2018).
892 39. Arefin TM*, et al.* Towards reliable reconstruction of the mouse brain corticothalamic
893 connectivity using diffusion MRI. *Neuroimage* **273**, 120111 (2023).
894 40. Arefin TM, Lee CH, White JD, Zhang J, Kaffman A. Macroscopic Structural and
895 Connectome Mapping of the Mouse Brain Using Diffusion Magnetic Resonance Imaging.
896 *Bio Protoc* **11**, e4221 (2021).
897 41. Asemi-Rad A, Ghiyamihoor F, Consalez GG, Marzban H. Ablation of Projection
898 Glutamatergic Neurons in the Lateral Cerebellar Nuclei Alters Motor Coordination in
899 Vglut2-Cre+ Mice. *Cerebellum*, (2023).
900 42. Carlson ES*, et al.* Catecholaminergic Innervation of the Lateral Nucleus of the Cerebellum
901 Modulates Cognitive Behaviors. *J Neurosci* **41**, 3512-3530 (2021).
902 43. Dumas DB, Gornati SV, Adolfs Y, Shimogori T, Pasterkamp RJ, Hoebeek FE. Anatomical
903 Development of the Cerebellothalamic Tract in Embryonic Mice. *Cells* **11**, (2022).
904 44. Houck BD, Person AL. Cerebellar Premotor Output Neurons Collateralize to Innervate the
905 Cerebellar Cortex. *J Comp Neurol* **523**, 2254-2271 (2015).
906 45. Locke TM*, et al.* Dopamine D1 Receptor-Positive Neurons in the Lateral Nucleus of the
907 Cerebellum Contribute to Cognitive Behavior. *Biol Psychiatry* **84**, 401-412 (2018).

908 46. Low AYT*, et al.* Reverse-translational identification of a cerebellar satiation network.
909 *Nature* **600**, 269-273 (2021).
910 47. Low AYT*, et al.* Precision of Discrete and Rhythmic Forelimb Movements Requires a
911 Distinct Neuronal Subpopulation in the Interposed Anterior Nucleus. *Cell Rep* **22**, 2322-
912 2333 (2018).
913 48. Frontera JL*, et al.* Bidirectional control of fear memories by cerebellar neurons projecting
914 to the ventrolateral periaqueductal grey. *Nat Commun* **11**, 5207 (2020).
915 49. Frontera JL*, et al.* The cerebellum regulates fear extinction through thalamo-prefrontal
916 cortex interactions in male mice. *Nat Commun* **14**, 1508 (2023).
917 50. Pisano TJ*, et al.* Homologous organization of cerebellar pathways to sensory, motor, and
918 associative forebrain. *Cell Rep* **36**, 109721 (2021).
919 51. Liu J*, et al.* Striatal glutamate delta-1 receptor regulates behavioral flexibility and
920 thalamostriatal connectivity. *Neurobiol Dis* **137**, 104746 (2020).
921 52. Trinh MA*, et al.* The eIF2alpha kinase PERK limits the expression of hippocampal
922 metabotropic glutamate receptor-dependent long-term depression. *Learn Mem* **21**, 298-
923 304 (2014).
924 53. Bicks LK, Koike H, Akbarian S, Morishita H. Prefrontal Cortex and Social Cognition in
925 Mouse and Man. *Front Psychol* **6**, 1805 (2015).
926 54. Parnaudeau S, Bolkan SS, Kellendonk C. The Mediodorsal Thalamus: An Essential
927 Partner of the Prefrontal Cortex for Cognition. *Biol Psychiatry* **83**, 648-656 (2018).
928 55. Calhoon GG, Tye KM. Resolving the neural circuits of anxiety. *Nat Neurosci* **18**, 1394-
929 1404 (2015).
930 56. Kim H, Lim CS, Kaang BK. Neuronal mechanisms and circuits underlying repetitive
931 behaviors in mouse models of autism spectrum disorder. *Behav Brain Funct* **12**, 3 (2016).
932 57. Lalonde R, Strazielle C. Behavioral effects of neonatal lesions on the cerebellar system.
933 *Int J Dev Neurosci* **43**, 58-65 (2015).

58. Manto M*, et al.* Consensus paper: roles of the cerebellum in motor control--the diversity of ideas on cerebellar involvement in movement. *Cerebellum* **11**, 457-487 (2012).

59. Tsai PT*, et al.* Autistic-like behaviour and cerebellar dysfunction in Purkinje cell Tsc1 mutant mice. *Nature* **488**, 647-651 (2012).

60. van der Heijden ME*, et al.* Maturation of Purkinje cell firing properties relies on neurogenesis of excitatory neurons. *Elife* **10**, (2021).

61. Prekop HT*, et al.* Sox14 Is Required for a Specific Subset of Cerebello-Olivary Projections. *J Neurosci* **38**, 9539-9550 (2018).

62. Liang B*, et al.* Striatal direct pathway neurons play leading roles in accelerating rotarod motor skill learning. *iScience* **25**, 104245 (2022).

63. Rose MF, Ahmad KA, Thaller C, Zoghbi HY. Excitatory neurons of the proprioceptive, interoceptive, and arousal hindbrain networks share a developmental requirement for Math1. *Proc Natl Acad Sci U S A* **106**, 22462-22467 (2009).

64. Cheng Y*, et al.* The Engrailed homeobox genes determine the different foliation patterns in the vermis and hemispheres of the mammalian cerebellum. *Development* **137**, 519-529 (2010).

65. Joyner AL. Engrailed, Wnt and Pax genes regulate midbrain--hindbrain development. *Trends Genet* **12**, 15-20 (1996).

66. Joyner AL, Herrup K, Auerbach BA, Davis CA, Rossant J. Subtle cerebellar phenotype in mice homozygous for a targeted deletion of the En-2 homeobox. *Science* **251**, 1239-1243 (1991).

67. Kuemerle B, Zanjani H, Joyner A, Herrup K. Pattern deformities and cell loss in Engrailed-2 mutant mice suggest two separate patterning events during cerebellar development. *J Neurosci* **17**, 7881-7889 (1997).

68. Millen KJ, Hui CC, Joyner AL. A role for En-2 and other murine homologues of Drosophila segment polarity genes in regulating positional information in the developing cerebellum. *Development* **121**, 3935-3945 (1995).

69. Millen KJ, Wurst W, Herrup K, Joyner AL. Abnormal embryonic cerebellar development and patterning of postnatal foliation in two mouse Engrailed-2 mutants. *Development* **120**, 695-706 (1994).

70. Orvis GD*, et al.* The engrailed homeobox genes are required in multiple cell lineages to coordinate sequential formation of fissures and growth of the cerebellum. *Dev Biol* **367**, 25-39 (2012).

71. Sgaier SK*, et al.* Genetic subdivision of the tectum and cerebellum into functionally related regions based on differential sensitivity to engrailed proteins. *Development* **134**, 2325-2335 (2007).

72. Sillitoe RV, Stephen D, Lao Z, Joyner AL. Engrailed homeobox genes determine the organization of Purkinje cell sagittal stripe gene expression in the adult cerebellum. *J Neurosci* **28**, 12150-12162 (2008).

73. Wurst W, Auerbach AB, Joyner AL. Multiple developmental defects in Engrailed-1 mutant mice: an early mid-hindbrain deletion and patterning defects in forelimbs and sternum. *Development* **120**, 2065-2075 (1994).

74. LeDoux MS, Lorden JF, Ervin JM. Cerebellectomy eliminates the motor syndrome of the genetically dystonic rat. *Exp Neurol* **120**, 302-310 (1993).

75. LeDoux MS, Lorden JF, Meinzen-Derr J. Selective elimination of cerebellar output in the genetically dystonic rat. *Brain Res* **697**, 91-103 (1995).

76. Grusser C, Grusser-Cornehls U. Improvement in motor performance of Weaver mutant mice following lesions of the cerebellum. *Behav Brain Res* **97**, 189-194 (1998).

77. Grusser-Cornehls U, Grusser C, Baurle J. Vermectomy enhances parvalbumin expression and improves motor performance in weaver mutant mice: an animal model for cerebellar ataxia. *Neuroscience* **91**, 315-326 (1999).

78. Badreddine N*, et al.* Spatiotemporal reorganization of corticostriatal networks encodes motor skill learning. *Cell Rep* **39**, 110623 (2022).

79. Augustin SM, Loewinger GC, O'Neal TJ, Kravitz AV, Lovinger DM. Dopamine D2 receptor signaling on iMSNs is required for initiation and vigor of learned actions. *Neuropsychopharmacology* **45**, 2087-2097 (2020).

80. Augustin SM, Gracias AL, Luo G, Anumola RC, Lovinger DM. Striatonigral direct pathway 2-arachidonoylglycerol contributes to ethanol effects on synaptic transmission and behavior. *Neuropsychopharmacology* **48**, 1941-1951 (2023).

81. Bailey KR, Mair RG. Lesions of specific and nonspecific thalamic nuclei affect prefrontal cortex-dependent aspects of spatial working memory. *Behav Neurosci* **119**, 410-419 (2005).

82. Matei V*, et al.* Smaller inner ear sensory epithelia in Neurog 1 null mice are related to earlier hair cell cycle exit. *Dev Dyn* **234**, 633-650 (2005).

83. Perl AK, Wert SE, Nagy A, Lobe CG, Whitsett JA. Early restriction of peripheral and proximal cell lineages during formation of the lung. *Proc Natl Acad Sci U S A* **99**, 10482-10487 (2002).

84. Kimmel RA, Turnbull DH, Blanquet V, Wurst W, Loomis CA, Joyner AL. Two lineage boundaries coordinate vertebrate apical ectodermal ridge formation. *Genes Dev* **14**, 1377-1389 (2000).

85. Bavley CC*, et al.* Rescue of Learning and Memory Deficits in the Human Nonsyndromic Intellectual Disability Cereblon Knock-Out Mouse Model by Targeting the AMP-Activated Protein Kinase-mTORC1 Translational Pathway. *J Neurosci* **38**, 2780-2795 (2018).

86. Tsai PT, *et al.* Sensitive Periods for Cerebellar-Mediated Autistic-like Behaviors. *Cell Rep* **25**, 357-367 e354 (2018).

87. Liu Y, McAfee SS, Van Der Heijden ME, Dhamala M, Sillitoe RV, Heck DH. Causal Evidence for a Role of Cerebellar Lobulus Simplex in Prefrontal-Hippocampal Interaction in Spatial Working Memory Decision-Making. *Cerebellum* **21**, 762-775 (2022).

88. Van Der Heijden ME, Gill JS, Rey Hipolito AG, Salazar Leon LE, Sillitoe RV. Quantification of Behavioral Deficits in Developing Mice With Dystonic Behaviors. *Dystonia* **1**, (2022).

89. Friard O, Gamba M. BORIS: a free, versatile open-source event-logging software for video/audio coding and live observations. *Methods in Ecology and Evolution* **7**, 1325-1330 (2016).

90. Johnson MA, *et al.* Chronic stress differentially alters mRNA expression of opioid peptides and receptors in the dorsal hippocampus of female and male rats. *J Comp Neurol* **529**, 2636-2657 (2021).

91. Blaess S, *et al.* Temporal-spatial changes in Sonic Hedgehog expression and signaling reveal different potentials of ventral mesencephalic progenitors to populate distinct ventral midbrain nuclei. *Neural Dev* **6**, 29 (2011).

92. Schindelin J, *et al.* Fiji: an open-source platform for biological-image analysis. *Nat Methods* **9**, 676-682 (2012).

93. Paxinos G, Watson C. *The rat brain in stereotaxic coordinates*, 6th edn. Academic Press/Elsevier (2007).

94. Aggarwal M, Mori S, Shimogori T, Blackshaw S, Zhang J. Three-dimensional diffusion tensor microimaging for anatomical characterization of the mouse brain. *Magn Reson Med* **64**, 249-261 (2010).

95. Jiang H, van Zijl PC, Kim J, Pearlson GD, Mori S. DtiStudio: resource program for diffusion tensor computation and fiber bundle tracking. *Comput Methods Programs Biomed* **81**, 106-116 (2006).

96. Wu D, Zhang J. In vivo mapping of macroscopic neuronal projections in the mouse hippocampus using high-resolution diffusion MRI. *Neuroimage* **125**, 84-93 (2016).

97. White JD*, et al.* Early life stress causes sex-specific changes in adult fronto-limbic connectivity that differentially drive learning. *Elife* **9**, (2020).

98. Bullmore E, Sporns O. Complex brain networks: graph theoretical analysis of structural and functional systems. *Nat Rev Neurosci* **10**, 186-198 (2009).

99. Wang J, Wang X, Xia M, Liao X, Evans A, He Y. GRETNA: a graph theoretical network analysis toolbox for imaging connectomics. *Front Hum Neurosci* **9**, 386 (2015).

100. Rubinov M, Sporns O. Weight-conserving characterization of complex functional brain networks. *Neuroimage* **56**, 2068-2079 (2011).

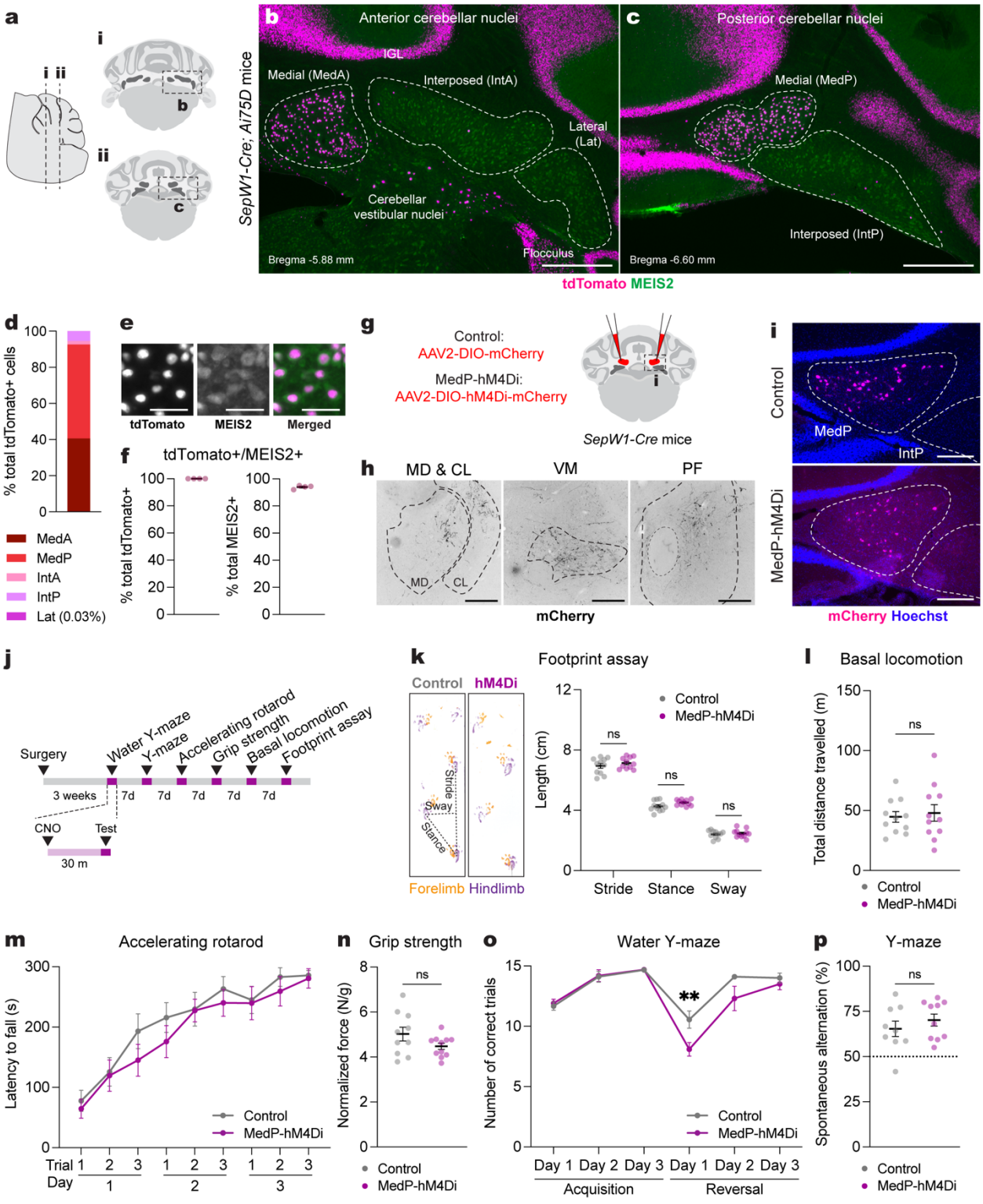


**Fig. 1 | Acute adult chemogenetic inhibition of MedP eCN impairs reversal learning and not motor behaviors.**

**a**, Schematic representation of a lateral sagittal plane of the mouse cerebellum on the left with vertical lines (**i** and **ii**) indicating the location of the anterior and posterior coronal schematics shown to right.

**b**,**c**, Representative coronal images of tdTomato expression in the anterior CN (**b**) and posterior (**c**) CN of *SepW1-Cre; Ai75D* mice. CN were subdivided into five subregions based on histological distinctions (Paxinos and Franklin, 2007) and MEIS2 immunostaining. Abbreviations: MedA=Anterior medial; MedP=Posterior medial; IntA=Anterior interposed; IntP=Posterior interposed; Lat=Lateral. Scale bars = 500 um.

**d**, Quantification of tdTomato+ cells on every second coronal section of *SepW1-Cre; Ai75D* mice (n=4) in the lateral CN (Lat) and subregions of the intermediate (Int) and medial (Med) CN (n=4 mice).

**e**, Representative image of tdTomato (magenta) and MEIS2 (green) co-expressing eCN in *SepW1-Cre; Ai75D* mice. Scale bars = 50 um.

**f**, Quantification of tdTomato+ cells that co-express MEIS2 and the reverse in *SepW1-Cre; Ai75D* mice (n=4 mice).

**g**, Schematic of viral injection to express mCherry (control) or hM4Di-mCherry (MedP-hM4Di) in adult MedP eCN. Dashed line indicates region shown in (**i**).

**h,** Representative images of MedP eCN mCherry+ axon terminals (black) in four thalamic nuclei of control mice. Fluorescent images were inverted using the look up table in Fiji. Abbreviations: MD=mediodorsal; CL=centrolateral; VM=ventromedial; PF=parafascicular. Scale bars = 250 um.

**i**, Representative images of viral mCherry expression in MedP eCN in control (top, AAV-DIO-mCherry) and MedP-hM4Di (bottom, AAV-DIO-hM4Di-mCherry) mice. Scale bars = 250 um.

**j**, Experimental timeline of surgery, CNO injection and behavioral tests.

**k**, (left) Representative images of footprints from control and MedP-hM4Di mice. (right) quantification of stride, stance, and sway (n=11 per group). Multiple Mann-Whitney *U* tests for

effect of genotype on stride ($U$ = 48, P = 0.4385), stance ($U$ = 34, P = 0.0843) and sway ($U$ = 58, P = 0.8851).

**l**, Total distance travelled during basal locomotion (n=11 per group; $t_{20}$ = 0.3910, P = 0.7000).

**m**, Latency to fall during the accelerating rotarod test (MedP-hM4Di: n=11, control: n=10). Repeated measure two-way ANOVA: main effect of time ($F_{4.750,90.25}$ = 27.51, P < 0.0001), but not of chemogenetics ($F_{1,19}$ = 0.9367, P = 0.3453) or interaction ($F_{5,152}$ = 0.3699, P = 0.9351).

**n**, Forelimb grip strength normalized to body weight (MedP-hM4Di: n=11, control: n=10; two-tailed unpaired t-test: $t_{19}$ = 1.677, P = 0.1099).

**o**, Total number of correct trials during the water Y-maze test (MedP-hM4Di: n=10, control: n=9). Repeated measure two-way ANOVA: main effect of time ($F_{5,85}$ = 27.65, P < 0.0001) and chemogenetics ($F_{1,17}$ = 9.855, P = 0.006), but not of interaction ($F_{5,85}$ = 2.257, P = 0.0559); with post hoc two-tailed t-tests with Šídák correction for effect of chemogenetics on Reversal Day 1 ($t_{102}$ = 3.386, P = 0.006), and not other comparisons ($P \geq 0.05$).

**p**, Percentage spontaneous alternations in the Y-maze (MedP-hM4Di: n=10, control: n=9; two-tailed unpaired t-test: $t_{17}$ = 0.9024, P = 0.3794).

ns, not significant: $P \geq 0.05$. Data are presented as mean values ± SEM.

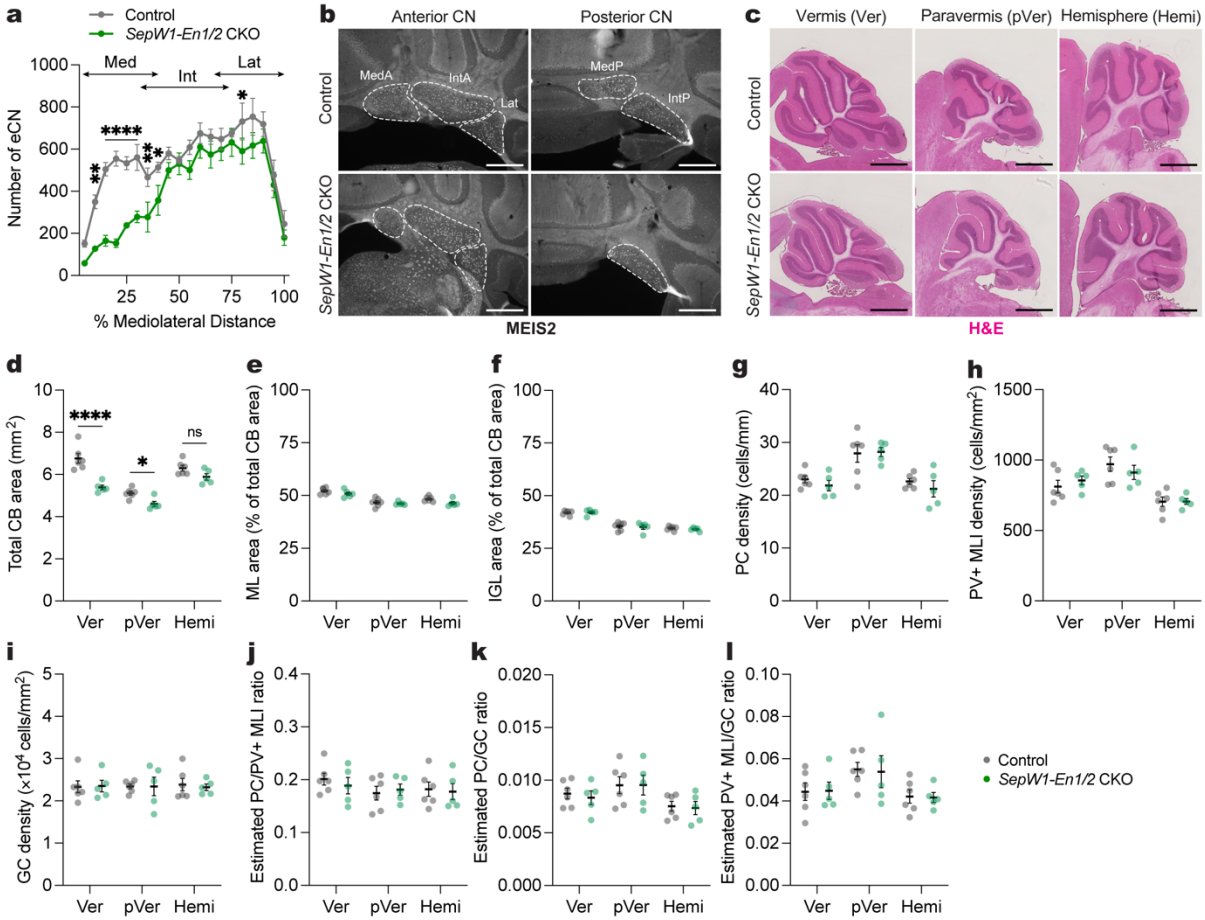


**Fig. 2 | Generation of mice lacking the MedP eCN by conditional knockout of *En1/2*.**

**a**, Quantification of eCN number (large (100-600 um$^2$) NeuN+ cells) along the medial-lateral axis in adult *SepW1-En1/2* CKOs (n=5) and littermate controls (n=6). Ordinary two-way ANOVA: main effect of mediolateral distance ($F_{19,180}$ = 24.02, P < 0.0001), genotype ($F_{1,180}$ = 86.54, P < 0.0001), and interaction ($F_{19,180}$ = 2.449, P < 0.0001); with post hoc two-tailed t-tests with uncorrected Fisher's LSD for effect of genotype for bin 5-10% ($t_{180}$ = 3.180, P = 0.0017), bins 10-30% (list of t value for each bin: $t_{180}$ = 4.858, 5.738, 4.218, 4.028; all P values: P < 0.0001), bin 30-35% ($t_{180}$ = 2.703, P = 0.0075), bin 35-40% ($t_{180}$ = 2.238, P = 0.0265), bin 75-80% ($t_{180}$ = 2.002. P = 0.0468), but not other comparisons (P ≥ 0.05). Abbreviations: Med=medial; Int=interposed; Lat=lateral.

**b**, Representative coronal images of MEIS2 labeling in the anterior and posterior CN of an adult *SepW1-En1/2* CKO and littermate control as indicated. Scale bars = 500 um.

**c**, Representative images of H&E labeled sagittal sections of vermis (Ver), paravermis (pVer), and hemisphere (Hemi) from a *SepW1-En1/2* CKO and littermate control. Scale bars = 1 mm.

**d**, Quantification of total cerebellar (CB) area of *SepW1-En1/2* CKOs (n=5) compared to littermate controls (n=6) in the vermis, paravermis and hemispheres. Ordinary two-way ANOVA: main effect of region ($F_{2,27}$ = 42.06, P < 0.0001) and genotype ($F_{1,27}$ = 37.13, P < 0.0001), and interaction ($F_{2,27}$ = 5.825, P = 0.0079); with post hoc two-tailed t-tests with uncorrected Fisher's LSD for effect of genotype for vermis ($t_{27}$ = 6.292, P < 0.0001), paravermis ($t_{27}$ = 2.359, P = 0.0258), and hemisphere (P = 0.0678).

**e**, Quantification of molecular layer (ML) area as a percent of total CB area in *SepW1-En1/2* CKOs (n=5) compared to littermate controls (n=6). Ordinary two-way ANOVA: main effect of region ($F_{2,27}$ = 32.11, P < 0.0001), genotype ($F_{1,27}$ = 5.236, P = 0.0302), but not of interaction (P = 0.5866).

**f**, Quantification of internal granule cell layer (IGL) area as a percent of total CB area in *SepW1-En1/2* CKOs (n=5) compared to littermate controls (n=6). Ordinary two-way ANOVA: main effect of region ($F_{2,27}$ = 82.04, P < 0.0001), but not of genotype (P = 0.6943) or interaction (P = 0.8641).

**g**, Quantification of Purkinje cell (PC) density in *SepW1-En1/2* CKOs (n=5) compared to littermate controls (n=6). Ordinary two-way ANOVA: main effect of region ($F_{2,18}$ = 18.34, P < 0.0001), but not of genotype (P = 0.4167) or interaction (P = 0.7216).

**h**, Quantification of PV+ MLI density in *SepW1-En1/2* CKOs (n=5) compared to littermate controls (n=6). Ordinary two-way ANOVA: main effect of region ($F_{2,27}$ = 16.66, P < 0.0001), but not of genotype (P = 0.8926) or interaction (P = 0.4617).

**i**, Quantification of granule cell (GC) density in the IGL of *SepW1-En1/2* CKOs (n=5) compared to littermate controls (n=6). Ordinary two-way ANOVA: no main effect of region (P = 0.9948), genotype (P = 0.8945) or interaction (P = 0.9502).

**j**, Quantification of the estimated ratio of the number of PCs to PV+ MLIs in *SepW1-En1/2* CKOs (n=5) compared to littermate controls (n=6). Ordinary two-way ANOVA: no significant main effect of region (P = 0.3807), genotype (P = 0.7618) or interaction (P = 0.7701).

**k**, Quantification of the estimated ratio of the number of PCs to GCs in *SepW1-En1/2* CKOs (n=5) compared to littermate controls (n=6). Ordinary two-way ANOVA: main effect of region ($F_{1,27}$ = 4.769, P = 0.0168), but no main effect of genotype (P = 0.7368) or interaction (P = 0.2521).

**l**, Quantification of the estimated ratio of the number of PV+ MLIs to GCs in *SepW1-En1/2* CKOs (n=5) compared to littermate controls (n=6). Ordinary two-way ANOVA: main effect of region ($F_{1,27}$ = 4.638, P = 0.0186), but not of genotype (P = 0.9195) or interaction (P = 0.9841).

ns, not significant: $P \geq 0.05$. Data are presented as mean values ± SEM.

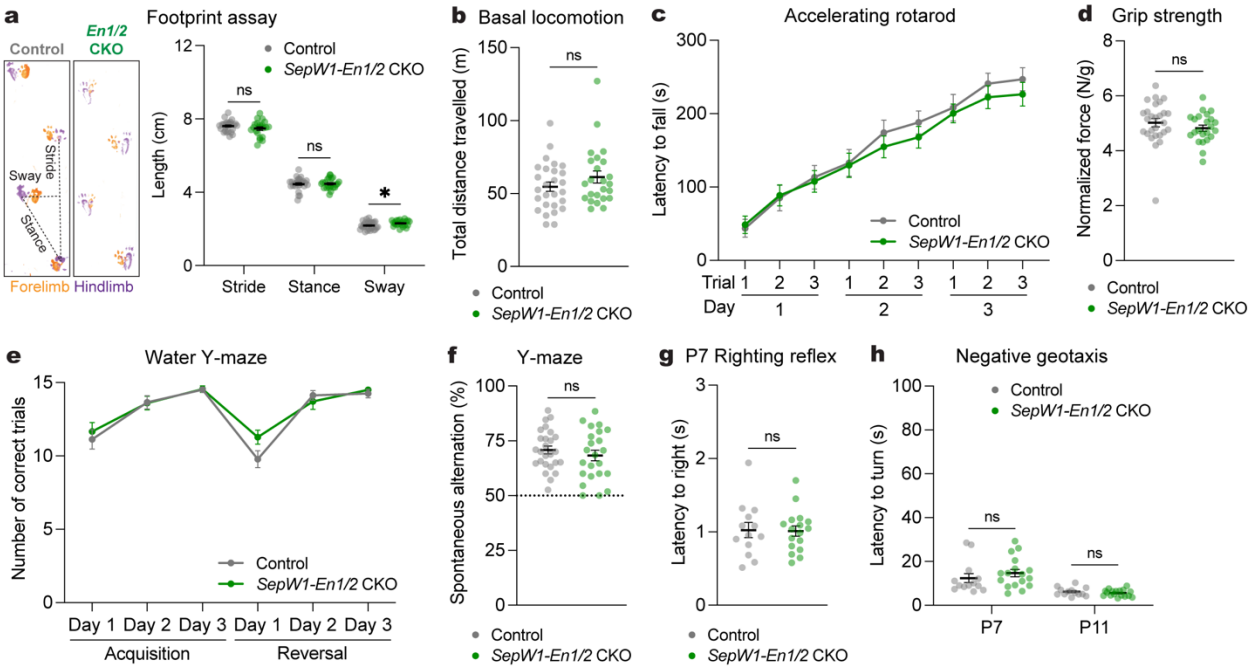


**Fig. 3 | Mice lacking MedP eCN have normal reversal learning as well as motor behaviors.**

**a**, (left) Representative images of footprints from one *SepW1-En1/2* CKO and littermate control. (right) Quantification of stride, stance, and sway (*SepW1-En1/2* CKOs: n=27, littermate controls: n=22). Multiple Mann-Whitney *U* tests showing effect of genotype on sway ($U$ = 188, P = 0.0276), but not stride ($U$ = 234, P = 0.2087) or stance ($U$ = 279, P = 0.7235).

**b**, Total distance travelled during basal locomotion (*SepW1-En1/2* CKOs: n=24, littermate controls: n=27; Mann-Whitney *U* test: $U$ = 264, P = 0.2640).

**c**, Latency to fall during the accelerating rotarod test (*SepW1-En1/2* CKOs: n=23, littermate controls: n=27). Repeated measure two-way ANOVA: main effect of time ($F_{4.590,220.3}$ = 69.92, P < 0.0001), but not of genotype ($F_{1,48}$ = 0.3434, P = 0.5606) or interaction ($F_{8,384}$ = 0.4280, P < 0.9041).

**d**, Forelimb grip strength coronal normalized to body weight (*SepW1-En1/2* CKOs: n=23, littermate controls: n=27; two-tailed unpaired t-test: $t_{48}$ = 1.1018, P = 0.6689).

**e**, Total number of correct trials during the water Y-maze test (*SepW1-En1/2* CKOs: n=18, littermate controls: n=23). Repeated measure two-way ANOVA: main effect of time ($F_{3.132,122.1}$ =

38.86, $P < 0.0001$), but not of genotype ($F_{1,39} = 0.5638$, $P = 0.4572$) or interaction ($F_{5,195} = 1.492$, $P = 0.1941$).

**f**, Percentage of spontaneous alternations in the Y-maze (*SepW1-En1/2* CKOs: n=23, littermate controls: n=26); two-tailed unpaired t-test: $t_{47} = 0.8600$, $P = 0.3942$).

**g**, Latency to right onto four paws at P7 (*SepW1-En1/2* CKOs: n=17, littermate controls: n=13; two-tailed unpaired t-test: $t_{28} = 0.1171$, $P = 0.9076$).

**h**, Latency to turn upward on a negative slope at P7 and P11 (*SepW1-En1/2* CKOs: n=17, littermate controls: n=13). Multiple Mann-Whitney *U* tests with Holm-Šídák correction for effect of genotype at P7 ($U = 79$, $P = 0.3562$) and at P11 ($U = 92.50$, $P = 0.4634$).

ns, not significant: $P \geq 0.05$. Data are presented as mean values ± SEM.

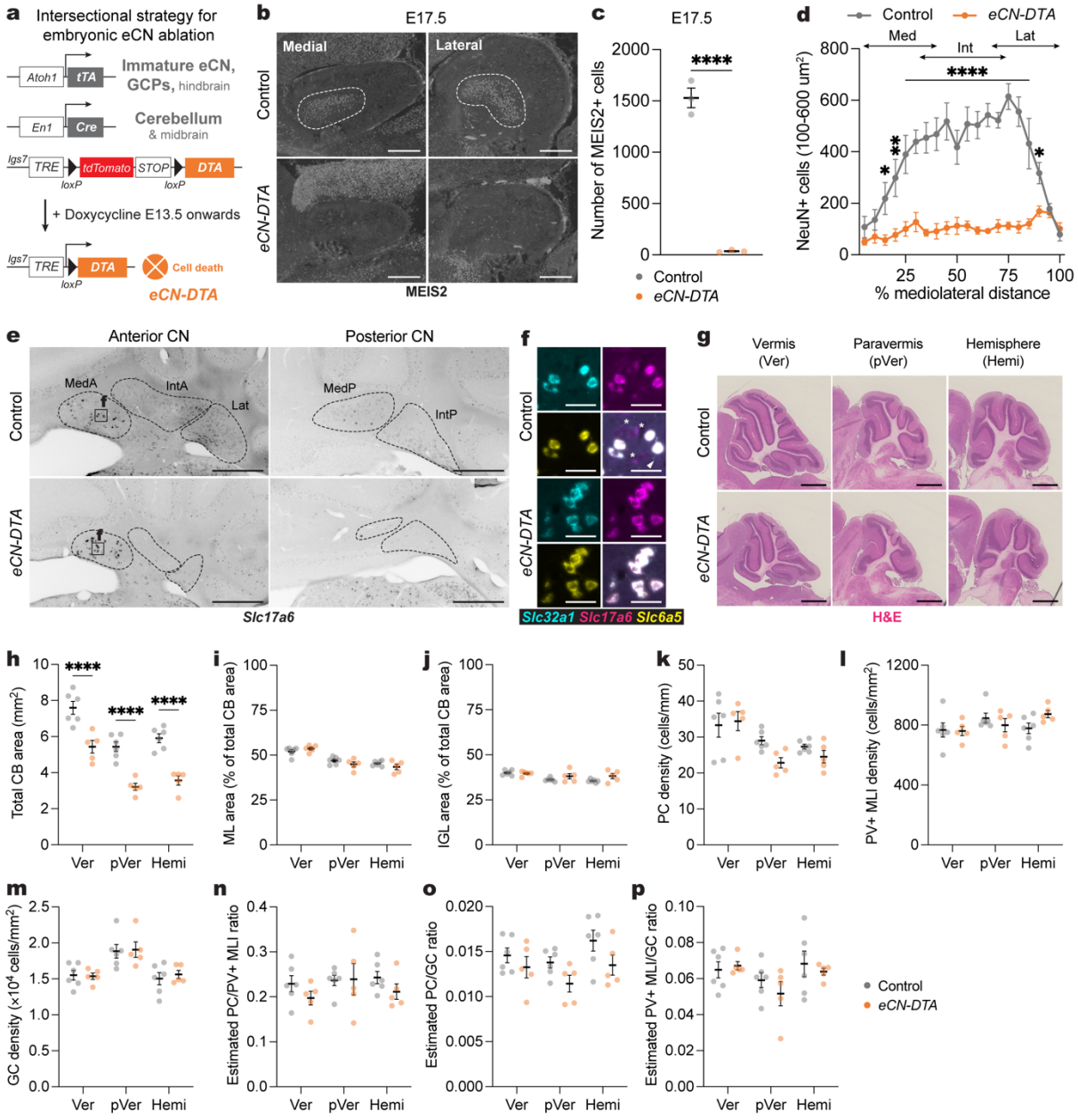


**Fig. 4 | Generation of mice in which all embryonic eCN are ablated using Diphtheria toxin.** **a**, Intersectional approach to pharmacogenetically ablate the embryonic eCN. A doxycycline (Dox)-controlled and recombinase activated gene overexpression allele (DRAGON) for attenuated diphtheria toxin fragment A (DTA) (*Igs7*$^{DRAGON\text{-}DTA}$) combined with an *Atoh1-tTA* transgene and *En1*$^{Cre}$ knock-in allele results in embryonic killing of eCN when Dox is administered starting at E13.5 via expression of DTA. The genotypes of littermate controls are *Atoh1-tTA* or *En1*$^{Cre}$ along with the *Igs7*$^{DRAGON\text{-}DTA}$ allele.

**b**, Representative images of sagittal sections stained for MEIS2 (white) in medial and lateral cerebellum of an E17.5 *eCN-DTA* and littermate control. Scale bars = 250 um.

**c**, Quantification of total number of MEIS2+ cells on every $10^{th}$ sagittal section of E17.5 *eCN-DTA* mice (n=3) compared to littermate controls (n=3) (two-tailed unpaired t-test: $t_4 = 15.62$, $P < 0.0001$).

**d**, Mediolateral distribution of NeuN+ large cells (100-600 $um^2$) in adult *eCN-DTA* mice (n=5) compared to littermate controls (n=6). Repeated measure two-way ANOVA: main effect of mediolateral distance ($F_{19,180} = 6.669$, $P < 0.0001$), genotype ($F_{1,180} = 359.5$, $P < 0.0001$), and interaction ($F_{19,180} = 5.745$, $P < 0.0001$); with post hoc two-tailed t-tests with uncorrected Fisher's LSD for effect of genotype show significance for bin 10-15% ($t_{180} = 3.327$, $P = 0.0163$), bin 15-20% ($t_{180} = 4.439$, $P = 0.0011$), bins 20-85% (list of t value for each bin: $t_{180} = 4.349, 4.684, 5.539, 5.676, 6.22, 4.587, 5.939, 6.153, 6.76, 6.181, 7.551, 6.744, 4.676$; all P values: $P < 0.0001$), bin 85-90% ($t_{180} = 2.229$, $P = 0.027$), but not other comparisons ($P \geq 0.05$). Abbreviations: Med=medial; Int=interposed; Lat=lateral.

**e**, Representative images of RNA *in situ* analysis of coronal sections for *Slc17a6* expression in the CN of *eCN-DTA* mice and littermate controls. Dotted outlines indicate the CN subregions. Images are single channel inverted using lookup table in Fiji. Scale bars = 500 um.

**f**, Representative images of triple RNA *in situ* of coronal sections in the medial CN showing some neurons co-express *Slc32a1*, *Slc17a6*, and *Slc6a5*. Arrowhead and asterisk indicate neurons expressing only *Slc32a1* or *Slc17a6* in controls, respectively. Scale bars = 50 um.

**g**, Representative images of H&E labeled vermis (Ver), paravermis (pVer), and hemisphere (Hemi) sagittal sections from an *eCN-DTA* and littermate control. Scale bars = 1 mm.

**h**, Quantification of total cerebellar (CB) area in *eCN-DTA* mice (n=5) and littermate controls (n=6) in the vermis, paravermis and hemispheres. Ordinary two-way ANOVA: main effect of region ($F_{2,27} = 32.08$, $P < 0.0001$) and genotype ($F_{1,27} = 89.64$, $P < 0.0001$), but not of interaction ($P = 0.9488$); with post hoc two-tailed t-tests with uncorrected Fisher's LSD for effect of genotype for vermis ($t_{27}$

= 5.260, P < 0.0001), paravermis ($t_{27}$ = 5.425, P < 0.0001), and hemisphere ($t_{27}$ = 5.713, P < 0.0001).

**i**, Quantification of molecular layer (ML) area as a percent of total CB area in *eCN-DTA* mice (n=5) compared to littermate controls (n=6). Ordinary two-way ANOVA: main effect of region ($F_{2,27}$ = 37.84, P < 0.0001), but not of genotype (P = 0.3540) or interaction (P = 0.1589).

**j**, Quantification of IGL area as a percent of total CB area in *eCN-DTA* mice (n=5) compared to littermate controls (n=6). Ordinary two-way ANOVA: main effect of region ($F_{2,27}$ = 7.249, P = 0.003), but not of genotype (P = 0.0545) or interaction (P = 0.1911); with post hoc two-tailed t-tests with uncorrected Fisher's LSD for effect of genotype for hemisphere ($t_{27}$ = 2.220, P = 0.0350), but not other comparisons ($P \geq 0.05$).

**k**, Quantification of PC density in *eCN-DTA* mice (n=5) compared to littermate controls (n=6). Ordinary two-way ANOVA: main effect of region ($F_{2,18}$ = 10.23, P = 0.0011), but not of genotype (P = 0.1660) or interaction (P = 0.2277).

**l**, Quantification of PV+ MLI density in *eCN-DTA* mice (n=5) compared to littermate controls (n=6). Ordinary two-way ANOVA: no main effect of region (P = 0.2153), genotype (P = 0.1660) or interaction (P = 0.2277).

**m**, Quantification of GC density in *eCN-DTA* mice (n=5) compared to littermate controls (n=6). Ordinary two-way ANOVA: main effect of region ($F_{2,18}$ = 10.08, P = 0.0012), but not of genotype (P = 0.6051) or interaction (P = 0.9220).

**n**, Quantification of the estimated ratio of the number of PCs to PV+ MLIs in *eCN-DTA* mice (n=5) compared to littermate controls (n=6). Ordinary two-way ANOVA: no significant main effect of region (P = 0.4484), genotype (P = 0.2061) or interaction (P = 0.5916).

**o**, Quantification of the estimated ratio of the number of PCs to GCs in *eCN-DTA* mice (n=5) compared to littermate controls (n=6). Ordinary two-way ANOVA: main effect of genotype ($F_{1,27}$ = 7.013, P = 0.0134), but not of region (P = 0.0913) or interaction (P = 0.7645).

**p**, Quantification of the estimated ratio of the number of PV+ MLIs to GCs in *eCN-DTA* mice (n=5) compared to littermate controls (n=6). Ordinary two-way ANOVA: no significant main effect of region ($P = 0.0680$), genotype ($P = 0.4415$) or interaction ($P = 0.6184$).

ns, not significant: $P \geq 0.05$. Data are presented as mean values ± SEM.

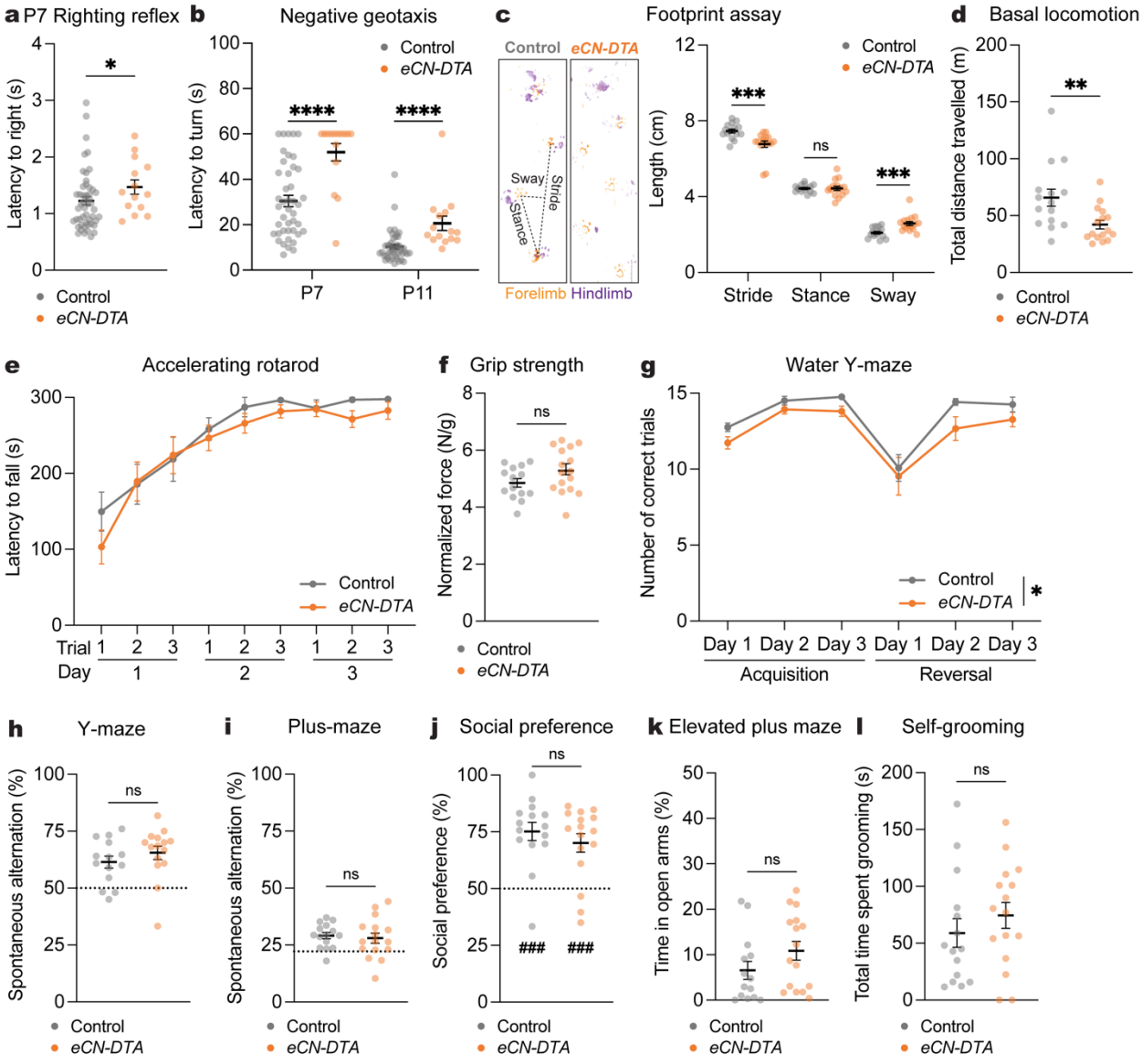


**Fig. 5 | Loss of all eCN impairs motor coordination, but not motor learning and non-motor behaviors.**

**a**, Latency to right onto four paws at P7 (*eCN-DTA* mice: n=15, littermate controls: n=43; Mann-Whitney *U* test: $U = 226$, $P = 0.0436$).

**b**, Latency to turn upward on a negative slope at P7 and P11 (*eCN-DTA* mice: n=15, littermate controls: n=43). Multiple Mann-Whitney *U* tests with Holm-Šídák correction for effect of genotype at P7 ($U = 109$, $P < 0.0001$) and at P11 ($U = 89$, $P < 0.0001$).

**c**, (left) Representative images of footprints from an *eCN-DTA* and littermate control. (right) Quantification of stride, stance, and sway (*eCN-DTA* mice: n=16, littermate controls: n=15). Multiple Mann-Whitney *U* tests for effect of genotype on stride ($U$ = 33, P = 0.00028) and sway ($U$ = 32, P = 0.00023), but not stance ($U$ = 113.5, P = 0.8073).

**d**, Total distance travelled during basal locomotion (*eCN-DTA* mice: n=16, littermate controls: n=15; two-tailed unpaired t-test: $t_{29}$ = 2.865, P = 0.0077).

**e**, Latency to fall in the accelerating rotarod test (*eCN-DTA* mice: n=15; littermate controls: n=15). Repeated measure two-way ANOVA: main effect of time ($F_{3.426,95.92}$ = 34.31, P < 0.0001), but not of genotype (P = 0.3873) or interaction (P = 0.6987).

**f**, Forelimb grip strength normalized to body weight (*eCN-DTA* mice: n=16, littermate controls: n=15; two-wailed unpaired t-test: $t_{28}$ = 1.684, P = 0.1033).

**g**, Total number of correct trials during the water Y-maze test (*eCN-DTA* mice: n=15, littermate controls: n=12). Repeated measure two-way ANOVA: main effect of time ($F_{1.667,41.67}$ = 17.92, P < 0.0001) and genotype ($F_{1,25}$ = 4.898, P = 0.0362), but not of interaction (P = 0.9183); with post hoc two-tailed t-tests with Šídák correction for effect of genotype all being $P \geq 0.05$.

**h**, Percentage of spontaneous alternations in the Y-maze (*eCN-DTA* mice: n=15, littermate controls: n=14; Mann-Whitney *U* test: $U$ = 76.50, P = 0.2209). Chance level performance is 50% (dotted line).

**i**, Percentage of spontaneous alternations in the plus-maze (*eCN-DTA* mice: n=16, littermate control: n=15; two-tailed unpaired t-test: $t_{29}$ = 0.4309, P = 0.6698). Chance level performance is 22.2% (dotted line).

**j**, Social preference (percent time nose spent within novel mouse contact zone) during the three-chamber social approach test (*eCN-DTA* mice: n=16, littermate controls: n=15; Mann-Whitney *U* test: $U$ = 102, P = 0.4945). Wilcoxon test against a null hypothesis (50%) in *eCN-DTA* mice ($W$ = 122, P = 0.0006) and littermate controls ($W$ = 116, P = 0.0002).

**k**, Percentage of time spent in the open arms of an elevated plus maze (*eCN-DTA* mice: n=16, littermate controls: n=14; Mann-Whitney *U* test: $U = 74$, $P = 0.1179$).

**l**, Total time spent self-grooming (*eCN-DTA* mice: n=16, littermate controls: n=15; Mann-Whitney *U* test: $U = 92$, $P = 0.2770$).

ns, not significant: $P \geq 0.05$. Data are presented as mean values ± SEM.

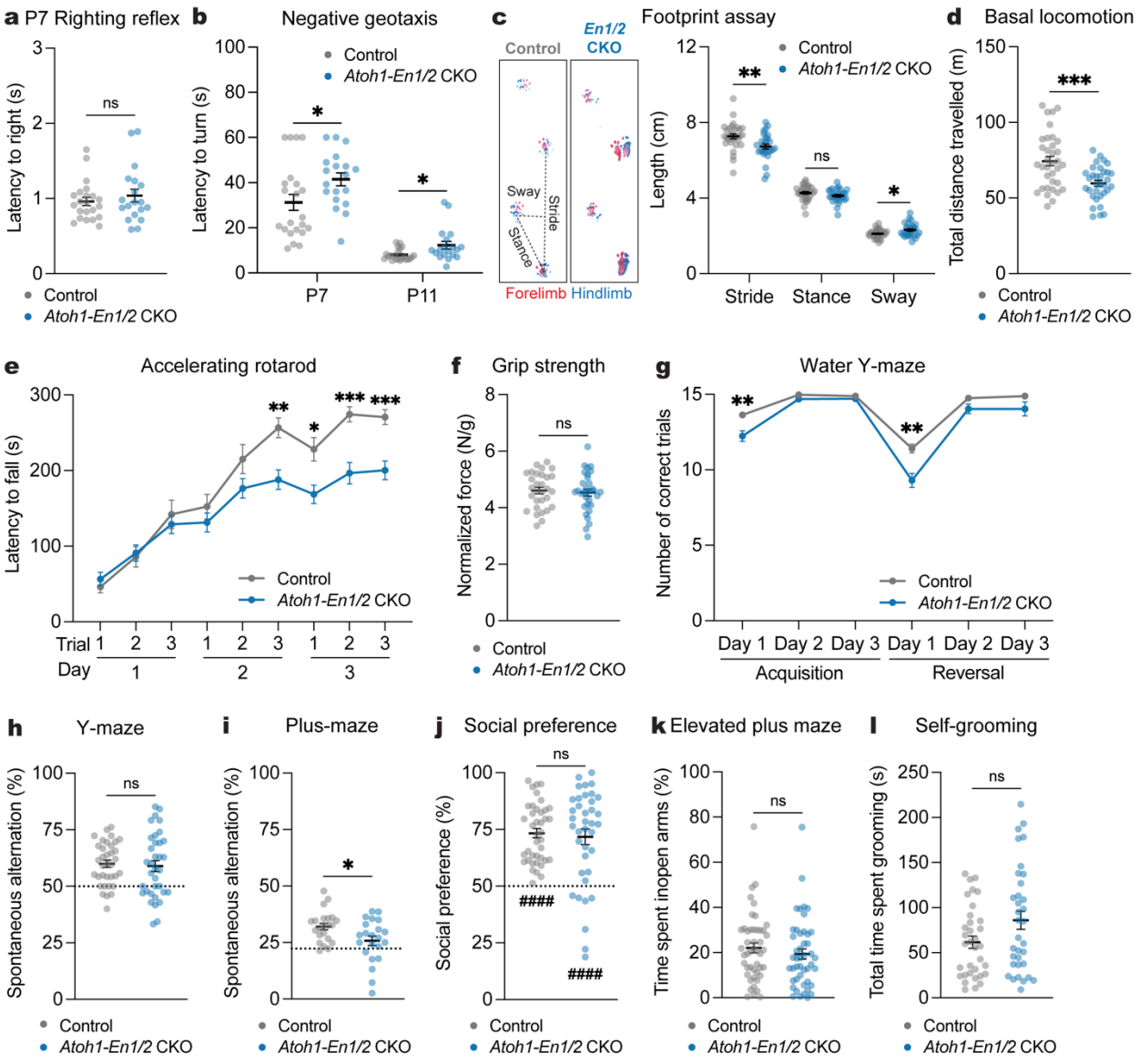


**Fig. 6 | Loss of *En1/2* in all eCN impairs motor coordination and learning, cognitive flexibility, and spatial working memory.**

**a**, Latency to right onto four paws at P7 (*Atoh1-En1/2* CKOs: n=19, littermate controls: n=22; Mann-Whitney *U* test: $U = 192.5$, $P = 0.6741$).

**b**, Latency to turn upward on a negative slope at P7 and P11 (*Atoh1-En1/2* CKOs: n=19, littermate controls: n=22). Multiple Mann-Whitney *U* tests with Holm-Šídák correction for effect of genotype at P7 ($U = 128$, $P = 0.0245$) and P11 ($U = 114.5$, $P = 0.033$).

**c**, (left) Representative images of footprints from an *Atoh1-En1/2* CKO and littermate control. (right) Quantification of stride, stance, and sway (*Atoh1-En1/2* CKOs: n=28, littermate controls: n=30). Multiple Mann-Whitney *U* tests for effect of genotype on stride ($U$ = 237, P = 0.0039) and sway ($U$ = 292.5, P = 0.047), but not stance ($U$ = 312, P = 0.0936).

**d**, Total distance travelled during basal locomotion (*Atoh1-En1/2* CKOs: n=33, littermate controls: n=35; two-tailed unpaired t-test: $t_{66}$ = 3.931, P = 0.0002).

**e**, Latency to fall in the accelerating rotarod test (*Atoh1-En1/2* CKOs: n=32, littermate controls: n=30). Repeated measure two-way ANOVA: main effect of time ($F_{5.648,338.9}$ = 90.56, P < 0.0001), genotype ($F_{1,60}$ = 7.791, P = 0.0070), and interaction ($F_{8,480}$ = 5.827, P < 0.0001); with post hoc two-tailed t-tests with Šídák correction for effect of genotype on day 2-trial 3 ($t_{59.83}$ = 3.721, P = 0.0040), day 3-trial 1 ($t_{55.69}$ = 3.019, P = 0.0338), day 3-trial 2 ($t_{55.46}$ = 4.502, P = 0.0003), day 3-trial 3 ($t_{57.98}$ = 4.416, P = 0.0004), and other comparisons ($P \geq 0.05$).

**f**, Forelimb grip strength normalized to body weight (*Atoh1-En1/2* CKOs: n=32, littermate controls: n=30; two-tailed unpaired t-test: $t_{60}$ = 0.4298, P = 0.6689).

**g**, Total number of correct trials during the water Y-maze test (*Atoh1-En1/2* CKOs: n=31, littermate controls: n=35). Repeated measure two-way ANOVA: main effect of time ($F_{3.003,192.2}$ = 118.4, P < 0.0001), genotype ($F_{1,64}$ = 21.47, P < 0.0001), and interaction ($F_{5,320}$ = 5.101, P = 0.0002); with post hoc two-tailed t-tests with Šídák correction for effect of genotype on Acquisition Day 1 ($t_{42.50}$ = 3.583, P = 0.0052), Reversal Day 1 ($t_{52.14}$ = 3.821, P = 0.0021), and no other comparisons ($P \geq 0.05$).

**h**, Percentage of spontaneous alternations in the Y-maze (n=35 per genotype; two-tailed unpaired t-test: $t_{68}$ = 0.3622, P = 0.7183). Chance level performance is 50% (dotted line).

**i**, Percentage of spontaneous alternations in the plus-maze (n=22 per genotype; two-tailed unpaired t-test: $t_{42}$ = 2.486, P = 0.0170). Chance level performance is 22.2% (dotted line).

**j**, Social preference (percent time nose spent within novel mouse contact zone) during the three-chamber social approach test (*Atoh1-En1/2* CKOs: n=38, littermate controls: n=40; Mann-Whitney *U* test: $U = 723$, $P = 0.7167$). Wilcoxon test against a null hypothesis (50%) in *Atoh1-En1/2* CKOs ($W = 605$, $P < 0.0001$) and littermate controls ($W = 820$, $P < 0.0001$).

**k**, Percentage of time spent in the open arms of an elevated plus maze (*Atoh1-En1/2* CKOs: n=46, littermate control: n=47; Mann-Whitney *U* test: $U = 923$, $P = 0.2266$).

**j**, Total time spent self-grooming (n=34 per genotype; Mann-Whitney *U* test: $U = 455$, $P = 0.1336$).

ns, not significant: $P \geq 0.05$. Data are presented as mean values ± SEM.

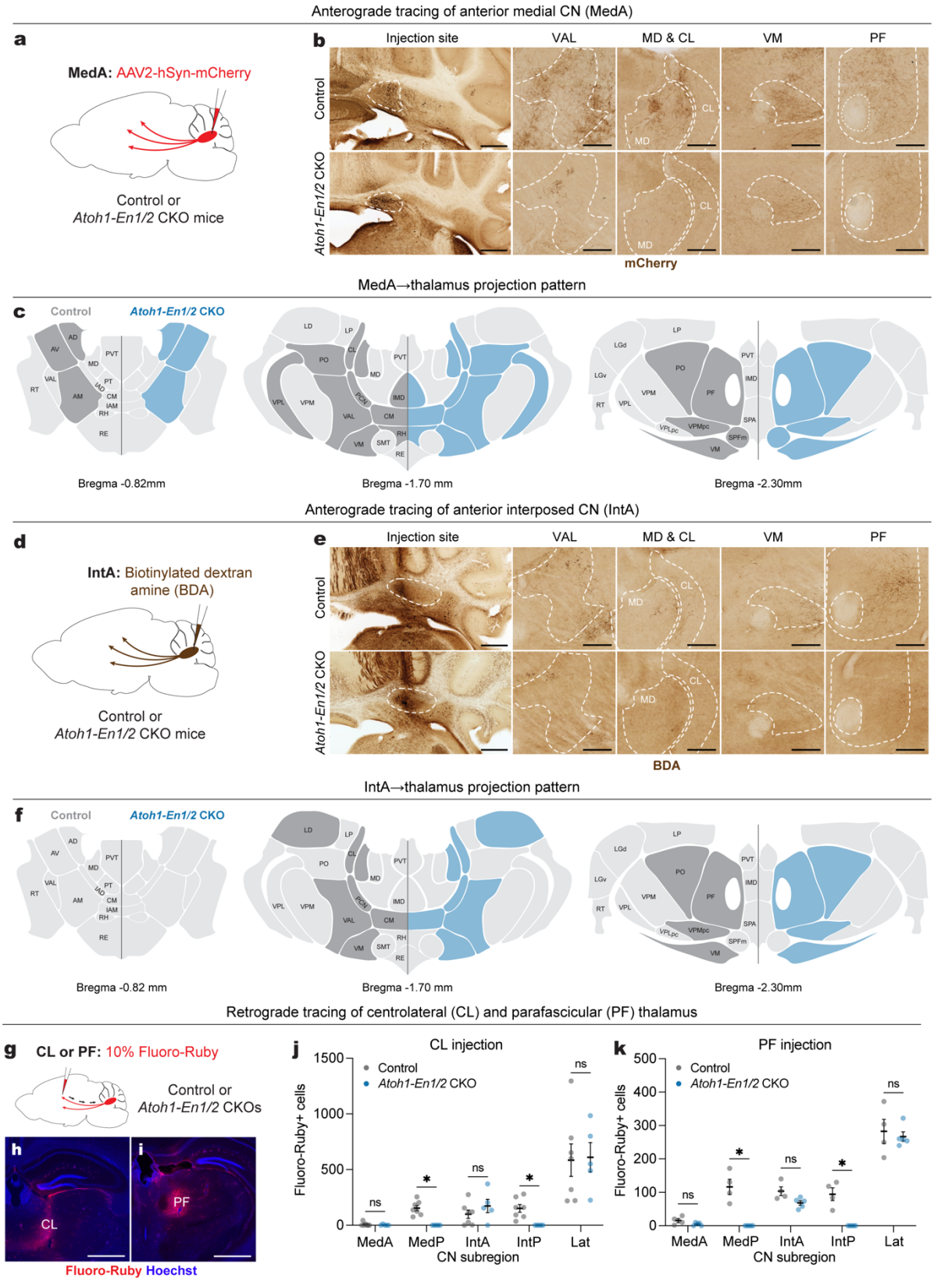

**Fig. 7 | *Atoh1-En1/2* CKOs have reduced cerebellothalamic projections, but no ectopic cerebellothalamic projections.**

**a**, Schematic of anterograde tracing of MedA CN cells in adult *Atoh1-En1/2* CKOs and littermate controls.

**b**, Representative images of coronal sections showing injection site and mCherry+ axon terminals (brown) in various thalamic regions from an *Atoh1-En1/2* CKO and littermate control. Scale bar: injection site = 1 mm and mCherry images = 250 um.

**c**, Summary of mCherry+ axon terminals observed in thalamic nuclei of *Atoh1-En1/2* CKOs (blue) versus littermate controls (dark grey) on three representative coronal planes adapted from Allen Brain Atlas. Blue indicates reduced density.

**d**, Schematic of anterograde tracing of anterior interposed CN (IntA) cells in adult *Atoh1-En1/2* CKOs and littermate controls.

**e**, Representative images of coronal sections showing injection site and biotinylated dextran amine (BDA)+ axon terminals (brown) in various thalamic regions from an *Atoh1-En1/2* CKO and littermate control. Scale bar: injection site = 1 mm and BDA images = 250 um.

**f**, Summary of BDA+ axon terminals observed in thalamic nuclei of *Atoh1-En1/2* CKOs (blue) and littermate controls (dark grey) versus on three representative coronal planes adapted from Allen Brain Atlas. Blue indicates reduced density.

**g**, (top) Schematic of retrograde tracing in adult *Atoh1-En1/2* CKOs and littermate controls.

**h**,**i**, Representative images of the injection site of Fluoro-Ruby (red) and Hoechst (blue) in centrolateral thalamus (CL, **h**) and parafascicular thalamus (PF, **i**). Scale bars = 1 mm.

**j**, Quantification of Fluoro-Ruby+ cells in CN subregions that are retrogradely labeled from CL injection. Multiple Mann-Whitney *U* tests with Holm-Šídák correction for effect of genotype on MedP ($U$ = 0, P = 0.0126) and IntP ($U$ = 0, P = 0.0126), but not on MedA ($U$ = 15.5, P = 0.9400), IntA ($U$ = 11, P = 0.6882), and Lat ($U$ = 15, P = 0.9400).

**k**, Quantification of Fluoro-Ruby+ cells in CN subregions that are retrogradely labeled from PF injection. Multiple Mann-Whitney *U* tests with Holm-Šídák correction for effect of genotype on MedP ($U = 0$, $P = 0.0390$) and IntP ($U = 0$, $P = 0.0390$), but not on MedA ($U = 3.5$, $P = 0.2516$), IntA ($U = 1$, $P = 0.0922$), and Lat ($U = 10$, $P > 0.9999$).

Abbreviations: AD=Anterodorsal nucleus; AM=Anteromedial nucleus; AV=Anteroventral nucleus of thalamus; CL=Central lateral nucleus; CM=Central medial nucleus; IAD=Interanterodorsal nucleus; IAM=Interanteromedial nucleus; IMD=Intermediodorsal nucleus; LD=Lateral dorsal nucleus of thalamus; LGv=Ventral part of the lateral geniculate complex; LP=Lateral posterior nucleus; MD=Mediodorsal nucleus of thalamus; PCN=Paracentral nucleus; PF=Parafascicular nucleus; PO=Posterior complex; PT=Parataenial nucleus; PVT=Paraventricular nucleus; RE=Nucleus of reuniens; RH=Rhomboid nucleus; RT=Reticular nucleus; SMT=Submedial nucleus; SPFm=Subparafascicular nucleus, magnocellular part; VAL=Ventral anterior-lateral complex; VM=Ventral medial nucleus; LGd=Dorsal part of the lateral geniculate complex; VPM=Ventral posteromedial nucleus; VPL=Ventral posterolateral nucleus; SPA=Subparafascicular area; VPMpc=Ventral posteromedial nucleus, parvicellular part; VPLpc=Ventral posterolateral nucleus, parvicellular part. ns, not significant: $P \geq 0.05$. Data are presented as mean values ± SEM.

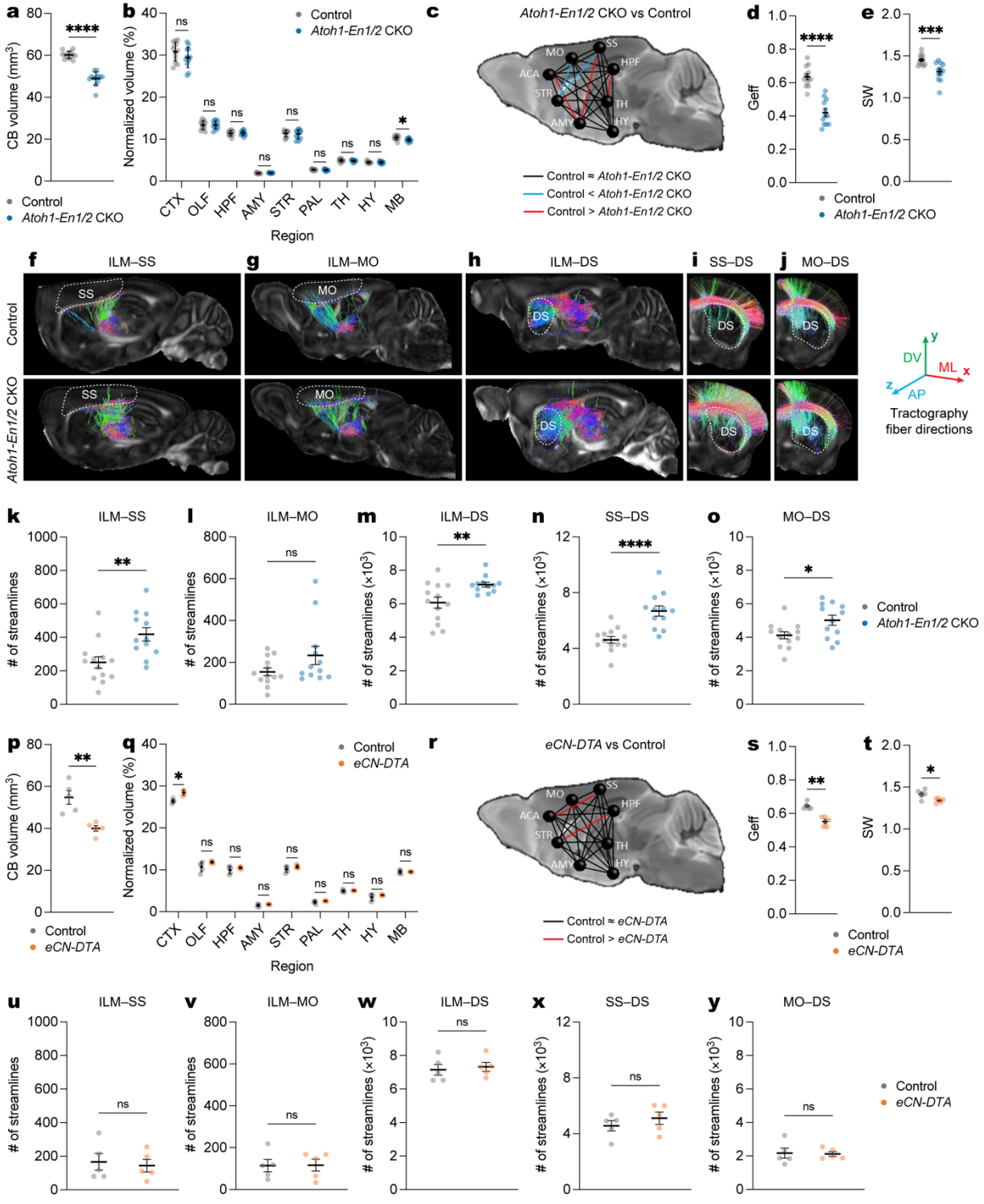


**Fig 8 | Diffusion MRI shows *Atoh1-En1/2* CKOs have connectivity changes outside the cerebellum that are distinct from *eCN-DTA* mice.**

**a**, Quantification of cerebellar (CB) volume in *Atoh1-En1/2* CKOs (n=12) compared to littermate controls (n=13) (two-tailed unpaired t-test: $t_{23} = 11.15$, $P < 0.0001$).

**b**, Quantification of regional volumes normalized to forebrain plus midbrain combined volume in *Atoh1-En1/2* CKOs (n=12) compared to littermate controls (n=13). Two-tailed unpaired t-tests to test for effect of genotype on MB ($t_{23} = 2.834$, $P = 0.0094$) and other comparisons $P \geq 0.05$.

**c**, Schematic representation of global connectivity in *Atoh1-En1/2* CKOs compared to littermate controls. Black lines indicate no significant difference, red lines indicate reduced connectivity in *Atoh1-En1/2* CKOs and blue lines indicate increased connectivity in *Atoh1-En1/2* CKOs compared to littermate controls (two-tailed unpaired t-tests with Welch's correction).

**d**, Quantification of global efficiency (Geff; *Atoh1-En1/2* CKOs: n=12, littermate controls: n=13; two-tailed unpaired t-test: $t_{23} = 7.876$, $P < 0.0001$).

**e**, Quantification of small worldness (SW; *Atoh1-En1/2* CKOs: n=12, littermate controls: n=13; two-tailed unpaired t-test: $t_{23} = 3.913$, $P = 0.0007$).

**f-j**, Representative images of ILM-SS (**f**), ILM-MO (**g**), ILM-DS (**h**), SS-DS (**i**), MO-DS (**j**) tractographies in right hemisphere of one *Atoh1-En1/2* CKO and littermate control. Target regions are outlined in dotted lines. The color of streamlines indicates their orientations, as indicated by the colored arrows on the right. Abbreviations: AP=anteroposterior; ML=mediolateral; DV=dorsoventral.

**k-o**, Quantification of average (left plus right hemispheres) of ILM-SS tractography (**k**, two-tailed unpaired t-test: $t_{23} = 3.225$, $P = 0.0038$), ILM-MO tractography (**l**, two-tailed unpaired t-test: $t_{23} = 1.701$, $P = 0.1024$), ILM-DS tractography (**m**, two-tailed unpaired t-test: $t_{23} = 2.902$, $P = 0.0080$), SS-DS tractography (**n**, two-tailed unpaired t-test: $t_{23} = 4.813$, $P < 0.0001$), and MO-DS tractography (**o**, two-tailed unpaired t-test: $t_{23} = 2.515$, $P = 0.0194$) in *Atoh1-En1/2* CKO compared to littermate controls (*Atoh1-En1/2* CKOs: n=12, littermate controls: n=13).

**p**, Quantification of cerebellar (CB) volume in *eCN-DTA* mice compared to littermate controls (n=5 per genotype; two-tailed unpaired t-test: $t_{8} = 4.295$, $P = 0.0026$).

**q**, Quantification of regional volume normalized to forebrain plus midbrain combined volume in *eCN-DTA* mice (n=5) compared to littermate controls (n=5). Two-tailed unpaired t-tests to test for effect of genotype on CTX ($t_8 = 5.876$, $P = 0.0004$) and other comparisons $P \geq 0.05$.

**r**, Schematic representation of global connectivity for *eCN-DTA* mice compared to littermate controls. Black lines indicate no significant difference and red lines indicate reduced connectivity in *eCN-DTA* mice compared to littermate controls (two-tailed unpaired t-tests with Welch's correction).

**s**, Quantification of global efficiency (Geff; n=5 per genotype; two-tailed unpaired t-test: $t_8 = 2.535$, $P = 0.035$).

**t**, Quantification of small worldness (SW; n=5 per genotype; two-tailed unpaired t-test: $t_8 = 1.591$, $P = 0.1503$).

**u-y**, Quantification of average (left and right hemispheres) ILM-SS tractography (**u**, two-tailed unpaired t-test: $t_8 = 0.3742$, $P = 0.7180$), ILM-SS tractography (**v**, two-tailed unpaired t-test: $t_8 = 0.0516$, $P = 0.9601$), ILM-SS tractography (**w**, two-tailed unpaired t-test: $t_8 = 0.4177$, $P = 0.6871$), ILM-SS tractography (**x**, two-tailed unpaired t-test: $t_8 = 0.9447$, $P = 0.3725$), and ILM-SS tractography (**y**, two-tailed unpaired t-test: $t_8 = 0.1414$, $P = 0.8911$) in *eCN-DTA* mice compared to littermate controls (n=5 per genotype).

Abbreviations: CTX=cerebral cortex; OLF=olfactory bulb; HPF=hippocampal formation; AMY=amygdala; STR=striatum; PAL=pallidum; TH=thalamus; HY=hypothalamus; MB=midbrain; HB=hindbrain; CB=cerebellum; ILM=intralaminar nuclei; SS=primary somatosensory cortex; MO=primary motor cortex; DS=dorsal striatum. ns, not significant: $P \geq 0.05$. Data are presented as mean values ± SD for **a**, **j** and mean value ± SEM for **d**,**e**,**k-o**,**s-y**.

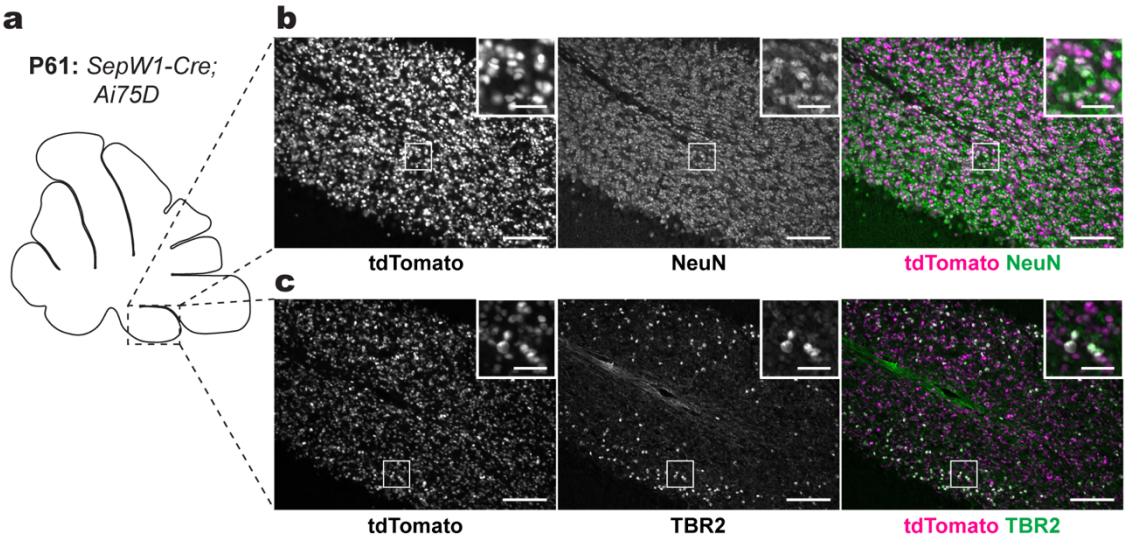


**Supplementary Fig. 1 | *SepW1-Cre* recombines in granule cells and unipolar brush cells.**

**a**, Schematic representation of sagittal plane of an adult mouse showing where **b** and **c** images were acquired.

**b**, Immunofluorescence images of tdTomato (magenta) and NeuN (green) co-expressing granule cells in adult *SepW1-Cre; Ai75D* mice. Scale bars = 100 um; inset scale bars = 25 um.

**c,** Immunofluorescence images of tdTomato (magenta) and TBR2 (green) co-expressing unipolar brush cells in adult *SepW1-Cre; Ai75D* mice. Scale bars = 100 um.

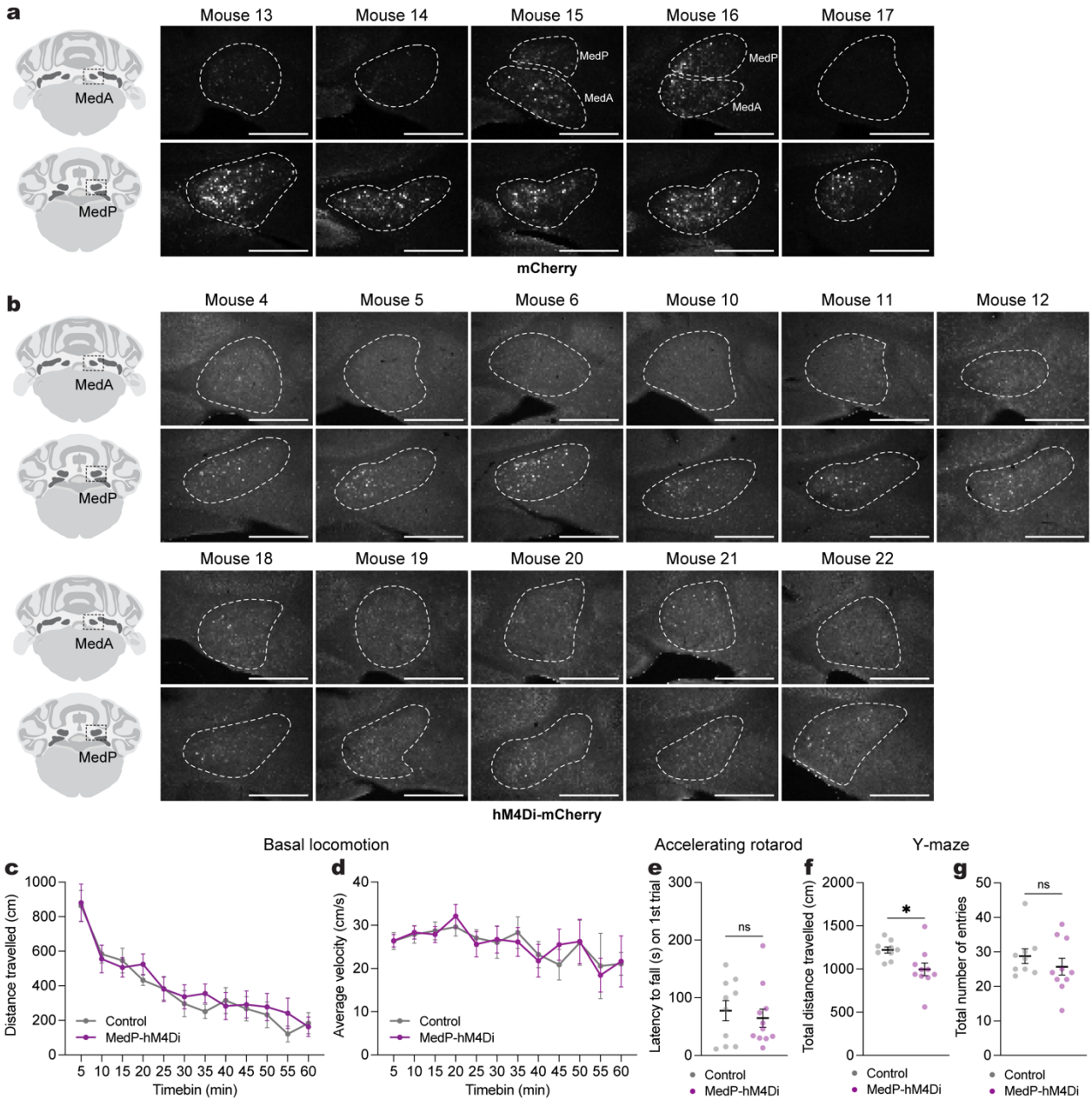


**Supplementary Fig. 2 | Motor coordination during behavior is largely intact after acute chemogenetic inhibition of adult MedP eCN.**

**a**, Schematic (left) and representative images of mCherry expression (right) in MedA (upper row) and MedP (lower row) CN in the five control mice. The other six control mice were Cre-negative (treated with CNO). Scale bars = 500 um.

**b**, Schematic (left) and representative images of hM4Di-mCherry expression (right) in MedA and MedP CN in the eleven MedP-hM4Di mice. Scale bars = 500 um.

**c**, Distance travelled during basal locomotion by 5 min time bins (n=11 per group). Repeated measure two-way ANOVA: no main effect of time (P = 0.0609), chemogenetics (P = 0.9730) or interaction (P = 0.9975).

**d**, Average velocity during basal locomotion by 5 min time bins (n=11 per group). Repeated measure two-way ANOVA: main effect of time ($F_{4.870,97.41}$ = 28.43, P < 0.0001), but not of chemogenetics (P = 0.7000) or interaction (P = 0.8668).

**e**, Latency to fall on the first trial of the accelerating rotarod test (MedP-hM4Di: n=11, control: n=10; Mann Whitney *U* test: *U* = 48, P = 0.6412).

**f**, Total distance travelled in the Y-maze (MedP-hM4Di: n=10, control: n=9; two-tailed unpaired t-test: $t_{17}$ = 2.648, P = 0.0169).

**g**, Total number of arm entries in the Y-maze (MedP-hM4Di: n=10, control: n=9; Mann Whitney *U* test: *U* = 30, P = 0.2326).

ns, not significant: $P \geq 0.05$. Data are presented as mean values ± SEM.

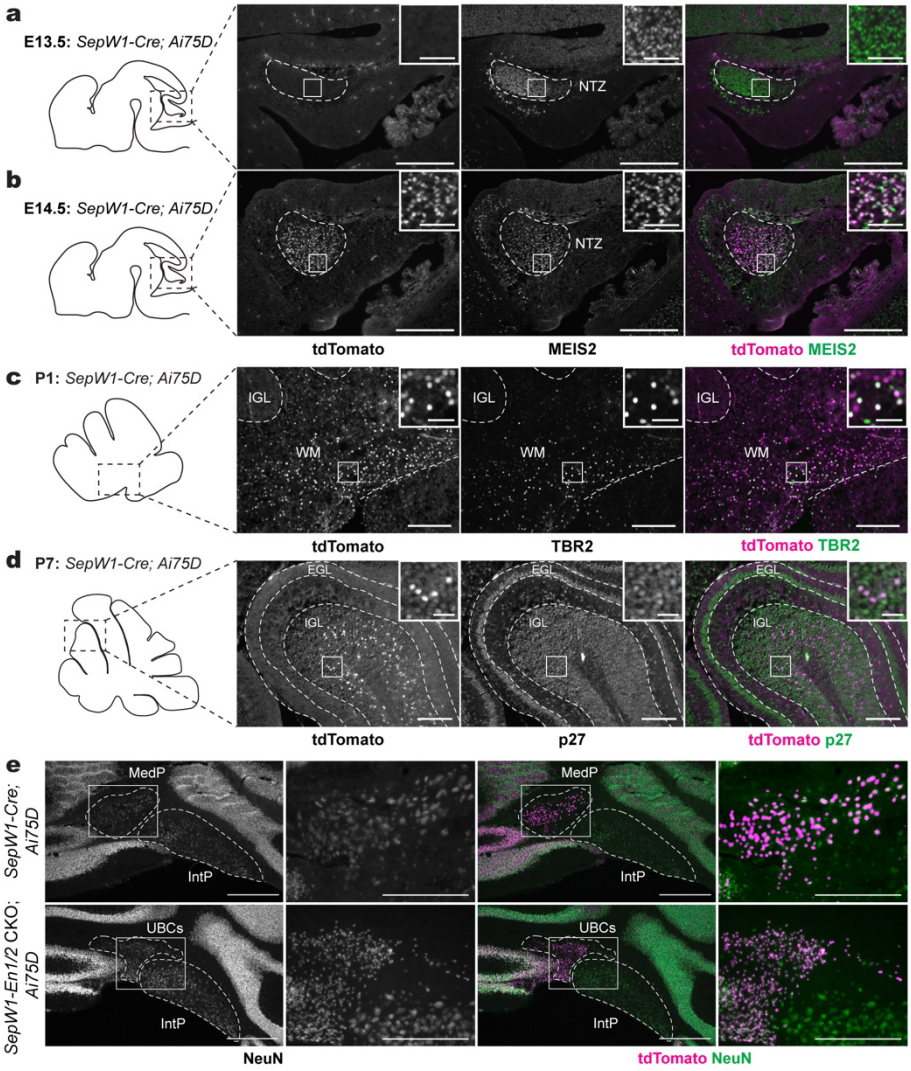


**Supplementary Fig. 3 | *SepW1-Cre* recombines in the developing excitatory cerebellar neurons and *SepW1-En1/2* CKOs have preferential loss of MedP CN.**

**a,b,** Schematic (left) and representative images (right) of sagittal sections stained for tdTomato (magenta) in *SepW1-Cre; Ai75D* mice showing recombination at E14.5 (**b**) but not at E13.5 (**a**) in eCN in the NTZ marked by MEIS2 (green). NTZ = nuclear transitory zone.

**c**, Schematic (left) and representative sagittal image (right) of tdTomato (magenta) expression in *SepW1-Cre; Ai75D* mice showing recombination at postnatal day (P1) in TBR2+ (green) unipolar brush cells.

**d**, Schematic (left) and representative sagittal images (right) of tdTomato (magenta) expression in *SepW1-Cre; Ai75D* mice showing recombination at P7 in p27+ (green) differentiated granule cells in the internal granule cell layer (IGL), but not in proliferating granule cell precursors in the external granule cell layer (EGL). Scale bars = 100 um; inset scale bars = 20 um.

**e**, Representative images of coronal sections stained for NeuN (single channel), NeuN (green) and tdTomato (magenta) co-labeling in the posterior CN of *SepW1-Cre; Ai75D* and *SepW1-En1/2* CKO; *Ai75D* mice (*SepW1-Cre/+; En1*$^{flox/flox}$*; En2*$^{flox/flox}$*; R26*$^{LSL\text{-}nls\text{-}tdTomato/+}$). NeuN labeling near the MedP of mutants are ectopic unipolar brush cells that are not TBR2+ or MEIS2+ (confirmed in Krishnamurthy et al., 2024). Abbreviations: MedP=Posterior medial; IntP=Posterior interposed. Scale bars for low magnification = 500 um; scale bars for high magnification = 100 um.

Scale bars in **a**, **b**, **c** = 250 um; inset scale bars = 50 um.

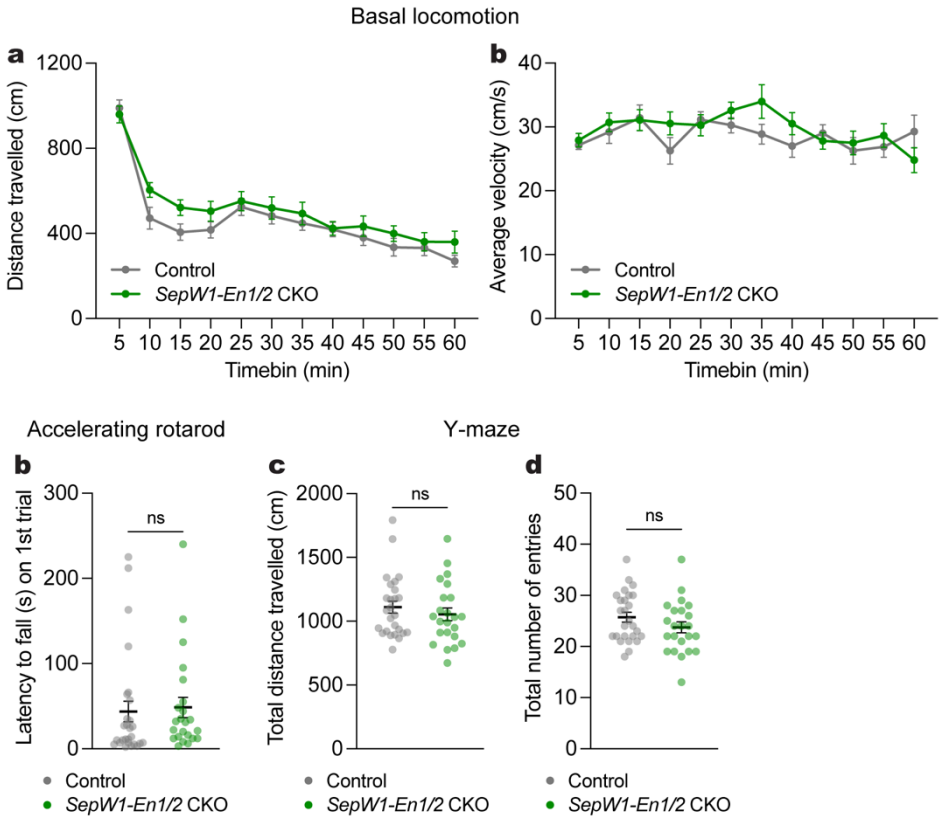


**Supplementary Fig. 4 | Motor coordination during behaviors is not altered in *SepW1-En1/2* CKOs.**

**a**, Distance travelled during basal locomotion by 5 min time bins (*SepW1-En1/2* CKOs: n=24, littermate controls: n=27). Repeated measure two-way ANOVA: main effect of time ($F_{5.410,265.1}$ = 71.20, P < 0.0001), but not of genotype (P = 0.2081) or interaction (P = 0.2042).

**b**, Average velocity during basal locomotion by 5 min time bins (*SepW1-En1/2* CKOs: n=24, littermate controls: n=27). Repeated measure two-way ANOVA: main effect of time ($F_{7.996,390.3}$ = 2.386, P = 0.0162), but not of genotype (P = 0.3429) or interaction (P = 0.1806).

**c**, Latency to fall on the first trial of the accelerating rotarod test (*SepW1-En1/2* CKOs: n=23, littermate controls: n=27; Mann-Whitney *U* test: *U* = 240.5, P = 0.1759).

**d**, Total distance travelled in the Y-maze (*SepW1-En1/2* CKOs: n=23, littermate controls: n=26; Mann-Whitney *U* test: *U* = 266, P = 0.5184).

**e**, Total number of arm entries in the Y-maze (*SepW1-En1/2* CKOs: n=23, littermate controls: n=26; two-tailed unpaired t-test: $t_{47} = 1.397$, $P = 0.1689$).

ns, not significant: $P \geq 0.05$. Data are presented as mean values ± SEM.

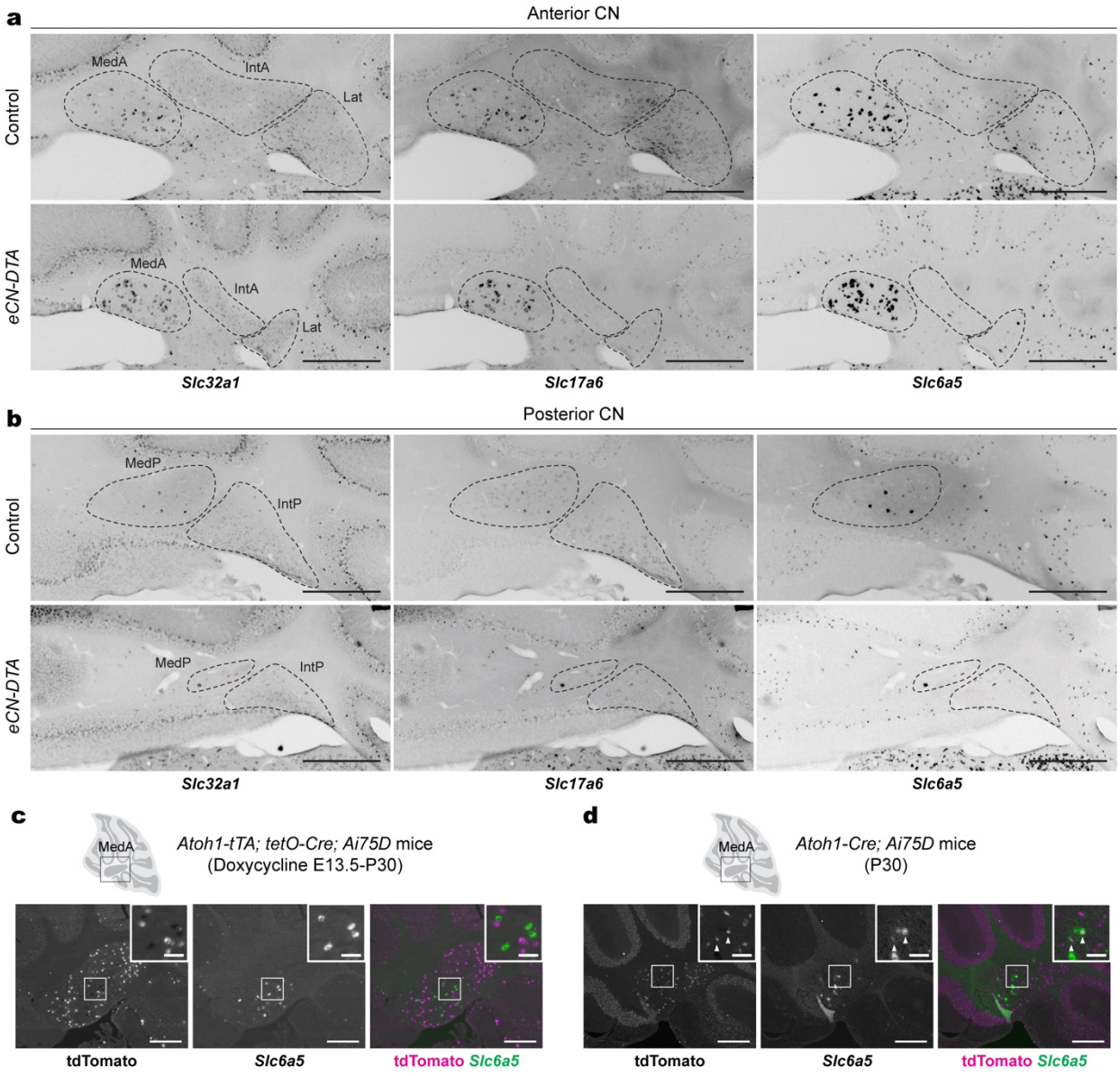


**Supplementary Fig. 5 | Remaining CN neurons in *eCN-DTA* mice are inhibitory neurons.**

**a**,**b**, Representative images of coronal sections of triple RNA *in situ* analysis of *Slc32a1*, *Slc17a6* and *Slc6a5* with single channel expression in anterior (**a**) and posterior (**b**) CN of *eCN-DTA* mice and littermate controls. Dotted outlines indicate the CN subregions. Abbreviations: MedA=Anterior medial; MedP=Posterior medial; IntA=Anterior interposed; IntP=Posterior interposed; Lat=Lateral. Scale bars = 500 um.

**c**, Representative images from the MedA region of double RNA *in situ* hybridization and immunofluorescence for *Slc6a5* and tdTomato in P30 *Atoh1-tTA; tetO-Cre; Ai75D* (*Atoh1-tTA/+;*

*tetO-Cre; R26*$^{LSL\text{-}nls\text{-}tdTomato/+}$) mice treated with doxycycline from E13.5 until P30. *Slc6a5*+ CN neurons are not labeled by the *Atoh1-tTA* transgene (tdTomato as a readout). Scale bars = 250 um; inset scale bars = 50 um.

**d**, Representative images from the MedA region of double RNA *in situ* hybridization and immunofluorescence for *Slc6a5* and tdTomato in P30 *Atoh1-Cre; Ai75D* mice. Subset of *Slc6a5*+ CN neurons are labeled by the *Atoh1-Cre* transgene (tdTomato as a readout). Scale bars = 250 um; inset scale bars = 50 um.

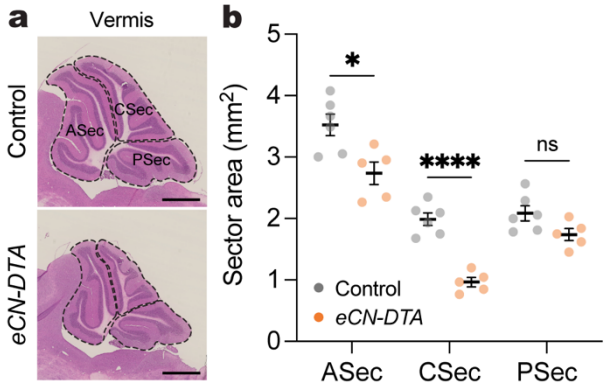


**Supplemental Fig. 6 | *eCN-DTA* mice show reduced growth in the anterior and central vermis.**

**a**, Representative images of H&E labeled vermis in *eCN-DTA* and littermate control mice. Anterior, central and posterior sectors (ASec, CSec, and PSec, respectively) are outlined in dotted lines. Scale bars = 1 mm.

**b**, Quantification of sector area in eCN-DTA mice (n=5) compared to littermate controls (n=6). Ordinary two-way ANOVA: main effect of genotype ($F_{1,9}$ = 17.96, P = 0.0022), main effect of sector ($F_{1.693,15.23}$ = 264.6, P < 0.0001), and interaction ($F_{2,18}$ = 10.65, P = 0.0009); with post hoc two-tailed t-tests with uncorrected Fisher's LSD for effect of genotype for ASec ($t_{8.779}$ = 3.100, P = 0.0131), CSec ($t_{8.706}$ = 8.001, P < 0.0001), and PSec (P = 0.0540).

ns, not significant: $P \geq 0.05$. Data are presented as mean ± SEM.

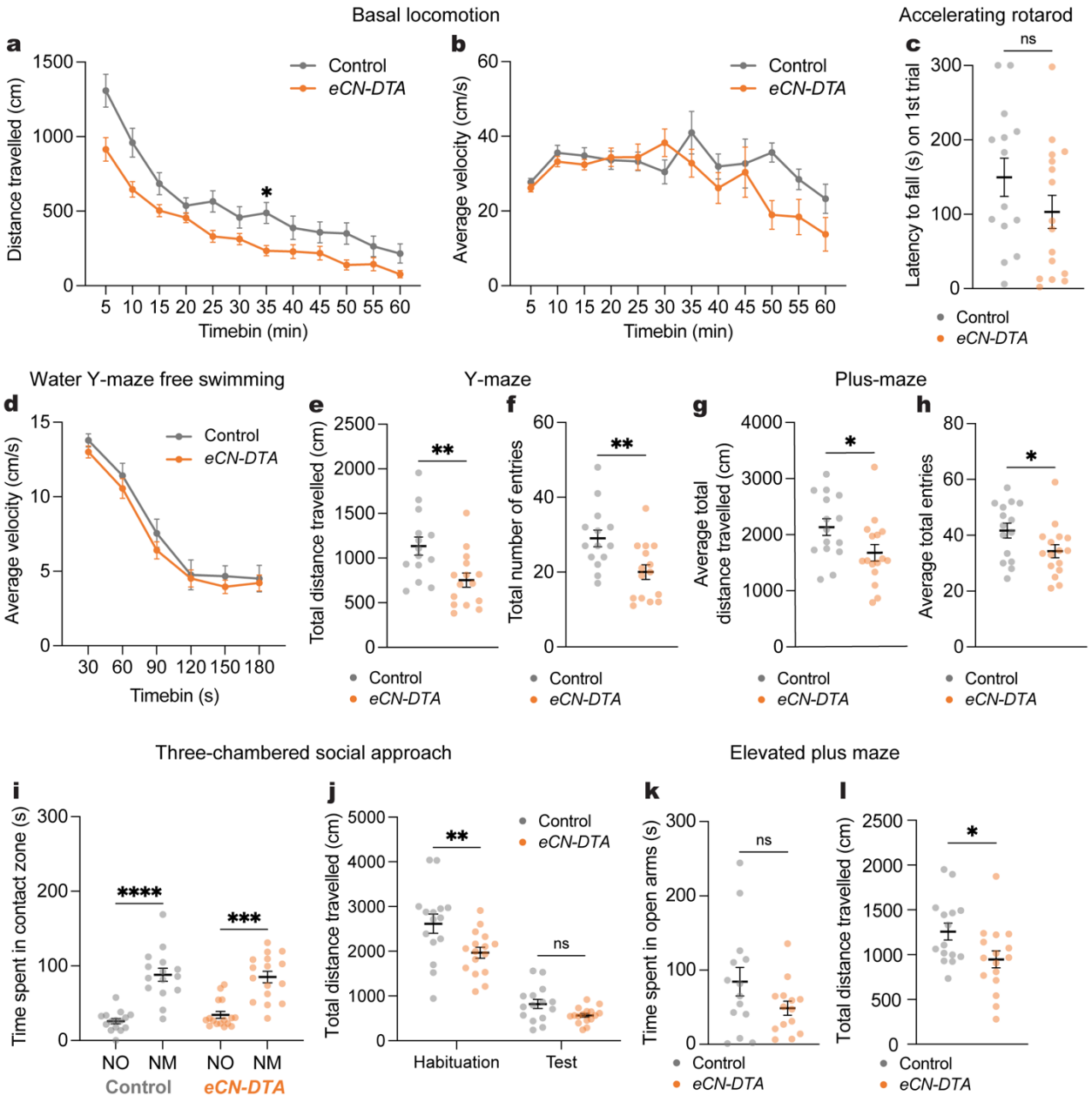


**Supplementary Fig. 7 | Motor coordination during behavior is task-dependent in *eCN-DTA* mice.**

**a**, Distance travelled during basal locomotion by 5 min time bins (*eCN-DTA* mice: n=16, littermate controls: n=15). Repeated measure two-way ANOVA: main effect of time ($F_{5.410,156.9}$ = 100.4, P < 0.0001), main effect of genotype ($F_{1,29}$ = 8.210, P = 0.0077), and interaction ($F_{11,319}$ = 2.629, P =

0.0032); with post hoc two-tailed t-tests with Šídák correction for effect of genotype for 30-35 min ($t_{20.48}$ = 3.245, P = 0.0466) but no other comparisons (P ≥ 0.05).

**b**, Average velocity during basal locomotion by 5 min time bins (*eCN-DTA* mice: n=16, littermate controls: n=15). Repeated measure two-way ANOVA: main effect of time ($F_{5.283,153.2}$ = 5.057, P = 0.0002), but not of genotype (P = 0.0883) or interaction (P = 0.0589).

**c**, Latency to fall on the first trial of the accelerating rotarod test (*eCN-DTA* mice: n=16, littermate controls: n=14; Mann-Whitney *U* test: *U* = 72.50, P = 0.1034).

**d**, Average swimming velocity during a three-minute swim (*eCN-DTA* mice: n=16, littermate controls: n=15). Repeated measure two-way ANOVA: main effect of time ($F_{5,145}$ = 137.8, P < 0.0001), but not of genotype (P = 0.3829) or interaction (P = 0.9235).

**e**, Total distance travelled during the Y-maze test (*eCN-DTA* mice: n=15, littermate controls: n=14; two-tailed unpaired t-test: $t_{27}$ = 3.027, P = 0.0054).

**f**, Total number of arm entries in the Y-maze (*eCN-DTA* mice: n=15, littermate controls: n=14; two-tailed unpaired t-test: $t_{27}$ = 2.969, P = 0.0062).

**g,** Average total distance travelled during two days of testing in the plus-maze (*eCN-DTA* mice: n=16, littermate controls: n=15: two-tailed unpaired t-test: $t_{29}$ = 2.211, P = 0.0350).

**h,** Average total number of entries during two days of testing in the plus-maze (*eCN-DTA* mice: n=16, littermate controls: n=15: two-tailed unpaired t-test: $t_{29}$ = 2.114, P = 0.0432).

**i,** Total time in which the animal's nose was within the contact zone of a novel mouse (NM) and novel object (NO) during the three-chambered social approach test (*eCN-DTA* mice: n=16, littermate controls: n=15). Repeated measure two-way ANOVA: main effect of location ($F_{1,29}$ = 53.64, P < 0.0001), but not of genotype (P = 0.5828) or interaction (P=0.4639); with post hoc two-tailed t-tests with Šídák correction for effect of location for littermate controls ($t_{29}$ = 5.614, P < 0.0001) and *eCN-DTA* mice ($t_{29}$ = 4.731, P = 0.0001) mice.

**j**, Total distance travelled during habituation and test phases of the three-chambered social approach test (*eCN-DTA* mice: n=16, littermate controls: n=15). Repeated measure two-way

ANOVA: main effect of phase ($F_{1,29}$ = 358.9, P < 0.0001), genotype ($F_{1,29}$ = 7.130, P = 0.0123), and interaction ($F_{1,29}$ = 5.461, P = 0.0266); with post hoc two-tailed t-tests with Šídák correction for effect of genotype for the habituation phase ($t_{58}$ = 3.433, P = 0.0022) but not test phase ($t_{58}$ = 1.344, P = 0.3343).

**k**, Total time spent in the open arms of an elevated plus maze (*eCN-DTA* mice: n=14, littermate controls: n=14; two-tailed unpaired t-test: $t_{26}$ = 1.662, P = 0.1086).

**l**, Total distance travelled in an elevated plus maze (*eCN-DTA* mice: n=15, littermate controls: n=16; two-tailed unpaired t-test: $t_{29}$ = 2.320, P = 0.0276).

ns, not significant: $P \geq 0.05$. Data are presented as mean values ± SEM.

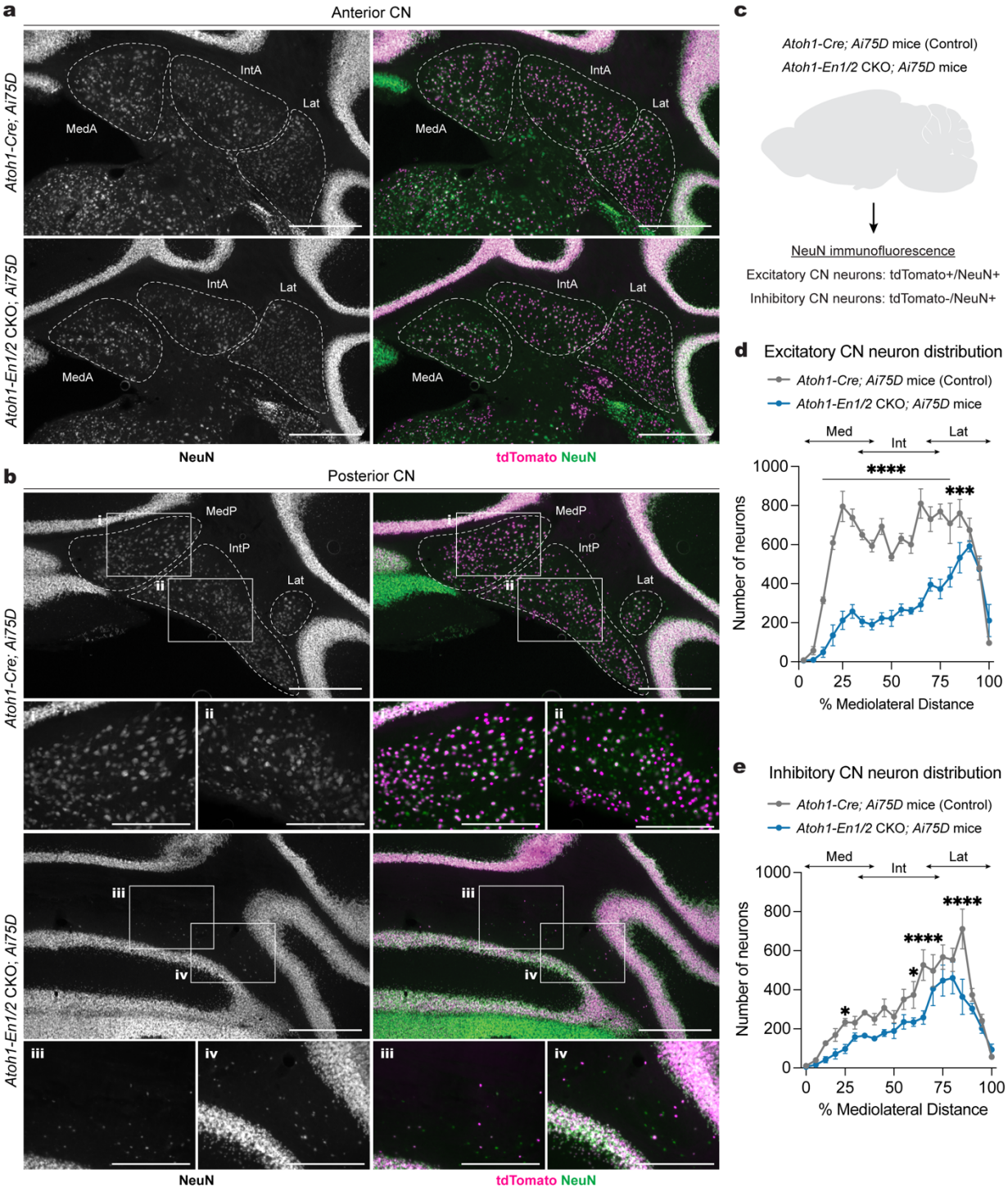


**Supplementary Fig. 8 | Inhibitory CN neurons are significantly reduced across the mediolateral axis in *Atoh1-En1/2* CKOs.**

**a**,**b**, Representative images of immunofluorescent staining NeuN (singe channel) and NeuN (green), tdTomato (magenta) co-labeling in of coronal sections of the anterior (**a**) and posterior

(**b**) CN of *Atoh1-Cre; Ai75D* and *Atoh1-En1/2* CKO; *Ai75D* mice. Abbreviations: MedA=Anterior medial; MedP=Posterior medial; IntA=Anterior interposed; IntP=Posterior interposed; Lat=Lateral. Scale bars = 500 um, scale bars for **i-iv** = 100 um.

**c**, Experimental design for quantifying excitatory and inhibitory CN neurons in *Atoh1-Cre; Ai75D* (*Atoh1-Cre/+; R26*$^{LSL\text{-}nls\text{-}tdTomato/+}$) and *Atoh1-En1/2* CKO; *Ai75D* (*Atoh1-Cre/+; En1*$^{flox/flox}$*; En2*$^{flox/flox}$*; R26*$^{LSL\text{-}nls\text{-}tdTomato/+}$) mice.

**d**, Quantification and distribution of excitatory CN neurons in half of the cerebellum (every second section). Two-way ANOVA: main effect of % mediolateral distance ($F_{19,120}$ = 31.38, P < 0.0001), genotype ($F_{1,120}$ = 400.1, P < 0.0001), and interaction ($F_{19,120}$ = 8.830, P < 0.0001); with post hoc two-tailed t-tests with uncorrected Fisher's LSD for effect of genotype for bin 10-80% (list of t value for each bin: $t_{120}$ = 4.029, 7.169, 8.828, 7.267, 6.726, 6.087, 7.103, 4.759, 5.516, 5.122, 7.85, 5.06, 6, 4.169; all P values: P < 0.0001), for bins 80-85% ($t_{120}$ = 3.435, P = 0.0008), and no other comparisons ($P \geq 0.05$). Abbreviations: Med=medial; Int=interposed; Lat=lateral.

**e**, Quantification and distribution of inhibitory CN neurons in half of the cerebellum (every second section). Two-way ANOVA: main effect of % mediolateral distance ($F_{19,120}$ = 23.97, P < 0.0001), and genotype ($F_{1,120}$ = 50.81, P < 0.0001), but not interaction ($F_{19,120}$ = 1.659, P = 0.0531); with post hoc two-tailed t-tests with uncorrected Fisher's LSD for effect of genotype for bin 20-25% ($t_{120}$ = 2.094, P = 0.0384), bin 55-60% ($t_{120}$ = 2.141, P = 0.0343), bin 60-65% ($t_{120}$ = 4.114, P < 0.0001), bin 80-85% ($t_{120}$ = 5.316, P <0.0001), and no other comparisons ($P \geq 0.05$). Abbreviations: Med=medial; Int=interposed; Lat=lateral.

Data are presented as mean values ± SEM.

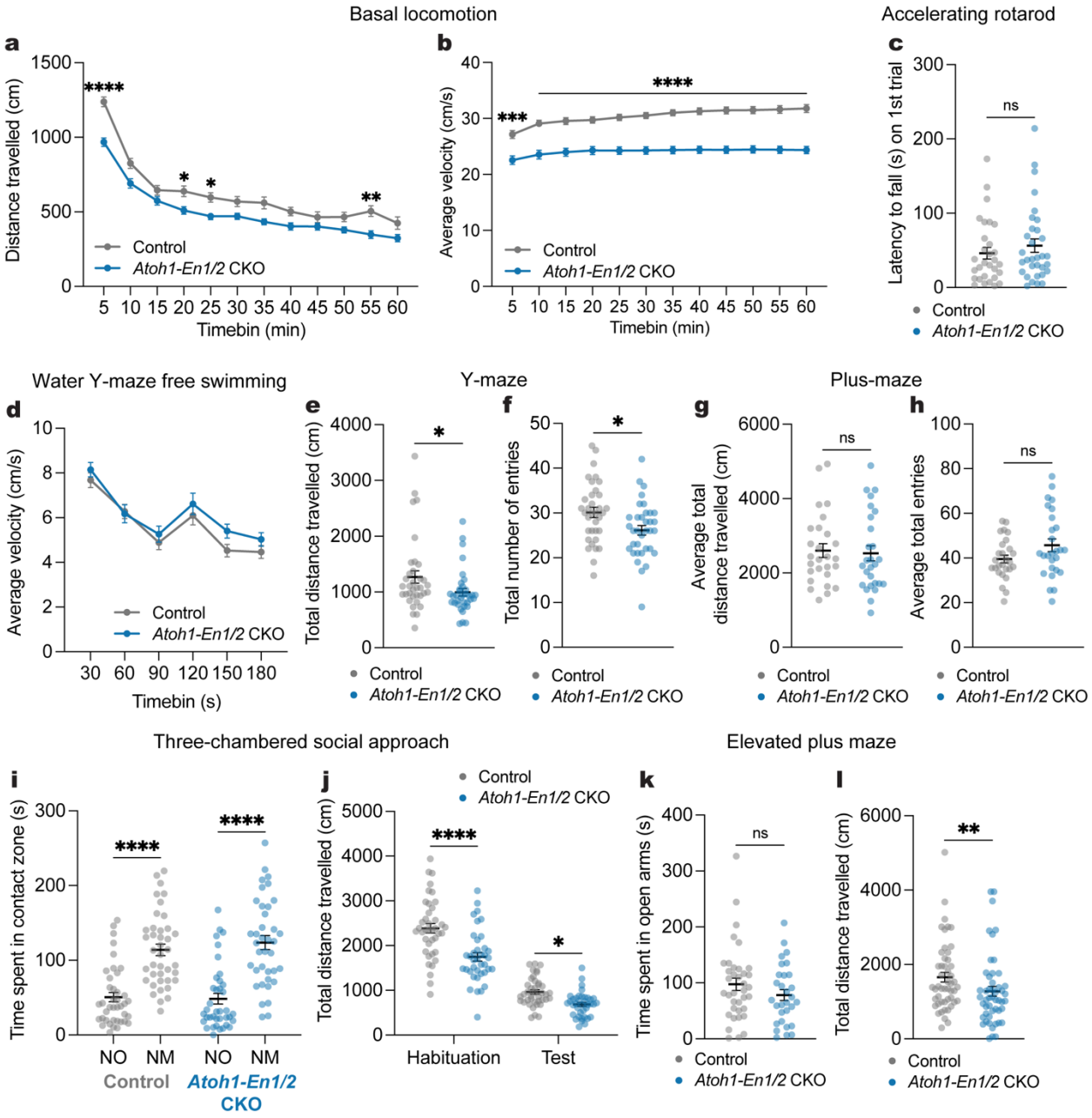


**Supplementary Fig. 9 | Motor coordination during behavior is task-dependent in *Atoh1-En1/2* CKOs.**

**a**, Distance travelled during basal locomotion by 5 min time bins (*Atoh1-En1/2* CKOs: n=33, littermate controls: n=35). Repeated measure two-way ANOVA: main effect of time ($F_{7.310,482.5}$ = 171.0, P < 0.0001), genotype ($F_{1,66}$ = 15.45, P = 0.0002), and interaction ($F_{11,726}$ = 3.120, P = 0.0004); with post hoc two-tailed t-tests with Šídák correction for effect of genotype on 0-5 min

($t_{65.21}$ = 6.250, P < 0.0001), 15-20 min ($t_{61.20}$ = 3.012, P = 0.0443), 20-25 min ($t_{59.87}$ = 3.358, P = 0.0163), 50-55 min ($t_{60.88}$ = 3.556, P = 0.0088), and no other comparisons ($P \geq 0.05$).

**b**, Average velocity during basal locomotion by 5 min time bins (*Atoh1-En1/2* CKOs: n=33, littermate controls: n=35). Repeated measure two-way ANOVA: main effect of time ($F_{2.435,160.7}$ = 171.0, P < 0.0001), genotype ($F_{1,66}$ = 57.43, P = 0.0002), and interaction ($F_{11,726}$ = 4.381, P < 0.0001); with post hoc two-tailed t-tests with Šídák correction for effect of genotype on 0-5 min ($t_{65.45}$ = 4.355, P = 0.0006) and 5-60 min (t value for each bin: $t_{65.45}$ = 4.355, $t_{61}$ = 5.693, $t_{63.58}$ = 5.927, $t_{62.8}$ = 5.916, $t_{63.54}$ = 6.755, $t_{61.95}$ = 7.332, $t_{62.74}$ = 7.867, $t_{65.1}$ = 7.819, $t_{65.56}$ = 7.863, $t_{65.83}$ = 7.695, $t_{66}$ = 7.698, $t_{65.53}$ = 7.589, all P values: P < 0.0001).

**c**, Latency to fall on the first trial of the accelerating rotarod test (*Atoh1-En1/2* CKOs: n=32, littermate controls: n=30; Mann-Whitney *U* test: *U* = 417, P = 0.3792).

**d**, Average swimming velocity during a three-minute swim (*Atoh1-En1/2* CKOs: n=35, littermate controls: n=31). Repeated measure two-way ANOVA: main effect of time ($F_{5,320}$ = 0.5563, P < 0.0001), but not of genotype (P = 0.1350) and interaction (P = 0.7335).

**e**, Total distance travelled during the Y-maze (n=35 per genotype; Mann-Whitney *U* test: *U* = 405, P = 0.0144).

**f**, Total number of arm entries in the Y-maze (n=35 per genotype; two-tailed unpaired t-test: $t_{68}$ = 2.548, P = 0.0131).

**g**, Average total distance travelled during two days of testing in the plus-maze (n=27 per genotype; Mann-Whitney *U* test: *U* = 332.5, P = 0.5857).

**h**, Average total number of arm entries during two days of testing in the plus-maze (n=27 per genotype; two-tailed unpaired t-test: $t_{52}$ = 1.839, P = 0.0717).

**i**, Total time in which the animal's nose was within the contact zone of a novel mouse (NM) and novel object (NO) during the three-chamber social approach test (*Atoh1-En1/2* CKOs: n=38, littermate controls: n=40). Repeated measure two-way ANOVA: main effect of location ($F_{1,152}$ = 81.64, P < 0.0001), but not of genotype (P = 0.6191) or interaction (P = 0.4360); with post hoc

two-tailed t-tests with Šídák correction for effect of location for *Atoh1-En1/2* CKOs ($t_{152}$ = 6.854, $P < 0.0001$) and littermate controls ($t_{152}$ = 5.913, $P < 0.0001$).

**j**, Total distance travelled during habituation and test phases in the three-chamber social approach test (*Atoh1-En1/2* CKOs: n=38, littermate controls: n=40). Repeated measure two-way ANOVA: main effect of phase ($F_{1,76}$ = 487.6, $P < 0.0001$), genotype ($F_{1,76}$ = 22.58, $P < 0.0001$), and interaction ($F_{1,76}$ = 10.31, P = 0.0019); with post hoc two-tailed t-tests with Šídák correction for effect of genotype for the habituation phase ($t_{152}$ = 5.772, $P < 0.0001$) and test phase ($t_{152}$ = 2.491, P = 0.0275).

**k**, Total time spent in the open arms of the elevated plus maze (n=50 per genotype; Mann-Whitney *U* test: *U* = 878, P = 0.01).

**l**, Total distance travelled in the elevated plus maze (n=50 per genotype; Mann-Whitney *U* test: *U* = 467, P = 0.2705).

ns, not significant: $P \geq 0.05$. Data are presented as mean values ± SEM.

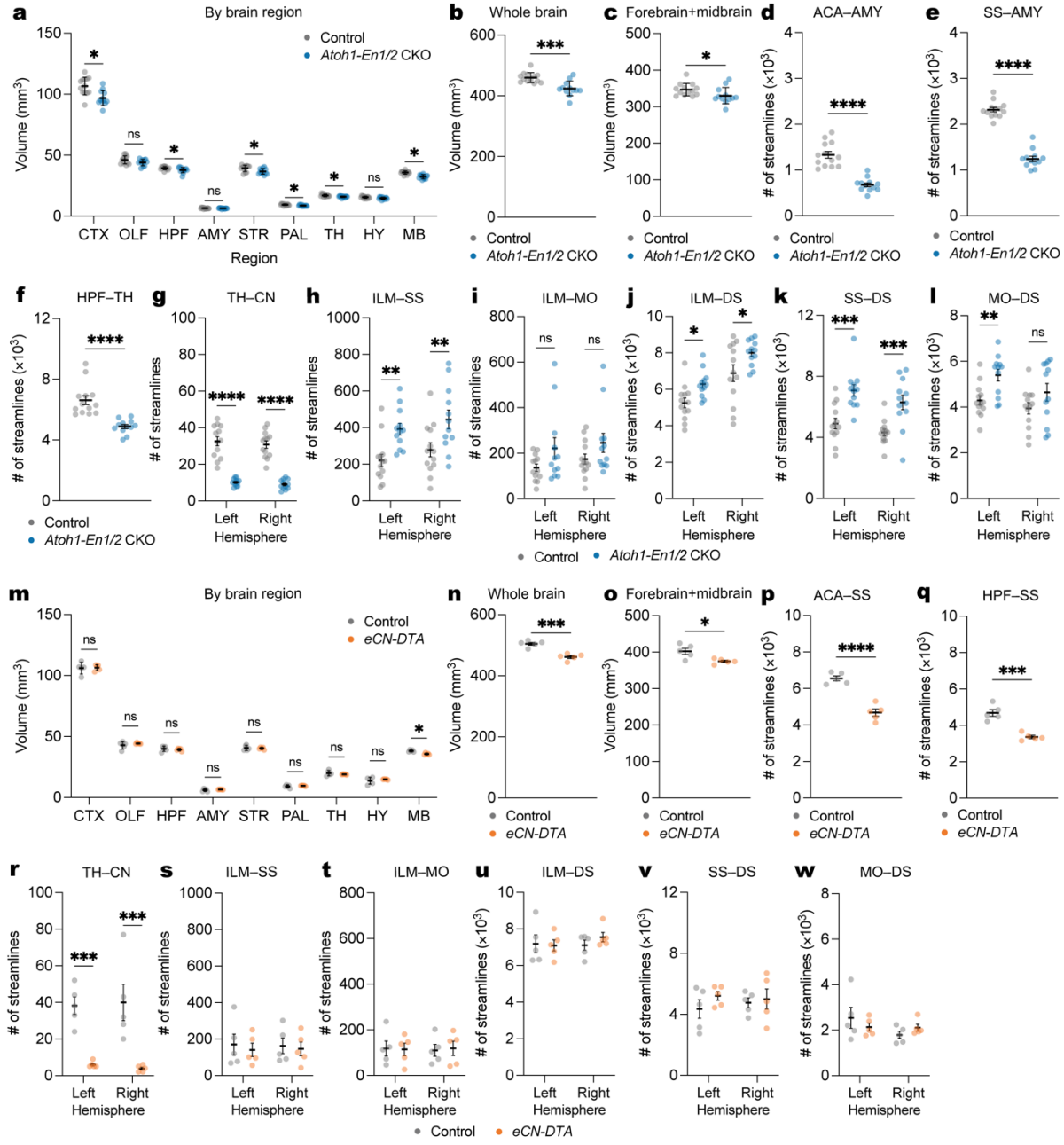


**Supplementary Fig. 10 | Brain volume and connectivity changes in *Atoh1-En1/2* CKO and eCN-DTA mice.**

**a**, Quantification of regional brain volumes in *Atoh1-En1/2* CKOs (n=12) compared to littermate controls (n=13). Two-tailed unpaired t-tests to test for effect of genotype on CTX ($t_{23}$ = 3.633, P = 0.0014), HPF ($t_{23}$ = 2.329, P = 0.03), STR ($t_{23}$ = 2.612, P = 0.016), PAL ($t_{23}$ = 3.143, P = 0.005),

TH ($t_{23}$ = 3.052, P = 0.006), MB ($t_{23}$ = 5.665, P < 0.0001), HB ($t_{23}$ = 11.16, P < 0.0001), CB ($t_{23}$ = 11.15, P < 0.0001), other comparisons $P \geq 0.05$.

**b**, Quantification of whole brain volume in *Atoh1-En1/2* CKOs compared to littermate controls (*Atoh1-En1/2* CKOs: n=12, littermate controls: n=13; two-tailed unpaired t-test: $t_{23}$ = 4.298, P = 0.0003).

**c**, Quantification of forebrain and midbrain combined volume in *Atoh1-En1/2* CKOs compared to littermate controls (*Atoh1-En1/2* CKOs: n=12, littermate controls: n=13; two-tailed unpaired t-test: $t_{23}$ = 2.087, P = 0.0481).

**d**, Quantification of average (left and right hemispheres) ACA-AMY tractography in *Atoh1-En1/2* CKOs compared to littermate controls (*Atoh1-En1/2* CKOs: n=12, littermate controls: n=13; two-tailed unpaired t-test: $t_{23}$ = 14.35, P < 0.0001).

**e**, Quantification of average (left and right hemispheres) SS-AMY tractography in *Atoh1-En1/2* CKOs compared to littermate controls (*Atoh1-En1/2* CKOs: n=12, littermate controls: n=13; Mann-Whitney *U* test: *U* = 0, P < 0.0001).

**f**, Quantification of average (left and right hemispheres) HPF-TH tractography in *Atoh1-En1/2* CKOs compared to littermate controls (*Atoh1-En1/2* CKOs: n=12, littermate controls: n=13; two-tailed unpaired t-test: $t_{23}$ = 4.298, P = 0.0003).

**g,** Quantification of TH-CN tractography in *Atoh1-En1/2* CKOs (n=12) compared to littermate controls (n=13). Ordinary two-way ANOVA: main effect of genotype ($F_{1,46}$ = 166.5, P < 0.0001), but not of hemisphere (P = 0.3838) or interaction (P = 0.8437); with post hoc two-tailed t-tests with uncorrected Fisher's LSD for effect of genotype for left hemisphere ($t_{46}$ = 9.265, P < 0.0001) and right hemisphere ($t_{46}$ = 8.985, P < 0.0001).

**h**, Quantification of ILM-SS tractography in *Atoh1-En1/2* CKOs (n=12) compared to littermate controls (n=13). Ordinary two-way ANOVA: main effect of genotype ($F_{1,46}$ = 18.16, P < 0.0001), but not of hemisphere (P = 0.1675) or interaction (P = 0.9536); with post hoc two-tailed t-tests

with uncorrected Fisher's LSD for effect of genotype for left hemisphere ($t_{46}$ = 3.055, P = 0.0037) and right hemisphere ($t_{46}$ = 2.972, P = 0.0047).

**i**, Quantification of ILM-MO tractography in *Atoh1-En1/2* CKOs (n=12) compared to littermate controls (n=13). Ordinary two-way ANOVA: main effect of genotype ($F_{1,46}$ = 5.585, P = 0.024), but not of hemisphere (P = 0.3553) or interaction (P = 0.8322); with post hoc two-tailed t-tests with uncorrected Fisher's LSD for effect of genotype for left hemisphere ($t_{46}$ = 1.822, P = 0.0750) and right hemisphere ($t_{46}$ = 1.520, P = 0.1353).

**j**, Quantification of ILM-DS tractography in *Atoh1-En1/2* CKOs (n=12) compared to littermate controls (n=13). Ordinary two-way ANOVA: main effect of genotype ($F_{1,46}$ = 11.94, P < 0.0001) and hemisphere ($F_{1,46}$ = 29.03, P < 0.0001), but not of interaction (P = 0.9007); with post hoc two-tailed t-tests with uncorrected Fisher's LSD for effect of genotype for left hemisphere ($t_{46}$ = 3.055, P = 0.0037) and right hemisphere ($t_{46}$ = 2.972, P = 0.0047).

**k**, Quantification of SS-DS tractography in *Atoh1-En1/2* CKOs (n=12) compared to littermate controls (n=13). Ordinary two-way ANOVA: main effect of genotype ($F_{1,46}$ = 32.43, P < 0.0001), but not of hemisphere (P = 0.0662) or interaction (P = 0.7773); with post hoc two-tailed t-tests with uncorrected Fisher's LSD for effect of genotype for left hemisphere ($t_{46}$ = 4.228, P = 0.0001) and right hemisphere ($t_{46}$ = 3.825, P = 0.0004).

**l**, Quantification of MO-SS tractography in *Atoh1-En1/2* CKOs (n=12) compared to littermate controls (n=13). Ordinary two-way ANOVA: main effect of genotype ($F_{1,46}$ = 10.60, P = 0.0021), but not of hemisphere (P = 0.0535) or interaction (P = 0.4680); with post hoc two-tailed t-tests with uncorrected Fisher's LSD for effect of genotype for left hemisphere ($t_{46}$ = 2.820, P = 0.0071) and right hemisphere ($t_{46}$ = 1.785, P = 0.0809).

**m**, Quantification of regional brain volumes in *eCN-DTA* mice (n=5) compared to littermate controls (n=5). Two-tailed unpaired t-tests to test for effect of genotype on MB ($t_8$ = 4.935, P = 0.001) and CB ($t_8$ = 3.130, P = 0.014), other comparisons $P \geq 0.05$.

**n**, Quantification of whole brain volume in *eCN-DTA* mice compared to littermate controls (n=5 per genotype; two-tailed unpaired t-test: $t_8 = 6.346$, P = 0.0002).

**o**, Quantification of forebrain and midbrain combined volumes in *eCN-DTA* mice compared to littermate controls (n=5 per genotype; two-tailed unpaired t-test: $t_8 = 3.055$, P = 0.0157).

**p**, Quantification of average (left plus right hemispheres) ACA-SS tractography in *eCN-DTA* mice compared to littermate controls (n=5 per genotype; two-tailed unpaired t-test: $t_8 = 7.743$, P < 0.0001).

**q**, Quantification of average (left plus right hemispheres) HPF-STR tractography in *eCN-DTA* mice compared to littermate controls (n=5 per genotype; two-tailed unpaired t-test: $t_8 = 6.324$, P = 0.0002).

**r**, Quantification of TH-CN tractography in *eCN-DTA* mice (n=5) compared to littermate controls (n=5). Ordinary two-way ANOVA: main effect of genotype ($F_{1,16} = 37.89$, P < 0.0001), but not of hemisphere (P = 0.9717) or interaction (P = 0.7233); with post hoc two-tailed t-tests with uncorrected Fisher's LSD for effect of genotype for left hemisphere ($t_{16} = 4.103$, P = 0.0008) and right hemisphere ($t_{16} = 4.613$, P = 0.0003).

**s**, Quantification of ILM-SS tractography in *eCN-DTA* mice (n=5) compared to littermate controls (n=5). Ordinary two-way ANOVA: no main effect of genotype (P = 0.6080), hemisphere (P = 0.9875) or interaction (P = 0.8883).

**t**, Quantification of ILM-MO tractography in *eCN-DTA* mice (n=5) compared to littermate controls (n=5). Ordinary two-way ANOVA: no main effect of genotype (P = 0.9440), hemisphere (P = 0.9600) or interaction (P = 0.8281).

**u**, Quantification of ILM-DS tractography in *eCN-DTA* mice (n=5) compared to littermate controls (n=5). Ordinary two-way ANOVA: no main effect of genotype (P = 0.6155), hemisphere (P = 0.5876) or interaction (P = 0.4505).

**v**, Quantification of SS-DS tractography in *eCN-DTA* mice (n=5) compared to littermate controls (n=5). Ordinary two-way ANOVA: no main effect of genotype (P = 0.2886), hemisphere (P = 0.8391) or interaction (P = 0.5482).

**w**, Quantification of MO-SS tractography in *eCN-DTA* mice (n=5) compared to littermate controls (n=5). Ordinary two-way ANOVA: no main effect of genotype (P = 0.8636), hemisphere (P = 0.1664) or interaction (P = 0.1924).

Abbreviations: CTX=cerebral cortex; OLF=olfactory bulb; HPF=hippocampal formation; AMY=amygdala; STR=striatum; PAL=pallidum; TH=thalamus; HY=hypothalamus; MB=midbrain; HB=hindbrain; CB=cerebellum; ILM=intralaminar nuclei; SS=primary somatosensory cortex; MO=primary motor cortex; ACA = anterior cingulate cortex. ns, not significant: $P \geq 0.05$. Data are presented as mean values ± SD for **a**,**b**,**g**,**h** and mean value ± SEM for **c**-**f**,**i**-**k**.

| **eCN phenotype & behavior** | **MedP-hM4Di** | ***SepW1-En1/2* CKOs** | ***Atoh1-En1/2* CKOs** | ***eCN-DTA*** |
|---|---|---|---|---|
| eCN phenotype | MedP eCN inhibited | MedP eCN gone MedA eCN reduced 50% | MedP & IntP eCN gone MedA & IntA eCN reduced 50% | All eCN gone |
| Negative geotaxis P7 & P11 | NA | P | X | X |
| Righting reflex P7 | NA | P | P | X |
| Footprint | P | P | X | X |
| Basal locomotion | P | P | X | X |
| Accelerating rotarod | P | P | X | P |
| Water Y maze | reversal | P | Initial & reversal | P |
| Y-maze | P | P | X | P |
| Plus-maze | NA | NA | X | P |
| Social Preference | NA | NA | P | P |
| Elevated Plus Maze | NA | NA | P | P |
| Grooming | NA | NA | P | P |
| Diffusion MRI | NA | NA | Increased connectivity thalamo-cortical-striatal | No change |
| Compensation | NA | From remaining eCN and/or extracerebellar circuits | Extracerebellar circuits interfere with non-motor behaviors | From extracerebellar circuits |

**Supplementary Fig. 11 | Summary of results.**

Legend: ✓ = no difference; NA = not applicable; X = impairment.

1694 **Table. 1 | Key resources and sources.**

| REAGENT OR RESOURCE | SOURCE | IDENTIFIER |
|---|---|---|
| **Antibodies** | | |
| Mouse monoclonal anti-NeuN (A60) | Millipore Sigma | Catalog No: MAB377 |
| Guinea pig polyclonal anti-NeuN | Millipore Sigma | Catalog No: ABN90 |
| Rabbit anti-Calbindin D-28k | Swant Inc | Catalog No: CD38 |
| Guinea pig polyclonal anti-Parvalbumin | Synaptic Systems | Catalog No: 195 044 |
| Chicken polyclonal anti-RFP | Rockland Immunochemicals | Catalog No: 600-901-379 |
| Mouse monoclonal anti-MEIS2 (H-10) | Santa Cruz Biotechnology | Catalog No: sc-515470 |
| Rabbit polyclonal anti-TBR2 | Abcam | Catalog No: ab23345 |
| Rabbit anti-p27 | BD Biosciences | Catalog No: 610241 |
| Goat Alexa Fluor 555 anti-chicken IgY (H+L) | Invitrogen | Catalog No: A21437 |
| Donkey Alexa Fluor 488 anti-rabbit IgG (H+L) | Invitrogen | Catalog No: A21206 |
| Donkey Alexa Fluor 647 anti-rabbit IgG (H+L) | Invitrogen | Catalog No: A31573 |
| Donkey Alexa Fluor 488 anti-mouse IgG (H+L) | Invitrogen | Catalog No: A21202 |
| Donkey Alexa Fluor 647 anti-mouse IgG (H+L) | Invitrogen | Catalog No: A31571 |
| Donkey Alexa Fluor 647 anti-guinea pig IgG (H+L) | Invitrogen | Catalog No: A21450 |
| Goat anti-mouse IgG antibody (H+L), Biotinylated | Vector Laboratories | Catalog No: BA-9200 |
| Goat anti-chicken IgG antibody (H+L), Biotinylated | Vector Laboratories | Catalog No: BA-9010 |
| **Virus strains** | | |
| AAV2-hSyn-mCherry (titer: 2.6 x $10^{13}$ GC/mL) | Addgene | Catalog No: 114472-AAV2 (Lot No: v53550) |
| AAV2-hSyn-DIO-mCherry (titer: 2.1 x $10^{13}$ GC/mL) | Addgene | Catalog No: 50459-AAV2 (Lot No: v122065) |
| AAV2-hSyn-DIO-hM4Di-mCherry (titer: 2.3 x $10^{13}$ GC/mL) | Addgene | Catalog No: 44362-AAV2 (Lot No: v117556) |
| **Chemicals** | | |
| 32% paraformaldehyde | Electron Microscopy Sciences | Catalog No: 15714 |
| Hematoxylin 2 | Richard-Allan Scientific | Catalog No: 7231 |
| Eosin-Y | Richard-Allan Scientific | Catalog No: 7111 |
| Bluing reagent | Richard-Allan Scientific | Catalog No: 7301 |
| Clarifier 2 | Richard-Allan Scientific | Catalog No: 7402 |
| Gadodiamide | Millipore Sigma | Catalog No: 131410-48-5 |
| Hoechst 33258, Pentahydrate (bis-Benzimide) | Invitrogen | Catalog No: H3569 |
| Dextran, Tetramethylrhodamine, 10,000 MW, Lysine Fixable (Fluoro-Ruby) | Thermo-Fisher Scientific | Catalog No: D1817 |
| Dextran, Biotin, 10,000 MW, Lysine Fixable (BDA-10K) | Thermo-Fisher Scientific | Catalog No: D1956 |
| Doxycycline hyclate | Sigma Aldrich | Catalog No: D9891 |
| VECTASTAIN Elite ABC-HRP Kit, Peroxidase (Standard) | Vector Laboratories | Catalog No: PK-6100 |
| 3,3'-Diaminobenzidine tetrahydrochloride (DAB) | Sigma Aldrich | Catalog No: D5905 |
| Fluoro-Gel | Electron Microscopy Sciences | Catalog No: 17985-10 |

| | | |
|---|---|---|
| Fluoromount-G | ThermoFisher Scientific | Catalog No: 00-4958-02 |
| Heparin sodium salt | Sigma Aldrich | Catalog No: H3393-50KU |
| UltraPure DNase/RNase-Free Distilled Water | ThermoFisher Scientific | Catalog No: 10977023 |
| Phosphate-Buffered Saline (10X) pH 7.4, RNase-free | ThermoFisher Scientific | Catalog No: AM9624 |
| Clozapine N-oxide | Enzo Life Sciences | Catalog No: BML-NS105-0025 |
| **Critical commercial assays** | | |
| RNAscope Multiplex Fluorescent Detection Kit v2 | Advanced Cell Diagnostics | Catalog No: 323110 |
| RNAscope Target Retrieval Reagents | Advanced Cell Diagnostics | Catalog No: 322000 |
| RNAscope Protease III | Advanced Cell Diagnostics | Catalog No: 322337 |
| RNAscope LS Multiplex TSA Buffer Pack | Advanced Cell Diagnostics | Catalog No: 322810 |
| Mm-Slc32a1-C1 | Advanced Cell Diagnostics | Catalog No: 319191 |
| Mm-Slc17a6-E2-C2 | Advanced Cell Diagnostics | Catalog No: 428871-C2 |
| Mm-Slc6a5-C3 | Advanced Cell Diagnostics | Catalog No: 409741-C3 |
| TSA Vivid fluorophore 520 | Advanced Cell Diagnostics | Catalog No: 323271 |
| TSA Vivid fluorophore 570 | Advanced Cell Diagnostics | Catalog No: 323272 |
| TSA Vivid fluorophore 650 | Advanced Cell Diagnostics | Catalog No: 323273 |
| **Experimental Models: Organisms/Strains** | | |
| Mouse: Swiss Webster | Taconic Biosciences | Stock No: SW |
| Mouse: *Atoh1-Cre*: *B6.Cg-Tg(Atoh1-Cre)1Bfri/J* | The Jackson Laboratory; Materi et al., 2005 | Stock No: 011104 |
| Mouse: *SepW1-Cre*: *B6.FVB(Cg)-Tg(Selenow-cre)NP39Gsat/Mmucd* | Mutant Mouse Resource & Research Centers (MMRRC); Gerfen, Paletzki & Heintz, 2013 | 037622-UCD (mice generously provided by N. De Marco Lab, Weill Cornell Medicine) |
| Mouse: *tetO-Cre: B6.Cg-Tg(TetO-cre)1Jaw/J* | The Jackson Laboratory | Stock No: 006234 |
| Mouse: 129S1/SvImJ | The Jackson Laboratory | Stock No: 002448 |
| Mouse: *En1*$^{Cre}$: *En1*$^{tm2(cre)Wrst}$/J | The Jackson Laboratory; Kimmel et al. 2000 | Stock No: 007916 |
| Mouse: *Atoh1-tTA* | Willett et al., 2019 | N/A |
| Mouse: *Igs7*$^{TRE\text{-}lox\text{-}tdTomato\text{-}STOP\text{-}lox\text{-}DTA*G128D}$ (Cre- and tTA- dependent DTA; *Igs7*$^{DRAGON\text{-}DTA}$ in manuscript; DRAGON = Doxycycline-controlled and Recombinase Activated Gene OverexpressioN): *Igs7*$^{tm2(tetO\text{-}tdTomato,\text{-}DTA*G128D)Rdiez}$/AljJ | The Jackson Laboratory; Ahmadzadeh et al., 2020 | Stock No: 034778 |
| Mouse: Ai75D (Cre-dependent nuclear tdTomato reporter, *Ai75* in manuscript): B6.Cg-G*t(ROSA)26Sor*$^{tm75.1(CAG\text{-}tdTomato*)Hze}$/J | The Jackson Laboratory; Daigle et al., 2018 | Stock No: 025106 |
| Mouse: *En1*$^{flox}$: *En1*$^{tm8.1Alj}$/*J* | The Jackson Laboratory; Sgaier et al., 2007 | Stock No: 007918 |
| Mouse: *En2*$^{flox}$: *En2*$^{tm6Alj}$/*J* | The Jackson Laboratory; Cheng et al., 2010 | Stock No: 008872 |
| Mouse: *En1*$^{flox/flox}$; *En2*$^{flox/flox}$ (littermate control in manuscript) | Willett et al., 2019 | N/A (generated with 007918 and 008872 in-house) |
| Mouse: *Atoh1-Cre/+; En1*$^{flox/flox}$; *En2*$^{flox/flox}$ (*Atoh1-En1/2* CKOs in manuscript) | Willett et al., 2019 | N/A (generated with 007918, 008872, and 011104 in-house) |

| | | |
|---|---|---|
| Mouse: *SepW1-Cre/+; En1$^{flox/flox}$; En2$^{flox/flox}$* (*SepW1-En1/2* CKOs in manuscript) | This manuscript | N/A (generated with 007918, 008872 in-house) |
| Mouse: *Atoh1-tTA/+; En1$^{Cre/+}$; lgs7$^{DRAGON-DTA/+}$* (*eCN-DTA* in manuscript) | This manuscript; Ahmadzadeh et al., 2020 | N/A (generated with *Atoh1-tTA*, 007916, and 034778 in-house) |
| **Software** | | |
| Fiji | ImageJ/Fiji | https://fiji.sc/ |
| Prism8 | GraphPad | https://www.graphpad.com/scientific-software/prism/ |
| ANY-maze | Stoelting Co | https://www.anymaze.co.uk/index.htm |
| BORIS | University of Torino | https://www.boris.unito.it |
| AMIRA | ThermoFisher Scientific | |
| DTIStudio | Jiang et al., 2006 | https://mristudios.org |
| MRtrix | Wu and Zhang (2016) | https://www.mrtrix.org/ |
| MATLAB R2022b | MathWorks | https://www.mathworks.com |

1695

1696 **Table. 2 | Primers and PCR conditions used for genotyping.**

| Allele | Primer sequence (5' to 3') |
|---|---|
| *Atoh1-Cre, En1$^{Cre}$* | GATATCTCACGTACTGACGG<br>TGACCAGAGTCATCCTTAGC |
| *SepW1-Cre* | ACTTGGTTTGCTCTGACTCGTGAGG<br>CGGCAAACGGACAGAAGCATT |
| *Atoh1-tTA* | GTACTGGCACGTGAAGAACAAGCG<br>GCTACTTGATGCTCCTGATCCTCC |
| *Igs7$^{DRAGON-WT}$* | CCCAACGGTCACTTACTTCC<br>CACACCTTTAATCCCGATGC |
| *Igs7$^{DRAGON-DTA}$* | CCCAACGGTCACTTACTTCC<br>GGTAACCGCGGCATAAAAC |
| *En1$^{lox}$* | GCTTGTTTGGTTTCCGAGTC<br>GGGCAGAGTAAGCCTTGAGA |
| *En2$^{lox}$* | GAAGGTCTCAAGTTTTAGCCGGTAGCC<br>CCCCTTCCTCCTACATAGTTGGCAGTG |
| *Ai75D* | CTGTTCCTGTACGGCATGG<br>GGCATTAAAGCAGCGTATCC |
| **For allele specific primers, refer to allele reference.* | |

1697

1698 **Table. 3 | Details of dye and viruses used in stereotaxic surgeries.**

| Tracer/virus | Serotype | Company | Catalog no. | Concentration/titer | Stereotaxic coordinate (distance from Bregma) | Injection volume |
|---|---|---|---|---|---|---|
| Dextran, Tetramethylrhodamine, 10,000 MW, Lysine Fixable (Fluoro-Ruby) | n/a | Thermo-Fisher Scientific | D1817 | 10% | CL: AP, -1.20 mm; ML, 0.69 mm; DV, -3.8 mm PF: AP, -2.1 mm; ML, 0.6 mm; DV, -3.5 mm | CL: 300 nL PF: 100 nL |
| Dextran, Biotin, 10,000 MW, Lysine Fixable (BDA-10K) | n/a | Thermo-Fisher Scientific | D1956 | 10% | IntA: AP, -6.24 mm; ML, 1.10 mm; DV, -3.80 mm | 300 nL |
| pAAV-hSyn-mCherry | AAV2 | Addgene | 114472-AAV2 (Lot No: v53550) | 2.6 x $10^{13}$ GC/mL | MedA: AP, -6.24 mm; ML, 0.85 mm; DV, -3.70 | 200 nL |
| pAAV-hSyn-DIO-mCherry | AAV2 | Addgene | 50459-AAV2 (Lot No: v122065) | 2.1 x $10^{13}$ GC/mL | MedP: AP, -6.7 mm; ML, ±0.9 mm; DV, -3.20 | 300 nl |
| pAAV-hSyn-DIO-hM4Di-mCherry | AAV2 | Addgene | 44362-AAV2 (Lot No: v117556) | 2.3 x $10^{13}$ GC/mL | MedP: AP, -6.7 mm; ML, ±0.9 mm; DV, -3.20 | 300 nl |

1699

**Table. 4 | Details of antibodies used for immunofluorescence.**

| Antibody (clone) | Species | Company | Catalog no. | IHC | Antigen retrieval | Temperature | Time |
|---|---|---|---|---|---|---|---|
| Anti-NeuN (A60) | Mouse mono | Millipore Sigma | MAB377 | 1:1000 | 20 m | 4°C | o/n |
| Anti-NeuN | Guinea pig poly | Millipore Sigma | ABN90 | 1:1000 | 20 m | 4°C | o/n |
| Anti-Calbindin D-28k | Rabbit | Swant Inc | CD38 | 1:1000 | 20 m | 4°C | o/n |
| Anti-Parvalbumin | Guinea pig poly | Synaptic Systems | 195 044 | 1:1000 | 20 m | 4°C | o/n |
| Anti-RFP | Chicken poly | Rockland Immunochemicals | 600-901-379 | 1:1000 (no antigen retrieval) 1:500 (with antigen retrieval) | No 20 m | 4°C | o/n or 48 h* |
| Anti-MEIS2 (H-10) | Mouse mono | Santa Cruz Biotechnology | sc-515470 | 1:1000 | 20 m | 4°C | o/n or 48 h* |
| Anti-TBR2 | Rabbit poly | Abcam | ab23345 | 1:500 | 20 m | 4°C | o/n |
| Anti-p27 | Mouse | BD Biosciences | 610241 | 1:500 | 20 m | 4°C | o/n |
| Alexa Fluor 555 anti-chicken IgY (H+L) | Goat | Invitrogen | A21437 | 1:500 | n/a | RT | 1 h |
| Alexa Fluor 488 anti-rabbit IgG (H+L) | Donkey | Invitrogen | A21206 | 1:500 | n/a | RT | 1 h |
| Alexa Fluor 647 anti-rabbit IgG (H+L) | Donkey | Invitrogen | A31573 | 1:500 | n/a | RT | 1 h or 2 h* |
| Alexa Fluor 488 anti-mouse IgG (H+L) | Donkey | Invitrogen | A21202 | 1:500 | n/a | RT | 1 h |
| Alexa Fluor 647 anti-mouse IgG (H+L) | Donkey | Invitrogen | A31571 | 1:500 | n/a | RT | 1 h or 2 h* |
| Alexa Fluor 647 anti-guinea pig IgG (H+L) | Goat | Invitrogen | A21450 | 1:500 | n/a | RT | 1 h |
| Anti-mouse IgG antibody (H+L), Biotinylated | Goat | Vector Laboratories | BA-9200 | 1:500 | n/a | RT | 1 h |
| Anti-chicken IgG antibody (H+L), Biotinylated | Goat | Vector Laboratories | BA-9010 | 1:500 | n/a | RT | 1 h |
| *Applicable for free-floating immunofluorescence or immunohistochemistry | | | | | | | |